Modeling Hydrological Impacts of Climate and Irrigation Changes in a Mediterranean Catchment

Dissertation
der Mathematisch-Naturwissenschaftlichen Fakultät
der Eberhard Karls Universität Tübingen
zur Erlangung des Grades eines
Doktors der Naturwissenschaften
(Dr. rer. nat.)

vorgelegt von
Diane von Gunten
aus
Gorgier, Schweiz

Tübingen
2015

Gedruckt mit Genehmigung der Mathematisch-Naturwissenschaftlichen Fakultät der Eberhard Karls Universität Tübingen.

Tag der mündlichen Qualifikation:
Dekan: Prof. Dr. Wolfgang Rosenstiel
1. Berichterstatter: Prof. Dr.-Ing. Olaf A. Cirpka
2. Berichterstatter: Dr. Thomas Wöhling
3. Berichterstatter: Prof. David L. Rudolph

Abstract

Climate change will have strong impacts on agriculture and hydrological processes, especially in semi-arid regions, where water resources are limited. However, these impacts are difficult to quantify. Apart from the uncertainties directly related to climate predictions (notably the prediction of future precipitation), the evaluation of hydrological effects of climate change also depends on the accurate simulation of water fluxes on the catchment scale, which are often uncertain. To simulate the catchment responses to climate change, different types of hydrological models have been used in the past, with various degrees of success. In this thesis, my aim is to evaluate the usefulness of integrated hydrological models to predict the impacts of climate change on water resources in semi-arid, Mediterranean catchments.

Integrated hydrological models, or *pde*-based models, are distributed hydrological models based on partial differential equations (*pde*). They usually simulate subsurface flow based on the Richards' equation and surface flow based on a simplification of the shallow-water equations. They account for surface-subsurface interactions in a spatially-distributed manner and they represent the main hydrological processes (infiltration, exchanges in the hyporheic zone, evapotranspiration, etc.) with some level of detail. However, they generally have high computational needs, which result in long simulation times. These long simulation times limit the applications of integrated hydrological models in realistic case studies, particularly because the model calibration and uncertainties qualification require a large number of model runs.

Because of the long simulation times and the large number of model parameters in many integrated hydrological models, model calibration can be a lengthy and tedious process. Hence, an important criterion to evaluate the practicability of integrated hydrological models in climate-impact studies is the feasibility of the model calibration. To accelerate the calibration procedure, I propose a method which is based on a set of computational grids of increasing resolution. I test this method in a particular case study, the Lerma catchment, situated in the Ebro basin (north-east Spain). In this case study, the model calibration is about eight times faster using the nested method than a direct manual calibration. Nevertheless, the model calibration is still considerably slower (about one month on a desktop computer) than the calibration of simpler conceptual models.

An important characteristic of the catchment which is modeled in this study is the rapid transition from rainfed to irrigated agriculture between 2006 and 2008. The calibrated hydrological model generally reproduces this transition with respect to changes in discharge and hydraulic heads. Consequently, this model is a valuable tool when studying the interactions between climate and irrigation changes, which are important to understand future impacts of climate change. For this purpose, I model the hydrological responses of the Lerma catchment to simultaneous climate and irrigation changes. To this end, climate scenarios for the region are developed, based on four regional climate models from the European ENSEMBLES project (http://www.ensembles-eu.org). The outputs from the regional climate models are downscaled using a calibrated weather generator and a quantile-based method. Based on the results from the hydrological simulations, it is found that responses to climate change significantly depend on the irrigation scenarios.

Hydraulic heads and base flow are larger under irrigated conditions, but they are more sensitive to climate change when irrigation is present. In contrast, responses of annual maximum flow to large precipitation events are more intense in the scenario without irrigation. In future climate, actual evapotranspiration in summer decreases under non-irrigated conditions due to the lower summer precipitation, and increases under irrigated conditions because of the larger soil moisture, which results in a higher sensitivity of actual evapotranspiration to temperature. This analysis would have been difficult, or even impossible, to conduct with other types of hydrological models.

In addition to mean climatic conditions, droughts are also examined. Droughts are a serious risk for the Ebro region notably because of the economical importance of the agricultural sector, which has large water needs. Changes in future droughts are often studied from a meteorological point of view. Drought indices (i.e., a single numerical value representing the dryness level based on one or more hydro-meteorological state variables) are computed based on the outputs from regional or global climate models in present and future climate. Differences in drought indices are then used to predict future drought conditions. I compare the results from this approach to the outputs of the integrated hydrological model during dry periods. Specifically, I examine the correlation between seven well-known drought indices and three modeled hydrological variables in the climate and irrigation scenarios used previously to study the interactions between irrigation and climate changes. In addition, I control the validity of the functional relationship between these indices and the hydrological variables under the predicted, future conditions. Correlations between the hydrological variables and drought indices are similar in all studied conditions. However, the relationships between the drought indices and the hydrological variables are often different in present and future climate. Hence, drought indices are adequate indicators of dry periods in all climates. However, a drought with a similar intensity (as defined by a particular drought index) might have different hydrological impacts in present and future climate. These differences cannot be captured by studying meteorological drought indices alone.

To conclude, integrated hydrological models have important advantages over other types of hydrological models in climate-impact studies: They allow for a joint analysis of surface and subsurface flow, they can be used to study interactions between land-use and climate changes, and they can be employed to test simpler methods, such as the use of drought indices. However, their use is hindered by their high computational needs. This obstacle can partially be overcome by simplifying the computational grid during part of the calibration process.

Kurzfassung

Der Klimawandel wird erhebliche Auswirkungen auf die Landwirtschaft und die Wasservorkommen habe; dies gilt insbesondere in semiariden Gebieten mit eingeschränkten Wasserressourcen. Diese Auswirkungen sind jedoch schwer zu quantifizieren. Neben den Unsicherheiten, die unmittelbar im Zusammenhang mit Klimaprognosen (besonders der Prognose des zukünftigen Niederschlags) stehen, hängt die Bewertung der hydrologischen Auswirkungen des Einflusses der Klimawandels von der Simulation des Wasserflusses ab, die ebenfalls unsicher ist. Um die Reaktion von Einzugsgebieten auf Klimaveränderungen zu simulieren, wurden vielfältige hydrologische Modellen verwendet. Mit der vorliegenden Doktorarbeit beabsichtige ich, die Zweckmäßigkeit von integrierten hydrologischen Modellen einzuschätzen, um hydrologische Auswirkungen der Klimaveränderung in semiariden Gebieten vorherzusagen.

Integrierte hydrologische Modelle (oder pde-basierte Modelle) sind räumlich verteilte hydrologische Modelle auf der Grundlage partieller Differenzialgleichungen (engl. Abk.: pde). Diese simulieren den unterirdischen Wasserfluss mit der Richardsgleichung und den oberirdischen Wasserfluss mit der Flachwassergleichung. Dadurch werden räumliche ober- und unterirdische Interaktionen berücksichtigt, und die meisten hydrologischen Prozesse (Wasserversickerung, Austausch in der hyporheischen Zone, Evapotranspiration, usw.) können hinreichend detailliert beschrieben werden. Sie erfordern jedoch häufig einen hohen Rechenaufwand, der in langen Simulationszeiten resultiert. Diese erschweren die Anwendung von integrierten hydrologischen Modellen in realistischen Fallstudien, da sie den Kalibrierungsprozess verlangsamen.

Aufgrund der hohen Anzahl von Parametern und langer Simulationszeiten kann die Kalibrierung von integrierten hydrologischen Modellen ein langwieriger und mühsamer Prozess sein. Deshalb ist die Geschwindigkeit der Modellkalibrierung ein wichtiges Kriterium, um die Nützlichkeit von integrierten hydrologischen Modellen in Klimafoldenstudien zu beurteilen. Um den Kalibrierungsprozess zu beschleunigen, schlage ich ein Kalibrierverfahren vor, das auf ineinander verschachtelten Rechengittern besteht. Ich teste diese Methode in einer Fallstudie über das Lermaeinzugsgebiet im Ebrobecken (Nordspanien). Durch die vorgeschlagene Methode ist die Modellkalibrierung achtmal schneller als eine direkte manuelle Kalibrierung. Sie dauert bei Verwendung eines Desktop-PCs ungefähr einen Monat. Das ist wesentlich länger als die Kalibrierung einfacher konzeptioneller Modelle. Dennoch war die Modellkalibrierung eine handhabbare Aufgabe.

Charakteristisch für das Gebiet meiner Fallstudie ist die schnelle Umwandlung der Landnutzung von regenabhängiger zu bewässerter Landwirtschaft in den Jahren zwischen 2006 und 2008. Das Modell reproduziert die Folgen dieses Wandels in Bezug auf den Gebiets und die Grundwasserstände. Deshalb können die Modellergebnisse genutzt werden, um die hydrologischen Folgen des Klimawandels in semiariden Gebieten unter dem Einsatz unterschiedlicher Bewässerungsstrategien zu verstehen und vorherzusagen. Für diesen Zweck habe ich die hydrologischen Reaktionen im Lermagebiet unter der gleichzeitigen Änderung der Bewässerung und

des Klimas modelliert. Basierend auf vier regionalen Klimamodellen des europäischen ENSEMBLES-Projektes (http://www.ensembles-eu.org), entwickle ich Klimaszenarien für das untersuchte Einzugsgebiet. Das Downscaling der Daten erfolgte durch einen kalibrierten Wettergenerator beziehungsweise einer "quantile-mapped" Methode. Davon ausgehend hängt die Reaktion auf die Klimaveränderungen maßgeblich von den Bewässerungsszenarios ab. Bewässerte Gebiete weisen zwar größere Piezometerhöhen und Basisabflüsse auf, reagieren jedoch anfälliger auf Klimaveränderungen. Im Gegensatz dazu kommt es in den Szenarios ohne Bewässerung zu intensiveren hydrologischen Reaktionen wie jährlichen Höchstabflüssen aufgrund heftiger werdender Niederschläge. In zukünftigen Klimaszenarien nimmt die aktuelle Verdunstung während des Sommers ab, steigt jedoch auf bewässerten Flächen. Zusätzlich ist die Bodenfeuchtigkeit größer auf bewässerten Flächen, wodurch die Sensitivität der aktuellen Evapotranspiration durch ansteigende Temperatur höher wird. Ohne Bewässerung führen niedrige Sommerniederschläge zu einer Abnahme der aktuellen Evapotranspiration. Diese Analysis ist kann mit anderen hydrologischen Modelltypen schwierig oder gar nicht durchgeführt werden. Daher sind integrierte hydrologische Modelle unabdingbar, um die Zusammenhänge zwischen Klima- und Landnutzungsänderungen umfassend zu untersuchen.

Zusätzlich zu den allgemeinen klimatischen Veränderungen, habe ich Extremereignisse wie Dürren untersucht. Aufgrund der wirtschaftlichen Bedeutung der Landwirtschaft im Ebrobecken sind Trockenzeiten dort eine ernst zu nehmende Gefahr. Veränderungen der Trockenperioden werden häufig meteorologisch untersucht. Dürreindizes sind einzelne numerische Werte, die den Trockenheitsgrad repräsentieren und auf einer oder mehreren meteorologischen Messgrößen beruhen. Sie werden aus den Ergebnissen lokaler oder globaler Klimamodelle für derzeitige oder zukünftige Klimata berechnet. Ich vergleiche die Stabilität der Beziehung zwischen diesen Indizes und den hydrologischen Variablen. Die Korrelationen zwischen den Dürreindizes und den untersuchten hydrologischen Zustandsgrößen sind für alle Klimaszenarien ähnlich. Jedoch verändern sich häufig die funktionalen Zusammenhänge beim Übergang von gegenwertigen zu zukünftigen Klimaszenarien. Daher sind Dürreindizes zwar angemessene Anzeiger für Trockenperioden in allen Klimaszenarien, aber sie verbergen unter Umständen wichtige Veränderungen durch die Folgen von zukünftigen Dürren.

Zusammenfassend kann festgestellt werden, dass die Zweckmäßigkeit von integrierten hydrologischen Modellen in Studien zu Klimaauswirkungen durch den hohen rechnerischen Zeitaufwand eingeschränkt wird. Dieses Hindernis kann durch die vorgestellte Kalibriermethode, die auf Gittervergröberungen in erste Kalibrierschritten beruht, teilweise umgangen werden. Kalibrierte integrierte hydrologische Modelle liefern wichtige Erkenntnisse bezüglich des Zusammenspiels von Bewässerungs- und Klimaveränderungen. Darüber hinaus sind sie hilfreich, um einfachere Ansätze zur Untersuchung der Folgen des Klimawandels, zu erproben und zu vergleichen.

Acknowledgments

First and foremost, I am very grateful to my actually-useful-and-available main advisor, Olaf Cirpka, and to the two best-ever, junior-only-by-name advisors, Claus Haslauer and Thomas Wöhling. Their support and guidance were a great help in the achievement of this thesis. Thanks a lot.

Secondly, I am deeply indebted to all my colleagues. Between coffee breaks, day-out and week-end in, you were definitely the place to go to celebrate the best and to go over the annoying. I cannot imagine how bland this period would have been without you: Alicia, Alexandra, Anneli, Atephe, Bijendra, Carolin (Lerma²), Chang, Karim, Jenia, Jeremy, Jürnjakob, Marvin, Matthias, Maxi, Reynolds, Shanghua, and Zhongwen. All my thanks also to my colleagues of the hydrogeology group: Alexander, Carsten, Chuanhe, Dominik, Julia, Kennedy, Emilio, Steven, etc. My cake-tasting ability is entirely their making.

I also gratefully acknowledge Michael Finkel, who supported the work of all the ITRG group, including mine, and Monika Jekelius. Her effectiveness and her supportive approach to administration are legendary.

In addition, I am very thankful to everybody who spent time and efforts on my all-time-favorite catchment. None of this study would have been possible without their results and measurements. I am especially grateful to Jesus Causapé and Daniel Merchán Elena. Special thanks go to Daniel, who supported me during my visit in Zaragoza. Empirical data show that the average research stay is improved three fold by the addition of tapas (personal communication: Sanz-Prat, 2014).

On the other side of the Atlantic, but closer in my mind, I thank David Rudolph for his support during my research stay and during my whole thesis. Canada was great and Waterloo was even better with his support. On the other side of the Rhine, but very close to my heart, I thank my parents to feed me, to support me, and to not kill me during my first 18 years. I love you both and I send some kisses to my sisters, brother and grand-parents as well.

Finally, I would like to thank the Deutsche Forschungsgemeinschaft (DFG) to fund this research project and the whole IRTG "Integrated Hydrosystem Modeling". Their financial support made my thesis possible.

Contents

1 Introduction

1.1 Motivation

The current increase in global mean temperature, resulting from the anthropogenic increase in CO_2 emissions (Meehl et al., 2007), will have strong impacts on hydrological processes, especially in semi-arid Mediterranean regions (e.g., Sánchez et al., 2004; Vargas-Amelin et al., 2014). Summer precipitation will probably decrease in the next 70 years, while potential evapotranspiration will likely increase, resulting in an overall dryer climate (Zambrano-Bigiarini et al., 2010). Simultaneously, irrigation needs and urban water demand will both increase (Milano et al., 2013). Hence, in these regions, water availability will decrease, which will complicate the management of local water resources (e.g., Bovolo et al., 2010). The competing water needs of agriculture and urban areas might not be met under the future climatic conditions. To plan the adaptation to these new conditions, accurate information about climate change and their impacts on hydrology is needed. However, the hydrological responses of local water bodies to climate change are highly uncertain (Ghosh et al., 2010), particularly because of the large disparities in the prediction of future precipitation between the different global climate models (Herrera et al., 2010).

In addition to the uncertainties related to climate predictions, the accuracy of hydrological models can have a large impact on the estimation of climate-change effects (Dams et al., 2015; Jiang et al., 2007). Various types of models have been used to predict hydrological effects of climate change, from simple conceptual models (e.g., Schaefli et al., 2007) to large integrated hydrological models (e.g., Goderniaux et al., 2009). Which hydrological models should be used to realistically represent water fluxes, and so which models should be used in climate-impact studies, is the subject of large discussions (e.g., Beven, 2002; Todini, 2007), which have not led yet to a general consensus. Theoretically, to simulate climate-change impacts, integrated hydrological models have various advantages over other hydrological model types (Section 3.3). However, only a low number of climate-impact studies have used an integrated hydrological model (e.g., Goderniaux et al., 2009; van Roosmalen et al., 2009). Indeed, integrated hydrological models are difficult to use in realistic case studies because of their long simulation time. Their high computational needs prohibit the use of the majority of methods for parameter estimation and uncertainty quantification (Blasone et al., 2008). Therefore, an important criterion to assess the usefulness of integrated hydrological models is the rapidity of their model calibration. Previous applications of integrated hydrological models have generally used manual calibration to estimate uncertain model parameters, which is a slow and tedious process (Goderniaux et al., 2009). A quicker and more practical calibration method would increase the interest of integrated hydrological models for climate-impact studies.

In addition, particular advantages of integrated hydrological models for climate-impact studies have not been investigated in detail before. For example, integrated hydrological models have been shown to be efficient in modeling the hydrological impacts of important land-use changes, such as irrigation changes (Pérez et al., 2011). In the Mediterranean region, irrigation onset is a particularly important case of land-use change because of

the scheduled increase in irrigated area. For instance, in the Ebro region, a significant increase (up to 300'000 hectare) in irrigated areas is planned in the next decades (Bielsa et al., 2015; Milano et al., 2013). At local and regional scales, the start of irrigation has important impacts on the hydrology (Merchán et al., 2013) and probably interacts with the catchment responses to climate change. Potential climate and irrigation changes should therefore be studied together. Indeed, the extent and the timing of the interactions between these two processes are not well-understood. As integrated hydrological models seem advantageous when separately modeling impacts of climate (Goderniaux, 2011) and irrigation changes (Pérez et al., 2011), they are good candidates to model catchment responses to synchronous changes in both climate and land use (van Roosmalen et al., 2009). However, previous studies have not investigated the simultaneous impacts of irrigation and climate changes in a realistic case-study. Consequently, it is not known if integrated hydrological models would bring new information on the interactions between climate and irrigation changes in realistic cases.

Another potential use of integrated hydrological models in climate-impact studies is to compare the outputs from integrated hydrological models with the results from other methods. Indeed, many simpler approaches to estimate climate-change impacts exist and often result in consequential time gain compared to the development and calibration of integrated hydrological models. For instance, a simplified approach to estimate the impact of climate change is the use of meteorological drought indices to estimate future drought impacts. Droughts strongly affect water resources and often cause tens of millions of euros of damage (Gil et al., 2011), notably because of the reduction in crop yield, decreasing water quality, and restriction in water use (Mishra et al., 2010). Hence, changes in drought frequency and duration must be examined. To this end, a meteorological perspective is often chosen (e.g., Kim et al., 2014; Kirono et al., 2011; Leng et al., 2015; Masud et al., 2015; Park et al., 2015; Tue et al., 2015; Zarch et al., 2015). Specifically, meteorological drought indices, i.e., summary metrics based on hydro-meteorological variables such as precipitation, are computed in present and future climate, based on outputs from global or regional climate models. Changes in drought indices are then used to estimate changes in drought risks, whereby no change in hydrological processes is considered. It is assumed that lower precipitation during dry periods will have a similar impact on streamflow or hydraulic heads in present and future climate. In addition, changes in potential evapotranspiration is often neglected (Vicente-Serrano et al., 2009). Because the impact of these simplifications have rarely been studied, a comparison between drought impacts simulated by a hydrological model, forced by future meteorological inputs, and droughts impacts derived simply from the calculation of drought indices could bring new insights into the estimation of future drought effects.

1.2 Objectives

The general objective of this thesis is to improve the quality of the predictions of hydrological impacts of climate change in Mediterranean climate. Specifically, my aim is to evaluate and improve the usefulness of integrated hydrological models in climate-impact studies.

In principle, integrated hydrological models have various advantages compared to simpler, conceptual models when studying climate-change impacts (Section 3.3). However, the parameter calibration of these models is difficult because of their long simulation time. Hence, my first objective is to simplify the calibration of integrated hydrological models.

My second objective is to study the interactions between irrigation and climate change effects. Concretely, I will investigate the differences in the catchment responses to climate change under different irrigation conditions, using an integrated hydrological model.

Finally, my third objective is to evaluate the efficiency of drought indices to predict changes in future drought risks. Practically, I will compare the estimation of future drought risks derived from drought indices to the outputs from the hydrological model.

1.3 Thesis structure

The remainder of this thesis is structured as follows:

- First, I present a summary of methods used for climate prediction. Next, I describe different hydrological modeling strategies used to predict the impacts of climate change on water resources.

- Three papers, constituting the main body of this thesis, are reproduced in Section 4, 5, and 6. Each of these publications present the accomplished work in each of three main objectives presented above (Section 1.2).

  1. The main subject of the first paper is an innovative calibration method, adapted to integrated hydrological models (or *pde*-based models). The central idea of this method is to use computational grids of increasing resolution during the model calibration.

  2. The second paper is a comparison of hydrological effects of climate change at catchment scale in irrigated and non-irrigated conditions. I use downscaled climate scenarios and an integrated hydrological model, calibrated under different irrigation conditions, to study the interactions between climate and irrigation changes in the Lerma catchment.

  3. The third paper is concerned with quantifying the efficiency of drought indices to predict hydrological impacts of droughts in future climate. I estimate the hydrological consequences of droughts (as simulated by the hydrological model) in different climate and irrigation scenarios. I compare these outputs with the prediction of future drought impacts derived from drought indices.

- Finally, I conclude with a general discussion and an outlook on possible future research.

2 Climate scenarios

Regional and global climate models are central to predict future climatic conditions. Since the outputs of these models are used as forcing in the hydrological simulations of this thesis, I give here a short review of these models, after a brief introduction to the emission scenarios of greenhouse gases. I then describe the adaptation of the climate-model outputs to a suitable format for hydrological studies (i.e., downscaling).

2.1 Greenhouse gases emission scenarios

The current increase in global temperature is driven by an increase in greenhouse-gas emissions, notably anthropogenic CO_2 (e.g., Meehl et al., 2007). In the year 2000, the Intergovernmental Panel on Climate Change (IPCC) developed a suite of emission scenarios, known as the SRES emission scenarios (Nakićenović et al., 2000). These scenarios are based on projections of demography, economic growth, and technological innovations.

In the last assessment report of climate change (Stocker et al., 2013), IPCC changed its focus from emission scenarios to representative concentration pathways (Vuuren et al., 2011). These representative concentration pathways or RCP are based on the difference in radiative forcing between pre-industrial time and the year 2100. For example, RCP6 is a scenario where the mean planetary radiative forcing is 6 W/m^2 higher in 2100 than in the last century (Meinshausen et al., 2011). These scenarios also contain an estimation of greenhouse gas emissions, but they focus on radiative forcing.
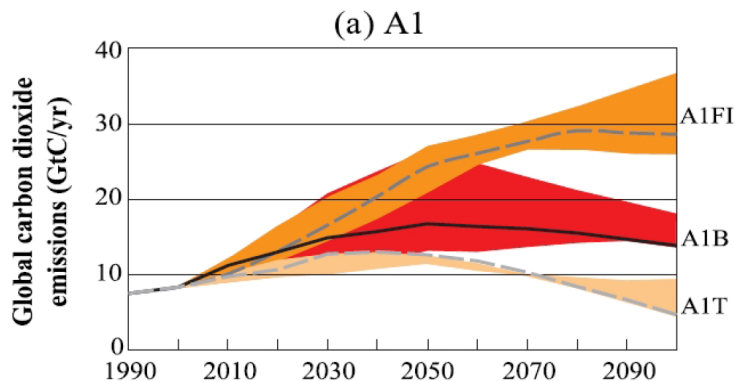

Figure 1: *Global annual CO_2 emission from 1990 to 2100 in the A1 scenarios in gigatonnes of carbon per year (GtC/y). The A1B emission scenarios is represented by the red colored band - Figure adapted from Nakićenović et al. (2000)*

Even if RCP is the current standard operated by IPCC (Stocker et al., 2013), I use the SRES scenarios in this thesis, because of the relatively low number of available regional climate simulations (Section 2.3) using RCP. More precisely, I use the climate scenario proposed by the ENSEMBLES project (Linden et al., 2009), which are based on the A1B emission scenario (Section 5). This scenario assumes a relatively homogeneous world with increased cultural interactions and a rapid economic growth (Nakićenović et al., 2000). Global population peaks in 2050 and declines after. Energy sources are balanced between

non-fossil and fossil. In the A1B scenario, global CO_2 emissions are maximal in 2050 with a yearly emission of about 16 GtC/yr (Figure 1). Differences in the climatic outcomes between the emission scenarios become apparent at the end of the 21st century, but they are less important until 2050. Hence, using more than one emission scenario for climate predictions before 2050 is of limited interest, according to Linden et al. (2009).

2.2 Global circulation models

Global circulation models (GCM), also called global climate models, are indispensable to the prediction of future climate. These large 3-dimensional models simulate the atmosphere, the land-surface, the ocean, and the exchanges between these different compartments on the global scale. Meteorological variables are predicted alongside with carbon fluxes and other biochemical variables. These models take solar radiation, land-use categories, and future CO_2 emissions, among other information (Goosse et al., 2015), as input.

The simulation of atmospheric processes is based on the conservation of mass, energy, and momentum. In other words, the representation of the atmosphere is derived from the Navier-Stokes equations (e.g., Bechtel et al., 2015) solved on a rotating sphere, and coupled with thermodynamical constraints. These conservation laws can be represented by a set of equations, which is then simplified to form the so-called "dynamic core" of the GCM. These simplifications or parameterizations are necessary because of the relatively low resolution of the GCMs (horizontal resolution: about 100-300 km^2, Buser et al. (2010)) and because of the strong non-linearity of the conservation laws (Randall, 2010). Many of these parametrizations are based on empirical knowledge and may introduce significant uncertainties (Déqué et al., 2007). One of the most important and uncertain parametrization is that of clouds, especially cumulus (Randall, 2010). Cumulus are especially difficult to simulate because their apparition depends on phase-changes of water, convective movements, and eddy fluxes, which are all sub-grid phenomena difficult to represent at grid scale. However, the simulation of cumulus is important because it has a large influence on modeled precipitation and radiation.

To numerically solve the equations forming the GCM dynamic core, the finite difference method was used in the majority of the early GCMs, such as the GFDL model (Smagorinsky et al., 1965). However, the finite difference method adapted for spherical coordinates results in the convergence of the meridians at the poles, which complicates the numerical calculations (Randall, 2010). To overcome this difficulty, current GCMs integrate a set of spectral methods to model the atmosphere, i.e., the dynamic cores of current GCMs often use a set of Fourier transform to numerically solve the differential equations. To overcome the tendency of spectral methods to create negative concentration of atmospheric constituents (particularly water vapor), semi-Lagrangian methods are used in addition or in replacement of spectral methods (Randall, 2010). In these schemes, the equations governing atmospheric motions are developed using the Lagrangian rate of change ($\frac{D}{Dt}$), but are solved on an Eulerian grid (e.g., Bonaventura, 2004).

Coupled with the dynamic core of the GCMs is the representation of land-surface and the oceans (Figure 2). Land-surface flow and run-off are drastically simplified (Milly et al.,
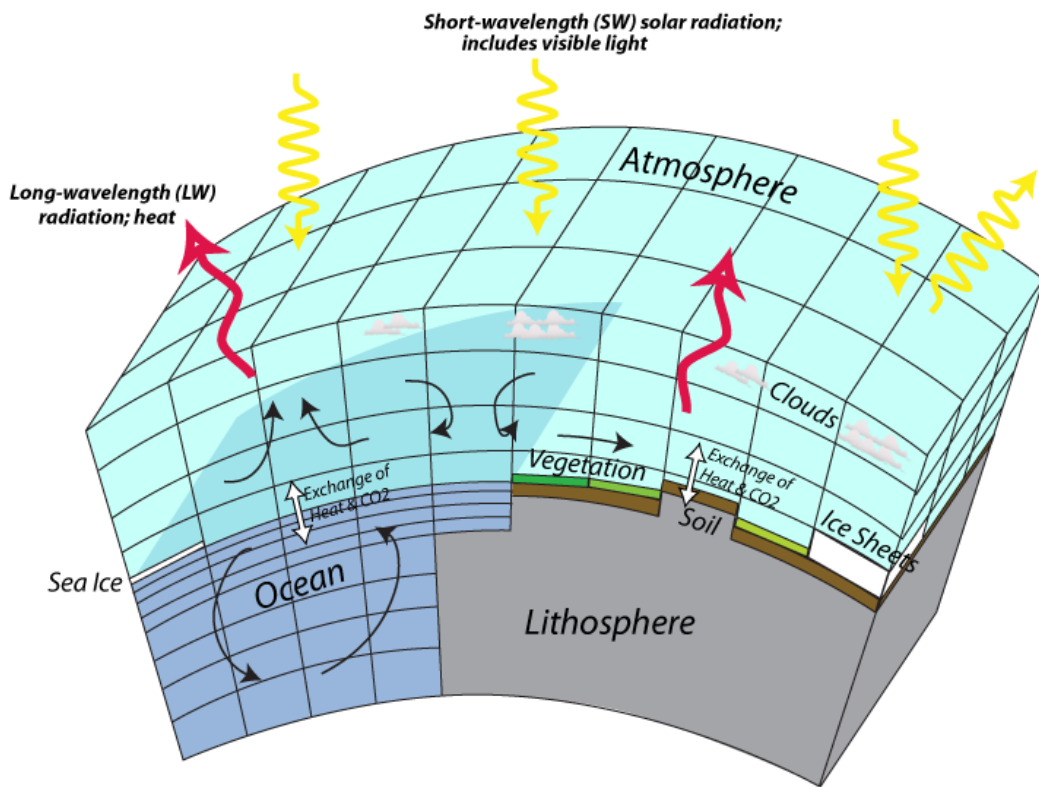
Figure 2: *Schematic structure of a GCM - Figure adapted from Bralower et al. (2015)*

2002). On the land-surface, surface temperature is the main link between the atmosphere and the surface (Roeckner et al., 2003). The surface temperature is derived from the energy balance of the soil or ocean surface (Roeckner et al., 2003). Ocean currents are simulated dynamically, based on conservation of momentum and mass. Energy and mass fluxes (water, CO_2, etc.) are exchanged between all three compartments. The CO_2 cycle is of special importance for climatic prediction and is modeled with some precision by modern GCMs. However, large uncertainties in the carbon cycle still exist, notably in the variations of the exchanges between the land and the atmosphere compartments (Randall et al., 2007).

Even if the GCM outputs reproduce the main characteristics and variations of the climate of our planet (Randall et al., 2007), variability between the different GCM outputs is relatively high, especially with respect to precipitation (Herrera et al., 2010). For example, predicted changes in mean summer precipitation in the Mediterranean region vary between -3% and -53% of the present precipitation for 2080-2100 in the A1B scenario (Christensen et al., 2007). Moreover, the low spatial resolution of GCM introduces errors, notably into the representation of topography and in phenomena at the sub-gird scale. Another important uncertainty source for climate prediction during the second-half of the 21st century is the difference between the CO_2 emission scenarios (Buser et al., 2010). To take into account these uncertainties, the majority of climate-impact studies use several GCMs to produce reliable climate scenarios.

2.3 Regional climate model and dynamical downscaling

Regional climate models (RCMs) function on the same basic principles as GCMs. However, RCMs only cover a part of the planet, usually one continent. Consequently, their horizontal resolution (under 100 km^2) is finer than the usual GCM resolution. Hence, topography, notably mountain ranges, is better represented and their influence on the atmosphere is simulated more realistically. In addition, atmospheric circulation can be modeled at finer scale, which allows for a more physically-based representation of the atmosphere (Giorgi et al., 2001).

RCMs are often used to increase the resolution and the realism of GCM outputs, a process called dynamical downscaling. This technique has been pioneered by Dickinson et al. (1989) and Giorgi et al. (1990), based on the nested modeling techniques from the field of numerical weather prediction (Giorgi et al., 2001). The GCM provides time-dependent lateral boundary conditions to the RCM. No feed-back from the RCM is returned to the GCM. The main advantage of dynamical downscaling over other downscaling techniques (Section 2.4) is that it is based on realistic atmospheric processes. However, it is computationally intensive and strongly depends on the accuracy of the GCM forcing (Fowler et al., 2007a).

Even if dynamical downscaling improves the realism of climate scenarios, it is not recommended to directly use RCM outputs as hydrological inputs (Wood et al., 2004). Indeed, the differences between the RCM outputs in the present climate and the measurements are often too important for this purpose. A statistical downscaling step (as explained in the next section) is necessary before using RCM outputs to force a hydrological model to predict climate change impacts.

2.4 Statistical downscaling of climate scenarios

Global and regional climate models simulate future climate at a relatively large scale (50-200km). Hence, small-scale features, such as elevation changes and local winds, are often neglected. However, these features also have a large influence on local climate. Statistical downscaling aims at integrating small and large scale factors into future climate prediction (Giorgi et al., 2001). Because of the importance of localized information for hydrological modeling, statistical downscaling of meteorological variables is an indispensable step to predict the hydrological impacts of climate change (Wilby et al., 1999). Many techniques have been proposed to downscale the output from global and regional climate models. They have been reviewed by Fowler et al. (2007a) and Prudhomme et al. (2002), among others. Among these various methods, three methods are highlighted here:

- Delta change approach: In this case, the measurements are modified to produce the future time series based on climate model indications (Fowler et al., 2007a). For example, monthly average temperature of the control and the future simulations are compared. This difference is then added to the measured temperature. For precipitation, the ratio between the average control and simulation is used to keep the frequency and duration of the dry/wet day series. The delta change method can

be expressed as follows:

$$\Delta_T = T_{RCM} - T_{RCM,CTL} \qquad\qquad \Delta_P = \frac{P_{RCM}}{P_{RCM,CTL}} \qquad (1)$$

$$T_{new} = T_{mes} + \Delta_T \qquad\qquad P_{new} = P_{mes} * \Delta_P \qquad (2)$$

in which T and P are temperature and precipitation. RCM, CTL is the control run in the current climate, RCM is the modeled future climate (a GCM could also be used), and mes is related to the measurements. Δ_T and Δ_P are calculated for each month. This statistical method is commonly used because of its simplicity. However, it does not allow for changes in variability. In addition, dry and wet days series are strictly identical in future and current climate (Goderniaux et al., 2011).

- Bias-correction and quantile-mapping approach: These methods use the outputs of GCMs or RCMs, the bias of which is corrected based on the difference between the measured times series and the control simulation of the climate model. In its more simple form, the difference in monthly average is used to modify the future time series (Fowler et al., 2007b). More complex approaches, for example based on the differences in the frequency distribution of one or more climatic variables, are possible (e.g. Kallache et al., 2011). This subset of bias-corrected approaches are more commonly called quantile-mapping approaches (Li et al., 2009) and are discussed further in Section 5. Bias-corrected methods and quantile-mapping methods are relatively simple to implement. In addition, changes in variability, such as an increase in intense rain events, are possible. However, the bias is assumed to be identical in present and future climate, which might not be true (Buser et al., 2010). Moreover, the physical consistency of the climate variables is not insured by bias-correction methods. Indeed, GCMs are physically-based models which create spatio-temporal fields consistent with atmospheric conservation laws. Bias correction methods alter these fields and violate conservation principles, in contrast to dynamical downscaling (Ehret et al., 2012).

- Weather generator: A weather generator is a model which extracts statistical properties from climatic data to create new time series with similar statistics. Statistical methods used to produce new time series differ greatly between weather generators. For example, the LARS weather generators (Racsko et al., 1991) is based on semi-empirical distributions of measured meteorological variables. Contrastingly, the RainSim weather generator (Burton et al., 2008; Kilsby et al., 2007) is based on Neyman-Scott rectangular process (Section 8.2). When weather generators are utilized to downscale climate scenarios, change factors are first extracted from the GCM or the RCM by comparing control and future simulations. These change factors are then used to modify the present statistics of the weather generator. Afterward, the weather generator creates meteorological time series representing the future (predicted) climate (Kilsby et al., 2007). Examples of statistical properties include the monthly mean and variance of precipitation, 1-day auto-correlation, and dry spell length. Weather generators are more complex to implement than other downscaling methods. Nevertheless, they are more flexible and can produce multiple time series for a given climate. Hence, weather variations can be better taken into account.

Any of these three methods can directly be used to downscale GCM outputs (e.g., Jyrkama et al., 2007). Otherwise, RCMs can be used first as dynamical downscaling step and a particular statistical method can be used as a second step (Goderniaux et al., 2011). Comparisons between downscaling methods have not found one method to be definitively superior to the others (Seguí et al., 2010). However, stochastic methods based on weather generators are often considered advantageous (Goderniaux et al., 2011; Holman et al., 2009) as they consider natural climate variability.

3   Hydrological modeling

Hydrological models are essential to the prediction of the hydrological impacts of climate change. In this thesis, integrated hydrological models are used for this purpose. However, many other types of hydrological models are available. This section gives a brief review of the different hydrological model types and their uses in climate-impact studies.

3.1   Types of hydrological models

Hydrological models are simplified representation of the hydrological cycle, which aim at simulating or predicting hydrological processes (Refsgaard, 1996). Hydrological models can be classified according to their integration of spatial information: In lumped models, the catchment is conceptualized as a single unit, while, in distributed models, the catchment is subdivided into different units, either based on topographic sub-catchments or using a computational grid (e.g., Pérez, 2011; Refsgaard, 1996). Semi-distributed models are a compromise between distributed and lumped models (Jajarmizadeh et al., 2012). They account for the spatial distribution of the contributing areas in a simplified manner. For instance, they lump zones with similar characteristics together, using averaged observable physical variables.

Hydrological models can be further classified based on the way they represent hydrological processes. Three types of models can be distinguished: empirical, conceptual, and integrated models (Refsgaard, 1996):

- Empirical models are data-driven and do not include a physical description of the system. They are based on functional relationships between a measurable input variable, such as precipitation, and an output variable, such as run-off. Artificial neural networks are often used for this purpose (Buerger et al., 2007).

- Conceptual models describe water flow and transport using semi-empirical relationships. These relationships are used to route water and solutes between the different storage compartments (e.g., Pérez, 2011).

- Integrated hydrological models, or *pde*-based models (i.e., models based on partial differential equations), aim at representing the surface and sub-surface hydrological processes using physical relationships. The goal is to describe the main hydrological processes using physical laws, which can be mathematically represented in three dimensions (Freeze et al., 1969). In most cases, the Richards' equation is used to

represent sub-surface flow. The shallow water equations are used for surface flow (Maxwell et al., 2014).

These different classes of models have all been used in different studies to predict the hydrological impacts of climate change, as described in the next section.

3.2 Hydrological modeling for climate-impact studies

Hydrological impacts of climate change have been a concern for many decades. The first studies on this subject (Manabe et al., 1975) directly used the outputs from simplified GCMs. However, the low resolution of GCMs, especially of early GCMs [1], hindered the investigation of hydrological impacts of climate change on the watershed scale. Hence, it was proposed to use hydrological models to study climate change impacts (Němec et al., 1982). In this approach, still used today, hydrological models are first calibrated using measured hydrological and meteorological variables. Next, the meteorological time series are modified to account for the predicted climate change (usually using a delta change approach in early studies, Section 2.4). These modified times series are used as model input and outputs from the hydrological model in present and predicted future climates are finally compared.

The first studies using this approach to study climate change impacts focused on surface flow (Green et al., 2011). For instance, early hydrological studies of climate change impacts investigated changes in the water budget in Belgium (Bultot et al., 1988) or run-off in the western United States (Revelle et al., 1983). In Spain, where my case study is situated, hydrological impacts of climate change is of special importance because of the limited water resources (Vargas-Amelin et al., 2014). In this country, one of the first research projects looking into future water resource was conducted by Ayala-Carcedo et al. (1996). They used a regional lumped model to simulate the main Spanish water basins. A mean decrease of 17% in the available surface- and subsurface-water was predicted for Spain (Estrela et al., 2012). Other empirical models, based on artificial neural networks, have been used in northern Spain to study the hydrological impacts of climate change (Buerger et al., 2007). A number of semi-distributed, conceptual models were also used for the same purpose on the national scale (Fernández, 2002; Iglesias et al., 2005). In parallel, similar models were applied on the catchment scale, for example, in the Gallego region (Majone et al., 2012), or in the Ebro basin (Candela et al., 2012; Zambrano-Bigiarini et al., 2010). Conceptual models have also widely been used outside of Spain in climate-impact studies. Examples extend from studies conducted in the Swiss Alps (Schaefli et al., 2007), in Turkey (Albek et al., 2004), or in Denmark (Thodsen, 2007), among other places.

The studies cited above generally neglect groundwater flow, even though aquifers are an important source of drinking water worldwide (Giordano, 2009). The simulation of climate-change effects on groundwater has become an important research topic only in the last decade (Taylor et al., 2013). Generally, groundwater has been shown to be sensitive to climate change (e.g., Döll, 2009). This sensitivity can be estimated from simple statistical relationships, based on measured hydraulic heads and precipitation

---

[1] grid size: about 300 km x 300km

(Barron et al., 2012; Chen et al., 2001, 2004). However, this method is often not precise enough for a quantitative assessment. Therefore, the prediction of climate-change impacts on aquifers is more frequently based on the outputs from a calibrated groundwater model (e.g., MODFLOW, Harbaugh et al., 2000) and an estimation of recharge, based on a simplified water balance. Candela et al. (2009) used this technique in Majorca, Serrat-Capdevila et al. (2007) in Arizona, and Allen et al. (2004) in British Columbia, among many others. Because processes leading to aquifer recharge are very simplified in this type of study, other authors (e.g., Bouraoui et al., 1999; Eckhardt et al., 2003; Jyrkama et al., 2007) have used soil models to improve the prediction of future recharge. However, groundwater flow was not considered or very simplified in these cases.

However, subsurface flow, and feedbacks between surface and subsurface flows, are important in climate-impact studies (Section 3.3). For instance, climate change influences river-groundwater interactions and surface recharge differently (Allen et al., 2004). If these two processes are not simulated explicitly, changes in the water-table depth or in river flow are difficult to estimate accurately. Hence, several authors have recently started modeling surface and subsurface flows as an integrated system. For example, van Roosmalen et al. (2007, 2009) applied a coupled model to a large-scale case study (about 6000 km² in Denmark) to estimate the hydrological effects of climate change. This model, using the MIKE-SHE code, simulated coupled surface and subsurface flow (Henriksen et al., 2003). However, unsaturated flow was based on a simplified water balance method, which is not always valid, especially in cases where the vadose zone is large (Goderniaux, 2011). To improve vadose zone modeling and surface/subsurface exchanges, Maxwell et al. (2008) used an integrated hydrological model (ParFlow, Kollet et al. (2006)) in the Great Plains in USA. There, they studied groundwater dynamics and land-atmosphere interactions in a changing climate. In the Geer basin, in Belgium, Goderniaux (2011) and Goderniaux et al. (2011, 2009) conducted a similar study, aiming at understanding climate change impacts on the hydrology, using HydroGeoSphere. HydroGeoSphere has the capacity to model the unsaturated zone in some detail, using the Richards' equation (Section 4). Hence, climate-change impacts on surface and saturated subsurface flows, as well as unsaturated subsurface flows, can be estimated. Even though other studies have used integrated hydrological models to estimate climate impacts (Davison et al., 2015), their use is still a rare occurrence in climate-impact studies (Goderniaux, 2011). Moreover, most of the applications have been made in humid climate. In the studies addressing hydrological effects of climate change in Mediterranean climate (e.g., Candela et al., 2009), integrated hydrological models were not used.

3.3 Pros and cons of integrated hydrological models

Advantages and limitations of various model types, notably of integrated hydrological models, have been widely discussed in the literature, notably by Beven (1989, 1993, 2002), Gupta et al. (2012), and Todini (2007). It is generally recognized that integrated hydrological models fail to completely integrate the complexity of the hydrological system (e.g., Beven, 1989). Their conceptualization are based on physical principles, as outlined by the blueprint of Freeze et al. (1969). However, the validity of the physical relationships used to describe the hydrological system is questionable when local heterogeneity is

neglected, and "effective" parameters are applied to a model with coarse resolution. Vogel et al. (2008) and Downer et al. (2004), among others, have noted that the hypotheses underlying the Richards' equation require a high spatial resolution, which is not generally achievable by integrated hydrological models. Moreover, even if the model grid would be sufficiently fine to represent the relevant heterogeneity, measurements of subsurface parameters on this scale would be practically impossible. Hence, in integrated hydrological models, Richards' equation is used in most cases as an effective law to model unsaturated flow, and not as a fundamental soil-physics law (e.g., Pérez, 2011). Furthermore, boundary conditions and initial states of the catchment are not precisely known even though they influence the model outputs. Hence, model calibration is still needed to apply an integrated hydrological model on the catchment scale. The calibration process is, however, hindered by the long simulation time associated with this category of models (e.g., Goderniaux et al., 2009), and by problems of parameter identifiability and non-uniqueness (Beven, 2002).

Nonetheless, integrated hydrological models have various advantages for climate-impact studies. Firstly, changes in surface and subsurface flows can be studied simultaneously. The consideration of surface and subsurface water bodies, and their interactions, is important to efficiently manage water resource. In addition, integrated hydrological models simulate feedbacks between different hydrological processes explicitly. Infiltration, exfiltration, run-off, and evapotranspiration are all represented. This is important as climate change influences these fluxes differently (Goderniaux et al., 2009). For example, the water table might be more influenced by changes in river levels than by changes in surface recharge (Allen et al., 2004). These differences might be impossible to represent without a distributed representation of surface/subsurface feed-backs. In addition, integrated hydrological models can simultaneously use more types of data in the calibration (discharge, hydraulic heads, evaporation measurement, etc.) and conceptualization process (irrigation volume, surface elevation, geological information, etc.) than simpler models. Accounting for diverse datasets might improve the simulation of hydrological processes on the catchment scale. Finally, even if integrated hydrological models are not entirely physically-based, they still rely less on empirically-based relationships than conceptual models. Moreover, a large number of scaling and simplification in integrated hydrological models is the result of subsurface heterogeneity, which can probably be considered constant in future and present climate. On the contrary, simplifications in conceptual models are more complicated and are often a mixed consequence of soil heterogeneity and climatic drivers, which will vary in future climate.

References

Albek, M., Ü.B. Ögütveren, and E. Albek (2004). "Hydrological modeling of Seydi Suyu watershed (Turkey) with HSPF". In: *J. Hydrol.* 285, pp. 260–271.

Allen, D.M., D.C. Mackie, and M.Wei (2004). "Groundwater and climate change: a sensitivity analysis for the Grand Forks aquifer, southern British Columbia, Canada". In: *Hydrogeol. J.* 12, pp. 270–290.

Ayala-Carcedo, F.J. and A. Iglesias López (1996). "Impactos del cambio climático sobre los recursos hídricos, el diseño y la planificación hidrológica en la España peninsular". In: *Tecnoambiente, (in Spanish)* 64, pp. 43–48.

Barron, O.V., R.S. Crosbie, W.R. Dawes, S.P. Charles, T. Picket, and M.J. Donn (2012). "Climatic controls on diffuse groundwater recharge across Australia". In: *Hydrol. Earth Syst. Sc.* 16, pp. 4557–4570.

Bechtel, S. E. and R. L. Lowe (2015). "Fluid mechanics". In: *Fundamentals of continuum mechanics*. Ed. by S.E. Bechtel and R.L. Lowe. Elsevier Academic Press, San Diego, USA, pp. 197–214.

Beven, K. (1989). "Changing ideas in hydrology - The case of physically-based models". In: *J. Hydrol.* 105, pp. 157–172.

— (1993). "Prophecy, reality and uncertainty in distributed hydrological modelling". In: *Adv. Water Resour.* 16, pp. 41–51.

— (2002). "Towards a coherent philosophy for modelling the environment". In: *P. Roy. Soc. Lond. A Mat.* 458, pp. 2465–2484.

Bielsa, J. and I. Cazcarro (2015). "Implementing integrated water resources management in the Ebro river basin: From theory to facts". In: *Sustainability* 7, pp. 441–464.

Blasone, R.-S., H. Madsenand, and D. Rosbjerg (2008). "Uncertainty assessment of integrated distributed hydrological models using GLUE with Markov chain Monte Carlo sampling". In: *J. Hydrol.* 353, pp. 18–32.

Bonaventura, L. (2004). *An introduction to semi-Lagrangian methods for geophysical scale flows*. Applied Mathematics Laboratory, Department of Mathematics, Politecnico di Milano.

Bouraoui, F., G. Vachaud, L. Li, H. Le Treut, and T. Chen (1999). "Evaluation of the impact of climate changes on water storage and groundwater recharge at the watershed scale". In: *Clim. Dyn.* 15, pp. 153–161.

Bovolo, C.I., S. Blenkinsop, B. Majone, M. Zambrano-Bigiarini, H.J. Fowler, A. Bellin, A. Burton, D. Barceló, P. Grathwohl, and J.A.C. Barth (2010). "Climate change, water resources and pollution in the Ebro Basin: Towards an integrated approach". In: *The Ebro river basin*. Ed. by D. Barceló and M. Petrovic. Springer-Verlag.

Bralower, T. and D. Bice (2015). *Earth in the Future, available at www.e-education.psu.edu*. The Pennsylvania State University.

Buerger, C.M., O. Kolditz, H.J. Fowler, and S. Blenkinsop (2007). "Future climate scenarios and rainfall-runoff modelling in the Upper Gallego catchment (Spain)". In: *Environ. Pollut.* 148, pp. 842–854.

Bultot, F., A. Coppens, G. Dupriez, D. Gellens, and F. Meulenberghs (1988). "Repercussions of a CO_2 doubling on the water cycle and on the water balance - a case study for Belgium". In: *J. Hydrol.* 99, pp. 319–347.

Burton, A., C.G. Kilsby, H. Fowler, P. S. P. Cowpertwait, and P.E. O'Conell (2008). "RainSim: A spatial-temporal stochastic rainfall modelling system". In: *Environ. Model. Softw.* 23, pp. 1356–1369.

Buser, C., H. Künsch, and A. Weber (2010). "Biases and uncertainty in climate projections". In: *Scand. J. Stat.* 37, pp. 179–199.

Candela, L., K. Tamoh, G. Olivares, and M. Gomez (2012). "Modelling impacts of climate change on water resources in ungauged and data-scarce watersheds. Application to the Siurana catchment (NE Spain)". In: *Sci. Total Environ.* 440, pp. 253–260.

Candela, L., W. von Igel, F.J. Elorza, and G. Aronica (2009). "Impact assessment of combined climate and management scenarios on groundwater resources and associated wetland (Majorca, Spain)". In: *J. Hydrol.* 376, pp. 510–527.

Chen, Z., S.E. Grasby, and K.G. Osadetz (2001). "Predicting average annual groundwater levels from climatic variables: An empirical model". In: *J. Hydrol.* 260, pp. 102–117.

— (2004). "Relation between climate variability and groundwater levels in the upper carbonate aquifer, southern Manitoba, Canada". In: *J. Hydrol.* 290, pp. 43–62.

Christensen, J.H, B. Hewitson, A. Busuioc, A. Chen, X. Gao, I. Held, R. Jones, R.K. Kolli, W.-T. Kwon, R. Laprise, V. Magana Rueda, L. Mearns, C.G. Menéndez, J. Räisänen, A. Rinke, A. Sarr, and P. Whetton (2007). "Regional climate projection". In: *Contribution of working group I to the fourth assessment report of the Intergovernmental Panel on Climate Change*. Ed. by S. Solomon, D. Qin, M. Manning, Z. Chen, M. Marquis, K.B. Averyt, M. Tignor, and H.L. Miller. Cambridge University Press, Cambridge, United Kingdom and New York, NY, USA.

Dams, J., J. Nossent, T. Belay Senbeta, P. Willems, and O. Batelaan (2015). "Multi-model approach to assess the impact of climate change on runoff, in press". In: *J. Hydrol.* X, pp. X–X.

Davison, J. H., H. Hwang, E. A. Sudicky, and J. C. Lin (2015). "Coupled atmospheric, land surface, and subsurface modeling: Exploring water and energy feedbacks in three-dimensions". In: *Adv. Water Resour., submitted.*

Déqué, M., D.P. Rowell, D. Lüthi, F. Giorgi, J.H. Christensen, B. Rockel, D. Jacob, E. Kjellström, M. Castro, and B. Hurk (2007). "An intercomparison of regional climate simulations for Europe: assessing uncertainties in model projections". In: *Clim. Change* 81, pp. 53–70.

Dickinson, R.E., R.M. Errico, F. Giorgi, and G.T. Bates (1989). "A regional climate model for the western United States". In: *Clim. Change* 15, pp. 383–422.

Döll, Petra (2009). "Vulnerability to the impact of climate change on renewable groundwater resources: a global-scale assessment". In: *Environ. Res. Lett.* 4, p. 035006.

Downer, C.W. and F.L. Ogden (2004). "Appropriate vertical discretization of Richards equation for two-dimensional watershed-scale modelling". In: *Hydrol. Process.* 18, pp. 1–22.

Eckhardt, K. and U. Ulbrich (2003). "Potential impacts of climate change on groundwater recharge and streamflow in a central European low mountain range". In: *J. Hydrol.* 284, pp. 244–252.

Ehret, U., E. Zeh, V. Wulfmeyer, K. Warrach-Sagi, and J. Liebert (2012). "Should we apply bias correction to global and regional climate model data?" In: *Hydrol. Earth Syst. Sc.* 16, pp. 3391–3404.

Estrela, T., M.A Pérez-Martin, and E. Vargas (2012). "Impact of climate change on water resource in Spain". In: *Hydrolog. Sci. J.* 57, pp. 1154–1167.

Fernández, P. (2002). "Estudio del impacto del cambio climático sobre los recursos hídricos. Aplicación en diecinueve cuencas en España." PhD thesis. (in Spanish), Universidad Politécnica de Madrid (Spain).

Fowler, H., S. Blenkinsop, and C. Tebaldi (2007a). "Linking climate change modelling to impacts studies: recent advances in downscaling techniques for hydrological modelling". In: *Int. J. Climatol.* 27.

Fowler, H. and C. Kilsby (2007b). "Using regional climate model data to simulate historical and future river flows in northwest England". In: *Clim. Change* 80, pp. 337–367.

Freeze, R. A. and R.L. Harlan (1969). "Blueprint for a physically-based digitally simulated hydrologic response model". In: *J. Hydrol.* 9, pp. 237–258.

Ghosh, S. and C. Misra (2010). "Assessing hydrological impacts of climate change: modeling techniques and challenges". In: *Open Hydrol. J.* 4, pp. 115–121.

Gil, M., A. Garrido, and A. Gómez-Ramos (2011). "Economic analysis of drought risk: An application for irrigated agriculture in Spain". In: *Agr. Water Manage.* 98, pp. 823–833.

Giordano, M. (2009). "Global Groundwater? Issues and Solutions". In: *Annu. Rev. of Environ. Res.* 34, pp. 153–178.

Giorgi, F., B. Hewitson, J. Christensen, M. Hulme, H. Von Storch, P. Whetton, R. Jones, L. Mearns, and C. Fu (2001). "Regional climate information, evaluation, and projections". In: *Contribution of working group I to the third assessment report of the Intergovernmental Panel on Climate Change.* Ed. by J.T. Houghton, Y. Ding, D.J. Griggs, M. Noguer, P.J. van der Linden, X. Dai, K. Maskell, and C.A. Johnson. Cambridge University Press, Cambridge, United Kingdom and New York, NY, USA.

Giorgi, F., M.-R. Marinucci, and G. Visconti (1990). "Use of a limited-area model nested in a general circulation model for regional climate simulation over Europe". In: *J. Geophys. Res. Atmos.* 95, pp. 18413–18431.

Goderniaux, P. (2011). "Impacts of climate change on groundwater reserves". PhD thesis. University of Liège.

Goderniaux, P., S. Brouyère, S. Blenkinsop, A. Burton, H.J. Fowler, P. Orban, and A. Dassargues (2011). "Modeling climate change impacts on groundwater resources using transient stochastic climatic scenarios". In: *Water Resour. Res.* 47, W12516.

Goderniaux, P., S. Brouyère, H.J. Fowler, S. Blenkinsop, R. Therrien, P. Orban, and A. Dassargues (2009). "Large scale surface-subsurface hydrological model to assess climate change impacts on groundwater reserves". In: *J. Hydrol.* 373, pp. 122–138.

Goosse, H., P.Y. Barriat, W. Lefebvre, M.F. Loutre, and V. Zunz (2015). *Introduction to climate dynamics and climate modeling.* Cambridge University Press.

Green, T.R., M. Taniguchi, H. Kooi, J.J. Gurdak, D.M. Allen, K. M. Hiscock, H. Treidel, and A.Aurel (2011). "Beneath the surface of global change: Impacts of climate change on groundwater". In: *J. Hydrol.* 405, pp. 532–560.

Gupta, H., M. Clark, J. Vrugt, G. Abramowitz, and M. Ye (2012). "Towards a comprehensive assessment of model structural adequacy". In: *Water Resour. Res.* 48, pp. 1–2.

Harbaugh, A.W., E.R. Banta, M.C. Hill, and M.G. McDonald (2000). *MODFLOW-2000, The U.S. Geological Survey modular groundwater model - User guide to modularization concept and the groundwater flow process*. U.S. Geological Survey.

Henriksen, H. J., L. Troldborg, P. Nyegaard, T.O. Sonnenborg, J.C. Refsgaard, and B. Madsen (2003). "Methodology for construction, calibration and validation of a national hydrological model for Denmark". In: *J. Hydrol.* 280, pp. 52–71.

Herrera, S., L. Fita, J. Fernández, and J. M. Gutiérrez (2010). "Evaluation of the mean and extreme precipitation regimes from the ENSEMBLES regional climate multimodel simulations over Spain". In: *J. Geophys. Res.* 115, p. D21117.

Holman, I.P., D. Tascone, and T.M. Hess (2009). "A comparison of stochastic and deterministic downscaling methods for modelling potential groundwater recharge under climate change in East Anglia, UK: implications for groundwater resource management". In: *Hydrogeol. J.* 17, pp. 1629–1641.

Iglesias, A., T. Estrela, F. Gallart, J. A. Alvarez, L.H. Barrios, and M.A. Pérez Martín (2005). "Impacts on hydric resource". In: *A preliminary general assessment of the impacts in Spain due to the effects of climate change*. Ed. by José Manuel Moreno-Rodríguez. Ministerio de medio ambiente. Chap. 7.

Jajarmizadeh, M., S. Harun, and M. Salarpour (2012). "A review on theoretical consideration and types of models in hydrology". In: *J. Environ. Sci. Technol.* 5, pp. 249–261.

Jiang, T., Y. D. Chen, C. Xu, X. Chen, X. Chen, and V. P. Singh (2007). "Comparison of hydrological impacts of climate change simulated by six hydrological models in the Dongjiang Basin, South China". In: *J. Hydrol.* 336, pp. 316–333.

Jyrkama, M.I. and J.F. Sykes (2007). "The impact of climate change on spatially varying groundwater recharge in the grand river watershed (Ontario)". In: *J.Hydrol.* 338, pp. 237–250.

Kallache, M., M. Vrac, P. Naveau, and Michelangeli P.-A. (2011). "Nonstationary probabilistic downscaling of extreme precipitation". In: *J. Geophys. Res.-Atmos.* 116.

Kilsby, C.G., P.D. Jonesand A. Burton, A.C. Ford, H.J. Fowler, C. Harpham, P. James, A. Smith, and R.L. Wilby (2007). "A daily weather generator for use in climate change studies". In: *Environ. Model. Softw.* 22, pp. 1705–1719.

Kim, B. S., I. H. Park, and S. R. Ha (2014). "Future projection of droughts over South Korea using representative concentration pathways (PCA)". In: *Terr. Atmos. Ocean Sci.* 25, pp. 673–688.

Kirono, D.G., D.M. Kent, K. Hennessy, and F. Mpelasoka (2011). "Characteristics of Australian droughts under enhanced greenhouse conditions: Results from 14 global climate models". In: *J. Arid Environ.* 75, pp. 566–575.

Kollet, S. and R. Maxwell (2006). "Integrated surface groundwater flow modeling: A free surface overland flow boundary condition in a parallel groundwater flow model". In: *Adv. Water Resour.* 29, pp. 945–958.

Leng, G., Q. Tang, and S. Rayburg (2015). "Climate change impacts on meteorological, agricultural and hydrological droughts in China". In: *Global Planet. Change* 126, pp. 23–34.

Li, H., J. Sheffield, and E. Wood (2009). "Bias correction of monthly precipitation and temperature fields from Intergovernmental Panel on Climate Change AR4 models using equidistant quantile matching". In: *J. Geophys. Res.* 115, p. D10101.

Linden, P. van der and J. Mitchell (2009). "Climate change and its impact: Summary of research and results from the ENSEMBLES project". In: *Met Office Hadley Centre, UK* 1, pp. 1–160.

Majone, B., I. Bovolo, Bellin, S. Blenkinsop, and H. J. Fowler (2012). "Modeling the impacts of future climate change on water resources for the Gallego river basin (Spain)". In: *Water Resour. Res.* 48, W01512.

Manabe, S. and R. Wetherald (1975). "The effects of doubling CO_2 concentration on the climate of a general circulation model". In: *J. Atmos. Sci.* 32, pp. 3–15.

Masud, M.B., M.N. Khaliq, and H.S. Wheater (2015). "Analysis of meteorological droughts for the Saskatchewan River Basin using univariate and bivariate approaches". In: *J. Hydrol.* 522, pp. 452–466.

Maxwell, R. and S. Kollet (2008). "Interdependence of groundwater dynamics and land energy feedbacks under climate change". In: *Nat. Geosci.* 1, pp. 655–659.

Maxwell, R., M. Putti, S. Meyerhoff, J.-O. Delfs, I.M. Ferguson, V. Ivanov, J. Kim, O. Kolditz, S.J. Kollet, M. Kumar, S. Lopez, J. Niu, C. Paniconi, Y.-J. Park, M.S. Phanikumar, C. Shen, E.A. Sudicky, and M. Sulis (2014). "Surface-subsurface model intercomparison: A first set of benchmark results to diagnose integrated hydrology and feedbacks". In: *Water Resour. Res.* 50, pp. 1531–1549.

Meehl, G.A., T.F. Stocker, W.D. Collins, P. Friedlingstein, A.T. Gaye, J.M. Gregory, A. Kitoh, R. Knutti, J.M. Murphy, A. Noda, S.C.B. Raper, I.G. Watterson, A.J. Weaver, and Z.C. Zhao (2007). "Global climate projections". In: *The physical science basis. Contribution of working group I to the fourth assessment report of the Intergovernmental Panel on Climate Change.* Ed. by S. Solomon, D. Qin, M. Manning, Z. Chen, M. Marquis, K.B. Averyt, M. Tignor, and H.L. Miller. Cambridge University Press, Cambridge, United Kingdom and New York, NY, USA.

Meinshausen, M., S. J. Smith, K. Calvin, J. S. Daniel, M. L. T. Kainuma, J-F. Lamarque, K. Matsumoto, S. A. Montzka, S. C. B. Raper, K. Riahi, A. Thomson, G. J. M. Velders, and D.P. P. van Vuuren (2011). "The RCP greenhouse gas concentrations and their extensions from 1765 to 2300". In: *Clim. Change* 109, pp. 213–241.

Merchán, D., J. Causapé, and R. Abrahao (2013). "Impact of irrigation implementation on hydrology and water quality in a small agricultural bassin in Spain". In: *Hydrolog. Sci. J.* 58, pp. 1400–1413.

Milano, M., D. Ruelland, A. Dezetter, J. Fabre, S. Ardoin-Bardin, and E. Servat (2013). "Modeling the current and future capacity of water resources to meet water demands in the Ebro basin". In: *J. Hydrol.* 500, pp. 114–126.

Milly, P.C. and A.B Shmakin (2002). "Global modeling of land water and energy balances. Part I: the land dynamics (LaD) model". In: *J. Hydrometeorol.* 3, pp. 283–299.

Mishra, A. and V. Singh (2010). "A review of drought concept". In: *J. Hydrol.* 391, pp. 202–216.

Nakićenović, N., O. Davidson, G. Davis, A. Grübler, T. Kram, E. Lebre La Rovere, B. Metz and T. Morita, W. Pepper, H. Pitcher, A. Sankovski, P. Shukla, R. Swart, R. Watson, and Z. Dadi (2000). "Emission scenarios - Summary for policymakers". In: *Intergovernemental Panel on Climate Change - Special Report.*

Němec, J. and J. Schaake (1982). "Sensitivity of water resource systems to climate variation". In: *Hydrolog. Sci. J.* 27, pp. 327–343.

Park, C.-H., H.-R. Byun, and and B.-R. Lee R. Deo (2015). "Drought prediction till 2100 under RCP 8.5 climate change scenarios for Korea". In: *J. Hydrol.* 526, pp. 221–230.

Pérez, A.J. (2011). "Physics-based numerical modeling of surface-groundwater flow and transport at catchment scale". PhD thesis. University of Tübingen.

Pérez, A.J., R. Abrahao, J. Causapé, O.A. Cirpka, and C.M. Bürger (2011). "Simulating the transition of a semi-arid rainfed catchment towards irrigation agriculture". In: *J. Hydrol.* 409, pp. 663–681.

Prudhomme, C., N. Reynard, and S. Crooks (2002). "Downscaling of global climate models for flood frequency analysis: where are we now?" In: *Hydrol. Process.* 16, pp. 1137–1150.

Racsko, P., L. Szeidl, and M. Semenov (1991). "A serial approach to local stochastic weather model". In: *Ecol. Model.* 57, pp. 27–41.

Randall, D. (2010). "The evolution of complexity in general circulation models". In: *The development of atmospheric general circulation models: Complexity, synthesis, and computation.* Ed. by W. Schubert L. Donner and R. Somerville. Cambridge University Press. Chap. 10.

Randall, D., R.A. Wood, S. Bony, R. Colman, T. Fichefet, J. Fyfe, V. Kattsov, A. Pitman, J. Shukla, J. Srinivasan, R.J. Stouffer, A. Sumi, and K.E. Taylor (2007). "Climate models and their evaluation". In: *Contribution of working group I to the fourth assessment report of the Intergovernmental Panel on Climate Change.* Ed. by S. Solomon, D. Qin, M. Manning, Z. Chen, M. Marquis, K.B. Averyt, M. Tignor, and H.L. Miller. Cambridge University Press, Cambridge, United Kingdom and New York, NY, USA.

Refsgaard, J.C. (1996). "Terminology, modelling protocols and classification of hydrological model codes". In: *Distributed hydrological modelling*. Ed. by M. Abbott and J.C. Refsgaard. Kluwer Academic Publishers.

Revelle, R. and P. Waggoner (1983). "Effects of a carbon dioxide-induced climatic change on water supplied in the western United States". In: *Changing climate: report of the carbon dioxide assessment committee*. The national academies press.

Roeckner, E., G. Bäuml, L. Bonaventura, R. Brokopf, M. Esch, M. Giorgetta, S. Hagemann, I. Kirchner, L. Kornblueh, E. Manzini, A. Rhodin, U. Schlese, U. Schulzweida, and A. Tompkins (2003). *The atmospheric general circulation model ECHAM5 Part 1-Model description*. Max Planck Institute for Meteorology.

Sánchez, E., C. Gallardo, M. Gaertner, A. Arribas, and M. Castro (2004). "Future climate extreme events in the Mediterranean simulated by a regional climate model: A first approach". In: *Global Planet. Change* 44, pp. 163–180.

Schaefli, B., B. Hingray, and A. Musy (2007). "Climate change and hydropower production in the Swiss Alps: Quantification of potential impacts and related modelling uncertainties". In: *Hydrol. Earth Syst. Sc.* 11, pp. 1191–1205.

Seguí, P. Quintana, A. Ribes, E. Martin, F. Habets, and J. Boé (2010). "Comparison of three downscaling methods in simulating the impact of climate change on the hydrology of Mediterranean basins". In: *J. Hydrol.* 383, pp. 111–124.

Serrat-Capdevila, A., J. Valdés, J. González Pérez, K. Baird, L. Mata, and T. Maddock (2007). "Modeling climate change impacts, and uncertainty, on the hydrology of a riparian system: The San Pedro Basin (Arizona/Sonora)". In: *J. Hydrol.* 347, pp. 48–66.

Smagorinsky, J., S. Manabe, and J. Leith Holloway (1965). "Numerical results from a nine-level general circulation model of the atmosphere". In: *Mon. Weather Rev.* Pp. 727–768.

Stocker, T.F., D. Qin, G.-K. Plattner, M. Tignor, S.K. Allen, J. Boschung, A. Nauels, Y. Xia, V. Bex, and P.M. Midgley (2013). *The physical science basis. contribution of working group I to the fifth assessment report of the Intergovernmental Panel on Climate Change*. Cambridge University Press, Cambridge, United Kingdom and New York, NY, USA.

Taylor, R.G., B. Scanlon, P. Döll, M. Rodell, R. van Beek, and Y. Wada (2013). "Ground water and climate change". In: *Nat. Clim. Change* 3, pp. 322–329.

Thodsen, H. (2007). "The influence of climate change on stream flow in Danish rivers". In: *J. Hydrol.* 333, pp. 226–238.

Todini, E. (2007). "Hydrological catchment modelling: past, present, and future". In: *Hydrol. Earth Syst. Sc.* 11, pp. 468–482.

Tue, V. M., S. V. Raghavan, P.M. Minh, and L. Shie-Yui (2015). "Investigating drought over the Central Highland, Vietnam, using regional climate models". In: *J. Hydrol.* 526, pp. 265–273.

van Roosmalen, L., B.S.B. Christensen, and T.O. Sonnenborg (2007). "Regional differences in climate change impacts on groundwater and stream discharge in Denmark". In: *Vadose Zone J.* 6, pp. 554–571.

van Roosmalen, L., T.O. Sonnenborg, and K.H. Jensen (2009). "Impact of climate and land use change on the hydrology of a large-scale agricultural catchment". In: *Water Resour. Res.* 45.7, W00A15.

Vargas-Amelin, E. and P. Pindado (2014). "The challenge of climate change in Spain: Water resources, agriculture and land." In: *J. Hydrol.* 518, pp. 243–249.

Vicente-Serrano, M.S., S. Beguería, and J. I. López-Moreno (2009). "A multiscalar drought index sensitive to global warming: The standardized precipitation evapotranspiration index". In: *J. Climate* 23, pp. 1696–1718.

Vogel, H.J. and O. Ippisch (2008). "Estimation of a critical spatial discretization limit for solving Richards equation at large scales". In: *Vadose Zone J.* 7, pp. 112–114.

Vuuren, D. P. van, J. Edmonds, M. Kainuma, K. Riahi, A. Thomson, K. Hibbard, and T. Kram G.C. Hurtt, V. Krey, J.-F. Lamarque, T. Masui, M. Meinshausen, N. Nakićenović, S.J. Smith, and S.K Rose (2011). "The representative concentration pathways: an overview". In: *Clim. Change* 109, pp. 5–31.

Wilby, R., L. Hay, and G. Leavesley (1999). "A comparison of downscaled and raw GCM output: Implications for climate change scenarios in the San Juan River basin, Colorado". In: *J. Hydrol.* 225, pp. 67–91.

Wood, S.E, S.E Leung, V. Sridhar, and D. Plettenmaier (2004). "Hydrological implications of dynamical and statistical appraches to downscaling climate model outputs". In: *Clim. change* 62, pp. 189–216.

Zambrano-Bigiarini, M., B. Majone, A. Bellin, C. I. Bovolo, S. Blenkinsop, and H.J Fowler (2010). "Hydrological impact of climate change on the Ebro river basin". In: *The Ebro river basin.* Ed. by D. Barceló and M. Petrovic. Springer-Verlag.

Zarch, M.A.A., B. Sivakumar, and A. Sharma (2015). "Droughts in a warming climate: A global assessment of standardized precipitation index (SPI) and reconnaissance drought index (RDI)". In: *J. Hydrol.* 526, pp. 183–195.

4   First publication

Title

Efficient calibration of a distributed *pde*-based hydrological model using grid coarsening

Journal

Journal of Hydrology (volume 519, pages 3290-3304)

Year

2014

Highlights

- A method is developed to reduce calibration time in integrated (or *pde*-based) hydrological models.

- Grids of various spatial resolutions are used for the calibration.

- Parameter transfers between coarse and fine grids are established and validated.

- The calibration method is applied successfully to the Lerma catchment in north-east Spain.

Contents lists available at ScienceDirect

Journal of Hydrology
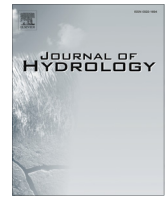
Efficient calibration of a distributed *pde*-based hydrological model using grid coarsening

D. von Gunten [a], T. Wöhling [a,c], C. Haslauer [a], D. Merchán [b], J. Causapé [b], O.A. Cirpka [a,*]

[a] *University of Tübingen, Center for Applied Geoscience, Hölderlinstr. 12, 72076 Tübingen, Germany*
[b] *Geological Survey of Spain IGME, C/Manuel Lasala no. 44, 9B, Zaragoza 50006, Spain*
[c] *Lincoln Agritech Ltd., Ruakura Research Centre, Hamilton, New Zealand*

ARTICLE INFO

SUMMARY

Partial-differential-equation based integrated hydrological models are now regularly used at catchment scale. They rely on the shallow water equations for surface flow and on the Richards' equations for subsurface flow, allowing a spatially explicit representation of properties and states. However, these models usually come at high computational costs, which limit their accessibility to state-of-the-art methods of parameter estimation and uncertainty quantification, because these methods require a large number of model evaluations. In this study, we present an efficient model calibration strategy, based on a hierarchy of grid resolutions, each of them resolving the same zonation of subsurface and land-surface units. We first analyze which model outputs show the highest similarities between the original model and two differently coarsened grids. Then we calibrate the coarser models by comparing these similar outputs to the measurements. We finish the calibration using the fully resolved model, taking the result of the preliminary calibration as starting point. We apply the proposed approach to the well monitored Lerma catchment in North-East Spain, using the model HydroGeoSphere. The original model grid with 80,000 finite elements was complemented with two other model variants with approximately 16,000 and 10,000 elements, respectively. Comparing the model results for these different grids, we observe differences in peak discharge, evapotranspiration, and near-surface saturation. Hydraulic heads and low flow, however, are very similar for all tested parameter sets, which allows the use of these variables to calibrate our model. The calibration results are satisfactory and the duration of the calibration has been greatly decreased by using different model grid resolutions.

1. Introduction

Recently, partial-differential-equation (*pde*) based hydrological models, that couple the shallow-water equations for surface flow and the Richards' equations for subsurface flow, have been successfully applied in various settings, from catchment scale (e.g., Condon et al., 2013; Goderniaux et al., 2011; Li et al., 2008; Shao et al., 2013) to continental scale (Lemieux et al., 2008). They are regarded as useful tools to represent hydrological processes, especially when studying spatially distributed surface–subsurface interactions or catchments driven by climatic or irrigation changes (Pérez et al., 2011), two problems difficult to analyze with simpler "bucket"-type models. However, *pde*-based models are usually computationally very demanding (Blasone et al., 2008) and sometimes require days of CPU time for a single forward run (Goderniaux et al., 2009) on a current desktop computer.

As a result, calibration of these models, which typically requires a large number of model evaluations, can be a slow, tedious, and subjective process. To reduce the number of simulations needed, model calibration of *pde*-based models is often limited to a trial-and-error process (e.g., Bonton et al., 2012; Calderhead et al., 2011; Goderniaux et al., 2009; Li et al., 2008; Pérez et al., 2011; Xevi et al., 1997), even though Blasone et al. (2008) and McMichael et al. (2006) have also proposed ensemble-based approaches. In the latter approaches, multiple parameters sets are generated by Monte-Carlo methods and weighted or modified depending on the likelihood of model outcomes in comparison to measurement (Beven and Binley, 1992). However, the large number of simulations needed renders approaches involving Monte-Carlo methods almost impossible for large *pde*-based models because of their long simulation times. The importance of sensitivity analysis to decrease the number of calibration parameters, and thus the required number of simulation runs, has also been recognized (e.g., Muleta and Nicklow, 2005; Christiaens and Feyen,

2002). Nevertheless, even for the most efficient calibration methods available today, the number of simulations needed would still be too large to apply these methods to integrated *pde*-based models. Therefore, model reduction is currently the only feasible option to calibrate such models.

Simulation time is known to greatly depend on spatial discretization (e.g., Vazquez et al., 2002). Typically, finer grids cause a non-linear increase of computational costs compared to coarser ones due to the larger number of unknowns. However, a sufficiently fine mesh is needed to realistically represent the topography of the catchment, which is important to properly simulate run-off, infiltration, and surface–subsurface exchange fluxes, or to characterize zones with large changeability in state variables. Therefore, to trade off model accuracy and simulation time, the spatial discretization should be chosen carefully in distributed models. Various studies have been conducted to find the minimum spatial discretization needed to adequately represent the catchment under consideration (e.g., Bruneau et al., 1995; Carrera-Hernandez et al., 2012; Chaplot, 2014; Chaubey et al., 2005; Cotter et al., 2003; Dutta and Nakayama, 2009; Kuo et al., 1999; Moglen and Hartman, 2001; Molnár and Julien, 2000). In general, the grid cell size must be smaller for catchments with highly uneven relief than for those with smooth topography (Chaplot, 2014). In addition, problems as the modeling of erosion (Hessel, 2005), spatially varying evapotranspiration (Sciuto and Diekkrüger, 2010), or reactive transport (Chaplot, 2005) are more sensitive to grid size than the simulation of hydraulic heads or discharge, especially low flow. The choice of spatial discretization therefore depends also on the simulation objectives (Cotter et al., 2003).

The importance of the resolution of spatial discretization has been recognized before, particularly in studies on reactive transport (Mehl and Hill, 2002). In this field, grid telescoping, i.e., the modeling of a reactive transport problem using two grids, namely a coarse grid representing the whole catchment and a fine one representing the surrounding area of the contaminated plume, is relatively common (Mehl and Hill, 2002; Mehl et al., 2006). However, grid telescoping requires a well defined inner domain of interest and an outer domain from which conditions can be extracted and used as boundary conditions for the inner domain. This is not suitable in all situations, e.g., it cannot be used for large non-point contamination problems, such as agricultural nitrate leaching from cultivated land.

Recently, more attention has been given to the influence of spatial discretization on model calibration of *pde*-based hydrological model. For example, Wildemeersch et al. (2014) analyzed parameter sensitivity, i.e., the influence of model parameters on the simulation output, and the linearized confidence interval for various spatial discretizations. These quantities were found to be very similar for all grid sizes, in this synthetic case study based on a Belgian catchment of approximately 300 km^2.

In the present study, we also focus on the links between model calibration and grid resolution. We propose a methodology to accelerate calibration in fully coupled *pde*-based hydrological models. Our main objective is to reduce simulation time, while obtaining a final model with a precise description of topography. To reach this objective, we vary the resolution of spatial discretization during the calibration. Moreover, we analyze how the changing grid resolution affects the model outcome and test the validity of our method in a case study in North-East Spain.

A prerequisite of the present analysis is that the subsurface structure and land-use at the surface is represented by zonation, which – in principle – is represented on all grid levels. Important questions of coarse-graining fine-scale information onto the resolution scale of larger grids are beyond the scope of the present study. Calibrating systems that account for internal heterogeneity

would require a multi-scale representation of the domain, robust coarse-graining rules, and the provision of fine-scale proxy data used in the calibration, which has been done in conceptual hydrological modeling (Samaniego et al., 2010) but not yet in *pde*-based catchment-scale models.

The remainder of this paper is structured as follows: First, we describe the principles of the proposed calibration method. Then, we present the governing equations of the numerical model HydroGeoSphere (Therrien, 2006), used in this study, and the study area. This is followed by the construction of the conceptual model for the test case. Afterward, we compare the outputs of the model when using different computational grids. Finally, we report the results of the sensitivity analysis and the calibration of our case study. We conclude with an evaluation of our calibration method.

2. Proposed calibration strategy

The proposed method to accelerate calibration utilizes a set of coarser grids on which simulations run faster than on the original fine grid. The coarser grids should be coarse enough to noticeably decrease computation time while capturing enough system behavior to be useful for calibration. We suggest to use two auxiliary grids, a coarse grid and an intermediate one.

The coarse grid is used to largely constrain model parameters in the full parameter space. The model outputs based on simulations using this grid and the fine grid should be comparable but may still show large differences, for example a consistent bias in model prediction along the parameters sets. Model results from simulations with the intermediate grid should be more comparable to those of the fine grid than the coarse-grid results, but differences may prevail. Indeed, if the intermediate grid would yield identical results in comparison to the fine grid, the latter grid would be unnecessary. We will show in the following that, upon grid refinement, hydraulic head and low flow can be adequately represented in a coarse grid while peak flow, evapotranspiration and saturation needs to be modeled on a finer grid, at least in the catchment under consideration in this study.

Conceptually, the proposed calibration method consists of the following seven steps, summarized in Fig. 1:

1. Set up of three computational grids:
   - a fine grid used in the final model,
   - an intermediate grid used to restrict the possible parameter space,
   - and a coarse grid used to estimate the possible parameter space.
2. Systematic comparison of the simulation results using different computational grids.
3. Parameter sensitivity analysis on the intermediate grid.
4. Constraining the feasible parameter space using the coarse grid.
5. Calibration of model parameters on the intermediate grid.
6. Transfer of the model parameters to the fine grid and eventual final parameter adjustments.
7. Model validation and evaluation on the fine grid.

The choice of the discretization for the coarse and intermediate grids depends on the impact of the grid coarsening on the model outputs used for calibration, such as stream flow hydrographs or hydraulic heads. This therefore also depends on catchment characteristics such as the topography or soil-hydraulic parameters. However, the size of the grid cells used in our case study, described in Section 6, may serve as a starting point in other applications. The method can be adapted to use more or less than three grids, depending on the complexity of the problem.
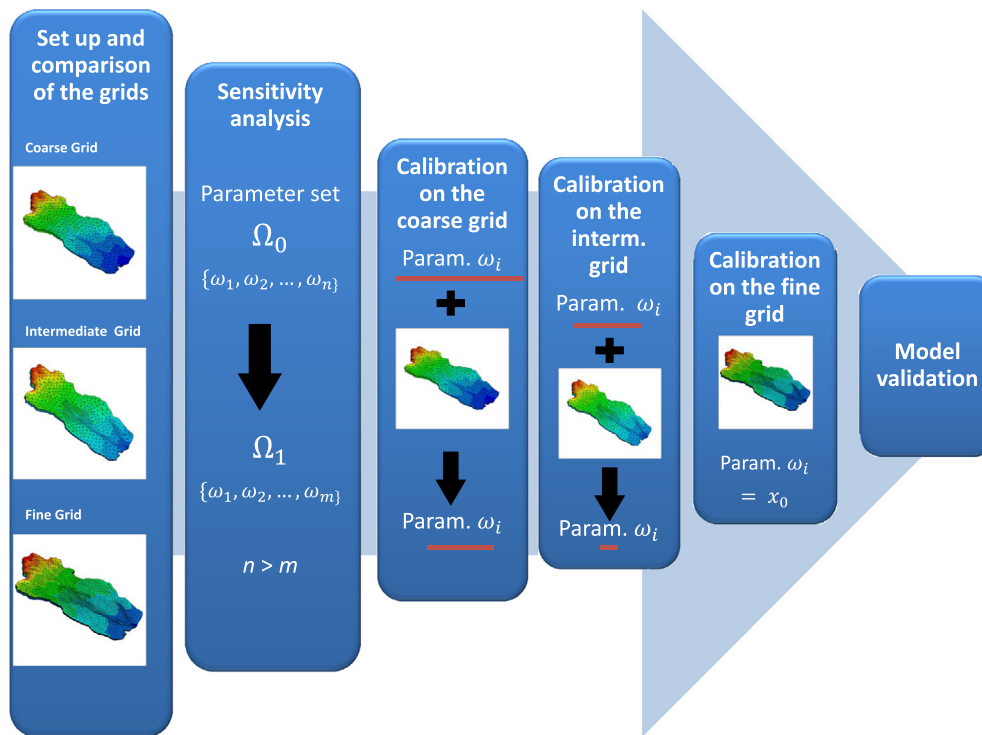
Fig. 1. A summary of the proposed calibration method.

In addition to determining the spatial discretization, the comparison between the grids also gives information about what part of the measured data should be used in each calibration step. It may be beneficial to use only part of the measured data on the coarse or intermediate grids and the whole data set at a later stage, when the fine grid is used. For example, in our case study, low flow is better represented on the coarse grid than peak flow. As a result, low flow can be used earlier during calibration, when the model is run with the coarse grid, while peak flow might be better considered on the fine grid.

3. Mathematical and numerical model

The calibration method described above could be applied to many grid-based distributed hydrological models. In this work, HydroGeoSphere has been selected, as it is a well established fully coupled *pde*-based numerical model used to simulate ground- and surface-flow processes at catchment scale (Therrien, 2006). In this section, the underlying assumptions and equations of HydroGeoSphere are briefly summarized. A more precise description is given by Therrien et al. (2010).

3.1. Subsurface flow

HydroGeoSphere uses the Richards' equation to model variably saturated sub-surface flow in porous media:

$$\frac{\partial(S_w \theta_s)}{\partial t} - \nabla \cdot (\mathbf{K} k_r \nabla h) = \sum \Gamma_{sub} \pm Q \tag{1}$$

in which S_w [–] represents the degree of water saturation, θ_s [–] is the saturated water content, assumed to be identical with the porosity, t [s] is time, $\mathbf{K}$ [m s^{-1}] is the saturated hydraulic conductivity tensor, k_r [–] represents the relative permeability, h [m] denotes the hydraulic head, Γ_{sub} [s^{-1}] is the fluid-exchange rate with the surface or the canopy layer and Q [s^{-1}] denotes the source/sink term from the outside of the domain.

To model the unsaturated flow field, constitutive relationships between hydraulic head, relative permeability and water saturation are needed, in addition to Eq. (1). For this purpose, we use the well-known van Genuchten parameterization (van Genuchten, 1980).

3.2. Surface flow

Surface flow is simulated using the diffusive-wave approximation of the two-dimensional Saint Venant equations (Moussa and Bocquillon, 2000). This approximation neglects local and convective acceleration terms of the momentum equation. It is generally applicable to catchments with a mild slope, thus lacking supercritical flow (Therrien et al., 2010). It can be written as followed:

$$\frac{\partial \phi_s h_s}{\partial t} - \frac{\partial}{\partial x}\left(k_{mx} d \frac{\partial h_s}{\partial x}\right) - \frac{\partial}{\partial y}\left(k_{my} d \frac{\partial h_s}{\partial y}\right) + d\Gamma_s \pm Q_s = 0 \tag{2}$$

where h_s [m] is the surface hydraulic heads, x and y [m] are the spatial coordinates, k_{mx} and k_{my} [m s^{-1}] are the surface conductances of the Manning equation in direction of x and y, d [m] is the water depth, Γ_s [s^{-1}] is the fluid exchange with the subsurface and the canopy layer and Q_s [m s^{-1}] are the external sources or sinks. ϕ_s [–] is the surface "porosity", introduced by Panday and Huyakorn (2004), which accounts for soil depression and obstruction, for example due to vegetation.

3.3. Surface–subsurface coupling

To model exchange between the surface and the subsurface, a Darcy-like equation is used. This so-called dual-node approach models the exchange flux as if a thin layer of a porous material controlled the infiltration/exfiltration of water (Therrien et al., 2010):

$$\Gamma_s d = \frac{k_r K_{zz}}{l_{ex}}(h - h_s) \tag{3}$$

where Γ_s [s^{-1}] represents the water exchange flux, d [m] is the water depth in the surface domain, K_{zz} [m s^{-1}] denotes the saturated vertical conductivity of the porous medium close to the surface, $h - h_s$ [m] is the difference in hydraulic head between the surface and the subsurface nodes, l_{ex} [m] is the coupling length or the depth of the conceptualized layer, separating surface and subsurface, and k_r [–] denotes the relative permeability. When water infiltrates, k_r is the relative permeability of the porous media. If the water is flowing from the subsurface to the surface, k_r depends on the water depth and the obstruction length, i.e., the height of the vegetation or the obstacles which hinder the surface flow (Therrien et al., 2010).

3.4. Interception and evapotranspiration

HydroGeoSphere models interception, transpiration and evaporation separately, following the model of Kristensen and Jensen (1975) (Therrien et al., 2010). Interception is modeled as a reservoir whose size depends on the leaf area index (LAI). This reservoir is filled by rain events and depleted by evaporation. Transpiration is modeled as a function of soil moisture, potential evapotranspiration (PET), evapotranspiration from the canopy layer, root depth, and LAI. Actual evaporation is a function of soil moisture and PET minus transpiration and evaporation from the canopy layer. Transpiration and evaporation are assumed to be zero below a certain saturation limit chosen by calibration, and transpiration stops as well in nearly water-saturated soils. The spatial distribution of evapotranspiration depends on available moisture, and is a function of the root distribution function, which decreases with depth.

4. Study area

We tested the calibration approach at the Lerma catchment (centered at 42.06°N, 1.14°W), which is a sub-catchment of the Arba catchment within the Ebro basin in North-East Spain. The surface catchment area is about 7.3 km^2 large and the altitude ranges between 330 and 490 m.a.s.l. Land use is predominantly agriculture (Pérez et al., 2011). While agriculture depended originally on natural rainfall, about half of the catchment area has been transformed into irrigated crop land starting in April 2006. The volume of irrigation water has changed from 0 m^3/year in 2005 to $2.1 \cdot 10^6$ m^3/year in 2011 (Merchán et al., 2013).

The climate in the Lerma catchment is semi-arid with a mean precipitation of 402 mm/year (2004–2011) and a mean potential evapotranspiration of 1301 mm/year (2004–2011, Merchán et al., 2013). Winter and summer are the driest seasons while spring is the wettest. The geology of the Lerma catchment is composed of two hydrogeologically relevant layers: The glacis layer on top and the so-called "buro" layer underneath. The glacis is made of clastic, permeable, and unconsolidated deposits of Quaternary age while the buro is a Tertiary bedrock made of lutite and marlstones. The glacis forms an aquifer whereas the buro can be considered as an aquitard even though the top first meters are likely weathered and play a role in the water circulation of the catchment. The Lerma soils are thin and composed of inceptisols (Pérez, 2011). No production wells are used in this catchment for groundwater abstraction.

The Lerma catchment has been extensively studied (Abrahao et al., 2011; Merchán et al., 2013; Pérez et al., 2011; Skhiri and Dechimi, 2011; Urdanoz and Aragüés, 2011) and data coverage is comprehensive, especially concerning surface properties and agricultural management. Irrigation data, regularly checked for plausibility, are available (Pérez et al., 2011). Crop type and planting dates are also known. Since 2002, daily meteorological data (precipitation, radiation, relative humidity and wind) have been measured at the station Ejea de los Caballeros, about 5 km away from the center of the Lerma catchment. Topographic information is available in the form of a digital elevation model with a horizontal resolution of 5 m (I.G.N., 2012). Surface flow discharge has been
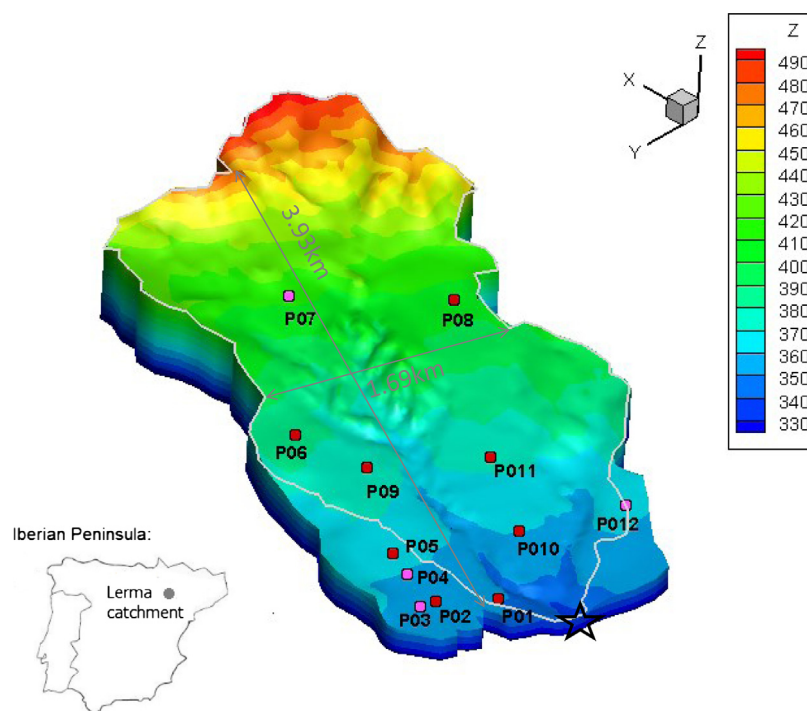

Fig. 2. Altitude of the Lerma catchment (m.a.s.l.) and position of the wells. The wells installed in 2008 are indicated by red dots, the ones installed in 2010 by purple dots, and the catchment outlet (42.06°N, 1.14°W) is indicated by a star. Vertical exaggeration is 5:1. The gray line represents the limits of the surface flow domain. (For interpretation of the references to colour in this figure legend, the reader is referred to the web version of this article.)

measured at the catchment outlet with a temporal resolution of 15 min, starting in 2006. Since May 2008, groundwater levels in the glacis layer have been measured in eight observation wells, usually with a monthly frequency. In addition, water tables in four additional wells have been measured since March 2010 (Fig. 2). Geological and soil type data are scarce even though a soil characterization campaign was conducted (Pérez, 2011). In general, the material forming the glacis consists of approximately 60% sand, 20% silt, and 20% clay. However, as measurements were taken at only 10 locations, this campaign probably does not reflect the heterogeneity of the catchment. In addition, the depth of the buro layer has been measured during the drilling of 12 wells as well as estimated at 63 additional locations using electrical sounding (Plata-Torres, 2012). Soil depth is more uncertain but is estimated to range between 30 and 45 cm over the buro and 50 and 90 cm over the glacis (Beltrán, 1986).

5. Conceptual model

An initial modeling study of the Lerma catchment was conducted by Pérez et al. (2011). With new information becoming available, a more detailed model has been developed for the present study. The updated model differs from that presented by Pérez et al. (2011) in the following aspects: The depth of the buro is now better constrained as a result of a geoelectrical-sounding campaign (Plata-Torres, 2012). Consequently, the depth of the unconsolidated materials, forming the aquifer, are now shallower in the model. In addition, feedbacks between soil moisture and evapotranspiration were neglected by Pérez et al. (2011), but are accounted for in the present study. Finally, we use an updated, more accurate digital elevation model and discriminate between soil and aquifer materials. This set of changes caused the need of a new calibration.

Pérez et al. (2011) performed a manual calibration of his model. However, this approach was slow. In addition, only very few parameter sets could be tested and uniform parameter values were used for the creation of the initial conditions. Consequently, we decided to develop a new calibration method in addition to a new conceptual model.

We apply a distributed *pde*-based model to the Lerma catchment because of the onset of irrigation in the catchment between 2006 and 2009. This spatially-variable water source influences the other hydrological processes such as evapotranspiration and is difficult to represent in "bucket-type" models (Pérez et al., 2011). In addition, we will use this model in the future to study climate-change impact where distributed modeling of recharge and evapotranspiration is an important advantage. The possibility of studying the unsaturated zone is another benefit of choosing a *pde*-based model for this study.

In the present model, the subsurface of the Lerma model is separated into six zones as shown in Fig. 3. The lower zone represents the "buro" material. The intermediate layer is divided into two zones. The first one represents the part of the domain where the buro is close to the surface and more permeable than in the rest of the buro layer. The second zone represents the glacis, i.e., the unconsolidated materials forming the aquifer in the lower part of the domain. The top layer represents the soil (top panel of Fig. 3). Three zones are considered therein: one directly above the buro, one representing the agricultural soils, and one standing for the bare soil in the rest of the domain. The zones are assumed to be homogeneous and horizontally isotropic, while the vertical hydraulic conductivity is assumed to be one order of magnitude smaller than the horizontal one. The domain is vertically subdivided into 22 computational layers. The thickness of these layers decreases in the vicinity of the surface.
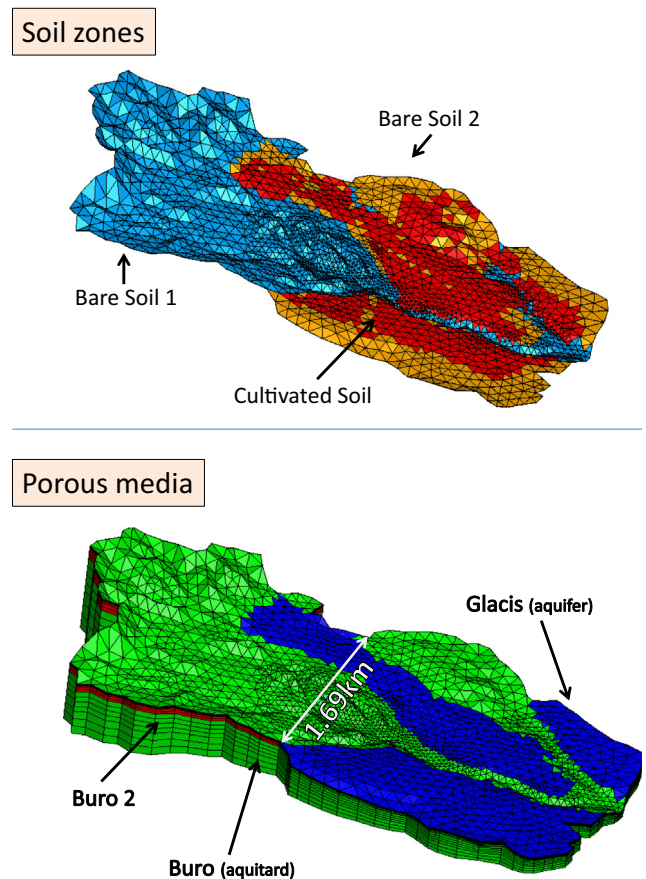

Fig. 3. Conceptual model of the catchment: soil and hydrogeological units. Extent of the cultivated soil is shown for the year 2008. Vertical exaggeration is 5:1.

The surface domain is separated into 56 sub-domains representing the different cropping and irrigation schemes. The known crop types consist mainly of corn, cereals, sunflower, and tomato. The actual evapotranspiration and the Manning coefficient depend on crop rotation patterns in the individual plots. Manning coefficients and other surface-flow parameters are taken from Pérez (2011). Actual evapotranspiration parameters are derived from a literature study, summarized in Section 7 and Table 5.

No-flow boundary conditions are assumed at the bottom and on the lateral sides of the subsurface model. For the surface domain, we assume a critical flow depth at the lateral limits (Pérez, 2011). The extent of the surface catchment (i.e. the watershed) is defined by the topography while the size of the aquifer is estimated based on the electrical sounding survey (Plata-Torres, 2012). The subsurface catchment is somewhat larger than the watershed constructed from topography. Groundwater flow and surface flow are nevertheless computed on the whole domain (Fig. 2). As a result of the boundary conditions, the fraction of the surface run-off that is generated

Table 1
Characteristics of the grids used. The simulation duration is based on an average of the four parameter sets used during the grid comparison, apart from the very fine grid case where only the second parameter set was used. The simulations were performed over the time period of one year on one core with a desktop computer Intel Core i7-2600 CPU @ 3.40 Ghz.

Grid name	No. of elements	No. of layers	Simulation time
Very fine grid	217,872	24	37 h 05 min
Fine grid	79,332	22	27 h 54 min
Intermediate grid	16,200	14	1 h 27 min
Coarse grid	10,448	14	40 min

outside of the watershed of the river gauge freely leaves the domain at the lateral surface boundaries.

To create the initial conditions, we started with a fully saturated model and repeatedly simulated one year with the meteorological forcing of 2005 until the hydrograph and the hydraulic heads achieved dynamic steady state (i.e., the temporal fluctuations were nearly identical from one simulation year to the next). Initial conditions were created separately for all grids, but for the fine grid the interpolated initial conditions of the intermediate grid were used as a starting point instead of a fully saturated model.

Irrigation and potential evapotranspiration are calculated using the FAO Penman–Monteith method (Allen et al., 1998) at daily time steps. Daily values of precipitation are used as model input as well, with the exception of days with intensive rainfall (higher than 25 mm/day). In this case, the total daily rain is considered to fall during 3 h in summer and spring. A duration of 9 h is assumed in winter and autumn. This approach aims to represent intensive convective events which are frequent in this catchment during spring and summer. The duration of smaller precipitation events has less impact on surface run-off and they have been kept as daily average to improve the model efficiency. The duration of the intense rain events is estimated using data with a resolution of 15 min from the meteorological station of Cola del Saso, which is situated about 10 km from the center of the catchment. Cola del Saso has a climate that is very similar to that of the Lerma catchment even though daily precipitation can show important short-term differences.

6. Comparison between the computational grids

As explained in Section 2, a coarse and an intermediate grid were used during calibration in addition to the fine grid, which forms the final model grid. In addition, a fourth refined grid was created and compared to the fine grid to test whether the spatial resolution of the final model, which we aim to calibrate, was adequate.

The size of the elements in each grid has been chosen to minimize the trade-off between time gain and modeling accuracy. The model using the coarse grid aims to generally represents the hydrological processes, notably the mean hydraulic heads, while the model using the intermediate grid has the additional goal of representing the low flow at the catchment outlet. The spatial resolution of the fine grid should be sufficient to model more complex hydrological processes as peaks flows and evapotranspiration. More precisely, the number of elements is decreased by a factor of eight for the coarse grid, compared to the grid of the original model. The element size is increased by about 50% and the vertical discretization is reduced to 12 layers, instead of 22 in the fine grid. For the intermediate grid, we use the coarse grid with some refinements in the cells along the streams. More detailed characteristics of all grids and their mean simulation time are presented in Table 1 and Fig. 4.

In this section, we compare the outputs of the Lerma model for all grids. Our goal is to assess the similarities and differences among the grids to optimize their use during the calibration process. Discharge at the catchment outlet, hydraulic heads in the eight piezometers installed in 2008, soil saturation, and evapotranspiration at the surface are analyzed. To imitate the calibration process, we do not use the parameters or the initial conditions used in the final model. Three parameter sets, whose values are coherent with the soil properties of the catchment, and two artificial initial conditions are arbitrarily chosen and listed in Table 2. Meteorological and irrigation data from the year 2009 are used for this comparison.
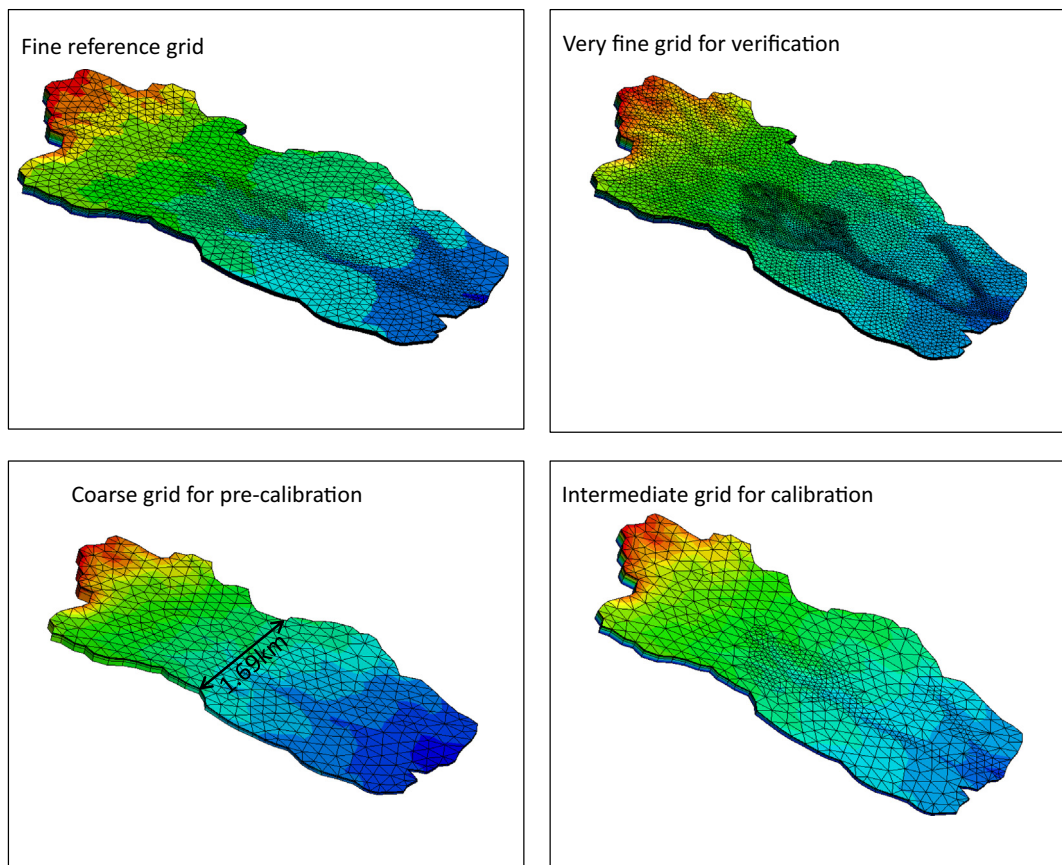

Fig. 4. Fine, very fine, coarse, and intermediate grids.

Table 2

Parameters set and initial conditions used during grid comparison. *K* is the hydraulic conductivity [m/s], α and β are the van-Genuchten parameters. All other parameters are kept constant at the value presented in Tables 4 and 5.

Parameter set	Param. 1	Param. 2	Param. 3	Param. 4
Bare soil 1				
K	$1.5 * 10^{-5}$	$5 * 10^{-5}$	$1.5 * 10^{-5}$	$1.5 * 10^{-5}$
α	3	5	3	3
β	2.25	2	1.5	2.25
Bare soil 2				
K	10^{-5}	10^{-4}	$1.5 * 10^{-5}$	10^{-5}
α	2	5	3	2
β	1.35	2	1.5	1.35
Cultivated soil				
K	$2 * 10^{-5}$	$4 * 10^{-5}$	$1.5 * 10^{-5}$	$2 * 10^{-5}$
α	2	5	3	2
β	1.25	2	1.5	1.25
Glacis				
K	0.0002	$2 * 10^{-6}$	$1.5 * 10^{-5}$	0.0002
α	2	5	3	2
β	1.5	2	1.5	1.5
Buro 2				
K	10^{-6}	10^{-5}	10^{-5}	10^{-6}
α	5	5	3	5
β	1.4	2	1.5	1.4
Buro				
K	$5 * 10^{-7}$	10^{-7}	10^{-7}	10^{-7}
α	3	5	3	3
β	1.8	2	1.5	1.8
Initial head	Surface	Surface	West: 380 m East: Surface	West: 380 m East: Surface

6.1. Discharge

Fig. 5 shows the hydrograph obtained with the fine, intermediate and coarse grids for parameter set 2. The results are very similar for the other parameters sets, as shown in Table 3. To quantitatively compare these hydrographs, two goodness-of-fit indicators are considered in Table 3 and during model calibration: The Nash-Stucliffe efficiency (NSE) and the root mean square error (RMSE). NSE is defined in Eq. (4) and compares the relative magnitude of the squared residuals to the variance of the measured data (Nash and Sutcliffe, 1970). RMSE is given in Eq. (5) and is constructed as the square-root of the mean squared difference between measured and modeled values, assuming a perfectly unbiased model.

$$NSE = 1 - \frac{\sum_{i=1}^{i=N}(Q_{mes} - Q_{obs})^2}{\sum_{i=1}^{i=N}(Q_{mes} - \overline{Q_{mes}})^2} \tag{4}$$

$$RMSE = \sqrt{\frac{1}{N}\sum_{i=1}^{i=N}(Q_{obs} - Q_{mes})^2} \tag{5}$$

where Q_{obs} is the observed discharge, Q_{mes} the measured discharge, and *N* the number of observations.

To compare discharge between the different grids, we separate peak and low flow. In this paper, low flow is defined as the total flow on days without precipitation on that day and the day before. Because of the small size of the catchment and because of the reasonably efficient irrigation management (Abrahao et al., 2011), significant run-off is not usually observed in periods without precipitation. Our definition of low flow is therefore similar to the base flow in dry days. More complex methods, which take advantage of the distributed nature of HydroGeoSphere (Partington et al., 2012), could be applied to separate base flow and run-off during wet days. However, we wanted to compare the full extent of peak flow and we therefore did not apply
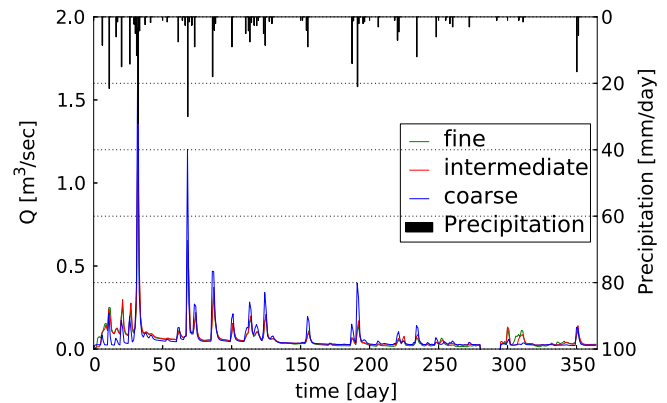

Fig. 5. Discharge comparison between the model results using the coarse, intermediate and fine grids for the parameter set 1. Meteorological input from 1st October 2008 to 30 September 2009.

Table 3

Goodness-of-fit measures of the hydrograph between the intermediate and fine grids.

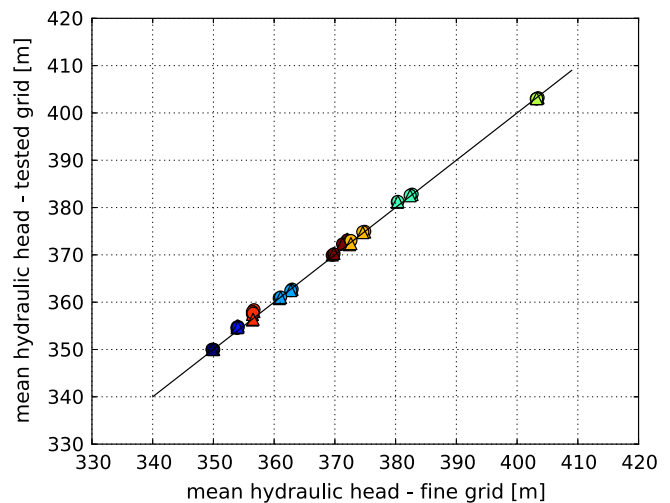| Parameter set	NSE	RMSE [%]
Param. 1	0.98	1.43
Param. 2	0.93	2.6
Param. 3	0.96	1.9
Param. 4	0.98	1.5

Fig. 6. Comparison of hydraulic heads computed on the various grids. The triangles show the hydraulic head comparison between the fine grid and the coarse grid, and the circles show the comparison between the fine grid and the intermediate grid for the four parameter sets. Average for one year. The wells are from the lowest to the highest hydraulic head: P01, P02, P010, P05, P011, P09, P06, P08.

base-flow separation method. Using the coarse grid results in less low flow compared to the fine grid (Fig. 5). We think this is caused by the coarse grid having a smaller surface slope than the fine grid because of the larger grid cells, which average elevation. This leads to a mismatch of run-off pathways (Chaplot, 2014) because flow is slower and more evenly distributed on the surface. However, we use this grid only to constrain the feasible parameter space. For this purpose, the difference between the model results is acceptably small. For the intermediate grid, the modeled discharge is very similar to that of the fine grid for all parameter sets (Table 3). As a consequence, the intermediate grid can be used for parameter calibration.
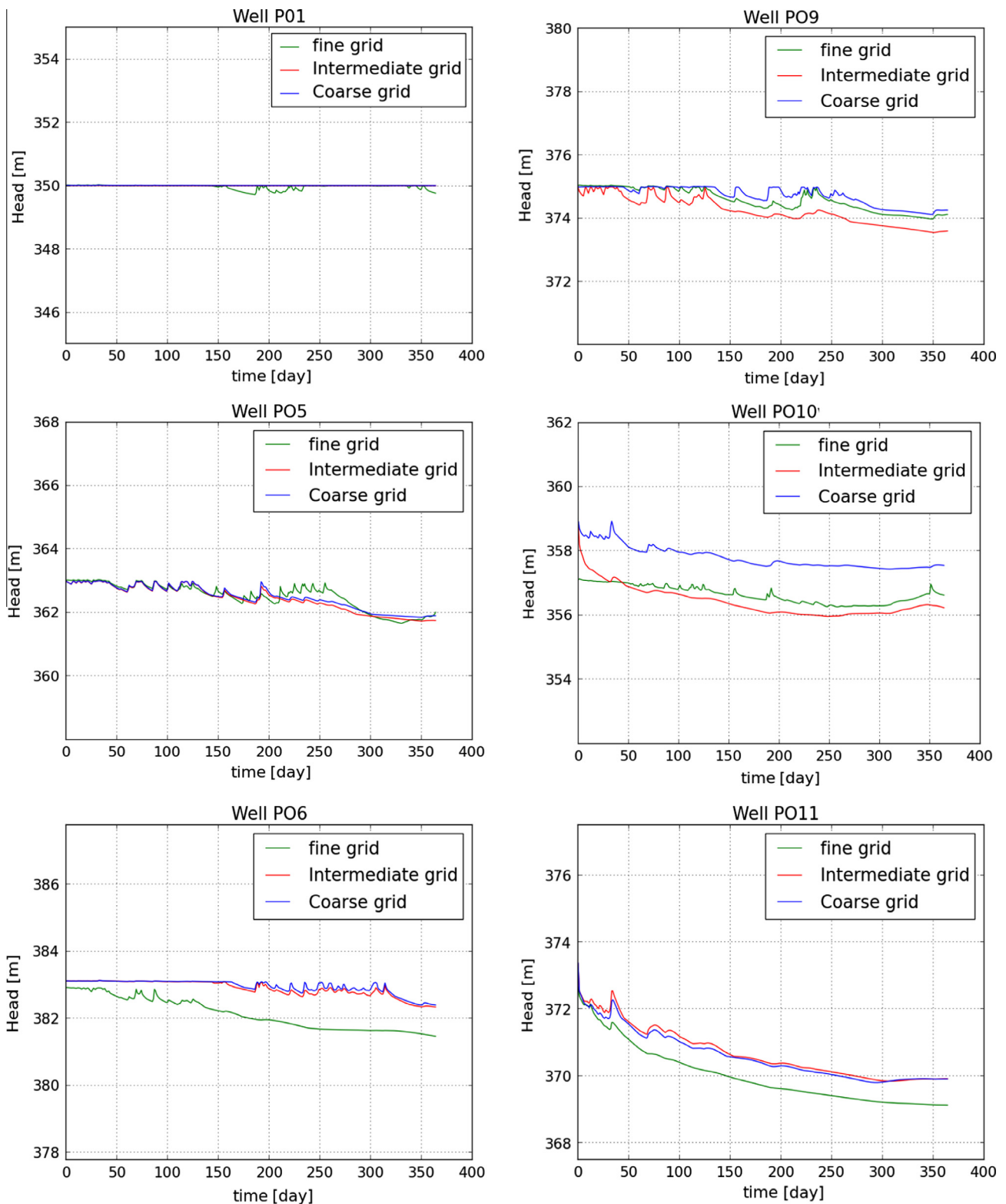
Fig. 7. Hydraulic-head variability for the hydrological year 2009 for the fine, intermediate, and coarse grids using parameter set 1.

Fig. 5 shows that the high-discharge peaks have a tendency to be lower on the fine grid than on the coarse one. A similar behavior has previously been observed (e.g., Moglen and Hartman, 2001; Wildemeersch et al., 2014), even though the opposite behavior has been reported as well (Chaplot, 2014). In our model this response is not consistent either, as peaks simulated using the fine grid are sometimes higher. Our model was tested with artificial precipitation input, and these simple tests show that peak height depends on the previous soil water content. A high water content before a precipitation event results in high peaks in the coarse or intermediate grid. On the contrary, a dry soil generally results in higher peaks on the fine grid. A possible explanation for this
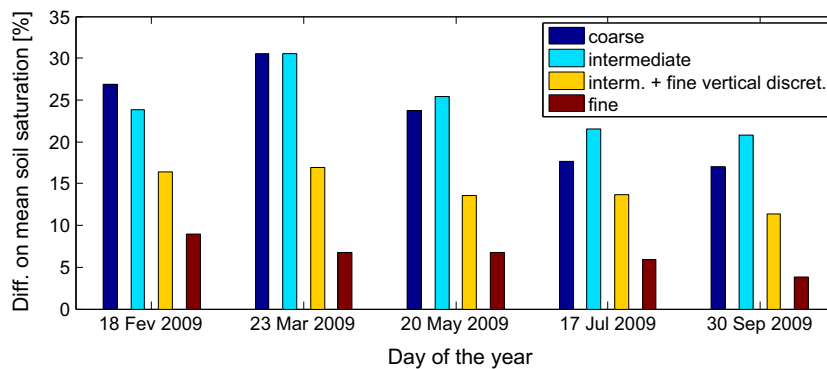
Fig. 8. Mean soil saturation (upper 40 cm) of each grid compared to the mean soil saturation of the very fine grid using parameter set 2.

difference is the soil saturation which is usually higher in the coarse and intermediate grids, as discussed in Section 6.3. Consequently, infiltration is higher in the coarse and intermediate grids when the soil is dry as the relative permeability is higher. On the contrary, when the soil is wet, the higher soil water content in the coarse and intermediate grids decreases infiltration. However, local topography and spatial difference in soil saturation, among other influences, complicates this simple picture.

6.2. Hydraulic heads

Fig. 6 presents the comparison between the fine, intermediate, and coarse grids with respect to hydraulic heads. In general, the simulation using the three different grids shows a close agreement for the average hydraulic head. Differences are mostly the result of the initial conditions as the chosen initial conditions depend on the surface elevation, which differs among the grids. Seasonal variability is similar between the grids as well (an example is shown in Fig. 7). However, during calibration on the intermediate and coarse grids, the average hydraulic heads were used as the target variables. Consequently, the variability of the hydraulic heads are of less importance for calibration.

6.3. Soil saturation and evapotranspiration

As mentioned in Section 5, the future purpose of the model is to study hydrological states and processes in a warmer climate, notably water saturation and evapotranspiration. These states and processes are sensitive to the vertical and horizontal spatial discretization of the model (Sciuto and Diekkrüger, 2010; Boone and Wetzel, 1996; Tiktak and Bouten, 1992). Therefore, it is necessary to ensure that the fine grid is accurate in simulating these states and processes, i.e., that this grid has the spatial precision needed to represent actual evapotranspiration and water saturation. To test this, a grid with even finer elements was developed and the results of the fine grid were compared to those of the very fine grid.

Because of the influence of evapotranspiration and the large variations in water content at the top of the unsaturated zone, the most important differences between the simulation results of the grids are found close to the surface. In addition, the strong relationship between (near-surface) soil-moisture and evapotranspiration has been found a key feature to represent water fluxes in coupled, integrated models, as large-scale land surface model (Gayler et al., 2014). Consequently, in Fig. 8, we compare the water saturation in the top soil (up to 40 cm depth) from each grid with the one obtained on the very fine grid at five specific dates. The soil water content of the soil was found to be constantly between 30% and 20% lower when using the very fine grid compared to the

intermediate grid. This bias is significant and explains why we could not use the intermediate grid in our final model. The mean water saturation on the fine grid is only between 9% and 3% higher than in the very fine grid, which is acceptable for our purpose. Indeed, this difference is significantly smaller than measured water saturation variability at small ($10 \, \text{m}^2$) scale (e.g., Schmitz and Sourell, 2000).

To compare the impact of vertical and horizontal discretization, we tested the intermediate grid with the vertical discretization of the fine grid. Fig. 8 shows that the vertical discretization explains about half of the bias. The horizontal discretization is therefore important. In addition, comparisons between the intermediate and the fine grid after 6 years of simulation show that the difference in soil water content is approximately constant with time. Indeed, the higher soil water content results in most cases in a lower infiltration in the model using the intermediate grid compared to the one using the fine grid as mentioned in Section 6.1. However, the variability in the soil water content was not studied in detail to confirm this finding.

The bias in soil water content is probably related to evapotranspiration. Indeed, mean daily evapotranspiration is about 7% lower in the intermediate grid than in the fine and very fine grids. Similar observations have been made before in HydroGeoSphere, notably by Sciuto and Diekkrüger (2010) who explained that spatial discretization influences total evapotranspiration in the following way: Transpiration is a function of soil moisture. Under and above a certain saturation, no transpiration occurs. Transpiration increases linearly from the low saturation limit to the next threshold, where transpiration is at maximum. However, larger elements average soil moisture and therefore decrease gradients in soil saturation.

In other words, in a dry climate, θ_{min}, the lower saturation threshold where no transpiration occurs anymore, is reached more rapidly in a coarse grid than in a fine one. As an example, let's examine a zone with the soil saturation θ_a, where $\theta_a < \theta_{min}$. If this zone is represented by a single model cell, transpiration will be zero. By contrast, if this zone is separated into n model cells, it is possible to have $\theta_i > \theta_{min}$ while satisfying the condition of $\theta_a = \frac{1}{n}\sum_{i=1}^{i=n}\theta_i \frac{A_i}{A_{tot}}$, where θ_i is the soil saturation of cell i, A_i represents the area of this cell and A_{tot} is the area of the entire zone. As cells with $\theta_i > \theta_{min}$ exist, the overall transpiration will be larger than zero when using the finer discretization.

6.4. Conclusion of the grid comparison

In summary, the simulation results using the intermediate and coarse grids show important differences to those of the fine grid, notably when surface saturation or evapotranspiration are examined. Nevertheless, sufficient similarities in simulated hydraulic heads and flow discharge, especially low flow, allow the use of the

coarse and intermediate grids as a proxy model during the first steps of calibration. Similar results between the simulations using the very fine grid and the fine grid show that the spatial resolution of our final model is sufficient to capture the hydrological processes of interest.

7. Sensitivity analysis

A *pde*-based model uses a large number of parameters. Some of them have a large impact on the output and others only a very small one. Therefore, to effectively calibrate a hydrological model, it is necessary to determine the parameters with the highest sensitivity to the model results (Christiaens and Feyen, 2002). This sensitivity analysis is done on the intermediate grid for the year 2008 because the intermediate grid is the one used most intensively during calibration. For each parameter, the model is run twice, once with a higher and once with a lower value than the original parameter value. The other parameters are kept constant. Description of the parameters, initial and modified values are shown in Tables 4 and 5. The choice of the parameters depends on the

Table 4
Parameters used during the sensitivity analysis, related to surface and subsurface flow.

Parameter name	Units	Value	Higher value	Lower value	Role
K_{bs1}	m/s	10^{-5}	10^{-4}	10^{-6}	Hydraulic conductivity – Bare Soil 1
K_{bs2}	m/s	10^{-5}	10^{-4}	10^{-6}	Hydraulic conductivity – Bare Soil 2
K_{cs}	m/s	10^{-4}	10^{-3}	10^{-5}	Hydraulic conductivity – Cultivated soil
K_{be}	m/s	10^{-7}	10^{-6}	10^{-8}	Hydraulic conductivity – Buro 2
K_{g1}	m/s	10^{-4}	10^{-3}	10^{-5}	Hydraulic conductivity – Glacis
K_b	m/s	10^{-7}	10^{-6}	10^{-8}	Hydraulic conductivity – Buro
α_{bs1}	1/m	4	5	3	Van Genuchten parameter – Bare Soil
α_{bs2}	1/m	4	5	3	Van Genuchten parameter – Bare Soil 2
α_{cs}	1/m	4	5	3	Van Genuchten parameter – Cultivated soil
α_{be}	1/m	4	5	3	Van Genuchten parameter – Buro 2
α_{g1}	1/m	4	5	3	Van Genuchten parameter – Glacis
α_b	1/m	4	5	3	Van Genuchten parameter – Buro
β_{bs1}	–	1.5	2	1.2	Van Genuchten parameter – Bare Soil 1
β_{bs2}	–	1.5	2	1.2	Van Genuchten parameter – Bare Soil 2
β_{cs}	–	1.5	2	1.2	Van Genuchten parameter – Cultivated soil
β_{be}	–	1.5	2	1.2	Van Genuchten parameter – Buro 2
β_{g1}	–	1.5	2	1.2	Van Genuchten parameter – Glacis
β_b	–	1.5	2	1.2	Van Genuchten parameter – Buro
S_{st}	1/m	10^{-4}	10^{-3}	10^{-5}	Specific storage for all soil zones
θ_s	–	0.3	0.4	0.2	Porosity for all soil zones
S_r	–	0.1	0.15	0.05	Residual Saturation for all soil zones
k_{bmx}, k_{bmy}	m/s	0.01	0.015	0.005	Manning parameter for bare soil (x and y direction)
k_{cmx}, k_{cmy}	m/s	0.04	0.05	0.03	Manning parameter for cultivated soil (x and y direction)
r_s	m	0.001	0.0015	0.0005	Average height of the soil depressions
o_s	m	0.05	0.07	0.03	Average height of the vegetation or other obstacles
l_{ex}	m	0.001	0.01	0.0001	Coupling between surface and subsurface

Table 5
Parameters used during the sensitivity analysis, related to evapotranspiration.

Param. name	Units	Value	Higher value	Lower value	Role	Reference
W_p	m	−150	−100	−200	Wilting point for all crops	Tolk (2003)
θ_a	–	0.9	0.95	0.85	Highest saturation where transpiration happens	Panday and Huyakorn (2004)
θ_o	–	0.8	0.87	0.73	Highest saturation where transpiration is not limited	Panday and Huyakorn (2004)
R_c	m	1	0.5	1.5	Root depth for corn	Canadell et al. (1996), Breuer et al. (2003)
R_w	m	1	0.5	1.5	Root depth for winter cereal	Breuer et al. (2003)
R_t	m	0.2	0.1	0.3	Root depth for tomato	Rosário et al. (1996)
C_1	–	0.31	0.5	0.1	1st Transpiration fit. param.	Li et al. (2008)
C_2	–	0.2	0.4	0.1	2nd Transpiration fit. param.	Li et al. (2008)
C_3	–	3.7	6.4	1	3rd Transpiration fit. param.	Li et al. (2008), Therrien et al. (2010)
E_d	m	0.2	0.3	0.1	Max. evaporation depth	Therrien et al. (2010)
e_1	–	0.83	0.73	0.93	Lowest saturation where evaporation happens	Panday and Huyakorn (2004)
LAI_c	–	Variable	6.5	4	LAI for corn	Gardiol et al. (2003), Mailhol et al. (1997), Howell et al. (1996), Breuer et al. (2003)
LAI_w	–	Variable	3	1.5	LAI for winter cereal	Breuer et al. (2003)
LAI_t	–	Variable	3.5	2	LAI for tomato	Koning (1994), Heuvelink (1995)
LAI_b	–	Variable	0.5	0.05	LAI for "bare soil" (i.e. for shrub and grass)	–
C_s	m	0.0035	0.0025	0.0045	Maximum height of the canopy storage	Kozak et al. (2007)

estimated limits of the parameter space, which are based on a literature study and previous work from Pérez (2011). The initial value is the mean of the limits of the respective parameter space. The modified values are half of the difference between the mean and the higher or lowest limits of the parameter space. The initial conditions are taken from the calibrated model.

Previously, the same sensitivity analysis has been done with artificial initial conditions, yielding similar results. In addition, we ran the same sensitivity analysis on the fine grid to confirm that parameter sensitivity is not greatly influenced by the spatial discretization (Wildemeersch et al., 2014). Results were again similar.

In this sensitivity analysis, the flow hydrograph at the outlet and the hydraulic heads measured at five observation wells (P02, P06, P09, P010 and P011) were analyzed. Based on the different simulations of these variables, the impact of each parameters on the model output was quantified as follows:

$$S_i = \frac{I_i}{\Delta b_i} \sum_{j=1}^{j=N_o} w_j \frac{RMSE(y_{i,j}, y_{0,j})}{\Delta_{max,j}} \tag{6}$$

where S_i is the sensitivity index of the parameter i, I_i is the estimated size of the parameter space for this parameter and Δb_i is the difference between the original and modified parameter value. By design, $\frac{I_i}{\Delta b_i} = 4$ in this analysis. N_o represents the type of outputs, i.e., the five observations wells and the hydrograph. $y_{0,j}$ is the jth output of the unmodified model while $y_{i,j}$ is the jth output of the model with the modified parameter b_i. The $RMSE$ is calculated by Eq. (5). The weights w_j are 0.5 for the hydrograph and 0.1 for each well. $\Delta_{max,j}$ is the maximum of the absolute difference between all modified models and the unmodified model for the output j. A high S_i indicates a parameter with a high influence on the model output.

Fig. 9 shows the S_i values for all parameters with a $S_i > 7\%$. These are 12 parameters out of 44 parameters. The saturated hydraulic conductivities have the largest impact on the simulated hydraulic heads and on the hydrograph, as found in other sensitivity analyses related to surface–subsurface modeling (Bonton et al., 2012). The van-Genuchten parameters of the zones close to the surface and the porosity ranked second in sensitivity. There are numerous parameters related to evapotranspiration but they have a small impact on the overall simulation results for hydraulics heads and hydrographs. Annual mean PET in the Lerma catchment is about three or four times the actual evapotranspiration. Consequently, soil water content controls actual evapotranspiration, a fact which limits the importance of the parameters related to evapotranspiration. The first and third fitting parameter of the
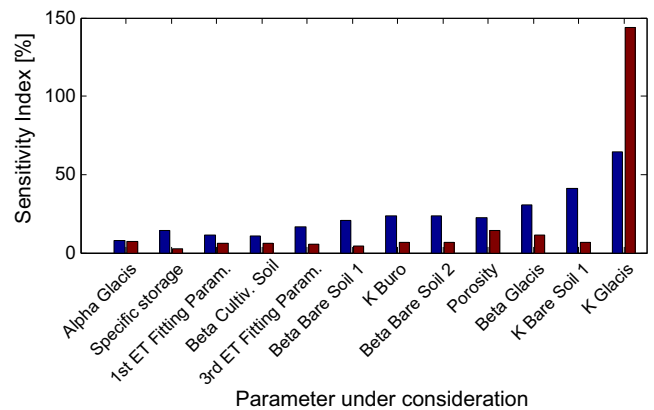

Fig. 9. Sensitivity indices of all parameters in the sensitivity analysis (Tables 4 and 5) with a mean sensitivity index above 7%. For each parameter, we tested an higher and lower value than the base case value. The higher value test is indicated in blue and the lower one in red. (For interpretation of the references to colour in this figure legend, the reader is referred to the web version of this article.)

transpiration function C_1 and C_3 are the most sensitive parameters of all evapotranspiration parameters, when hydraulics heads or the flow hydrograph is considered.

The S_i value of LAI is difficult to compare to the other parameters because it varies with time but, based on tests with different constant LAI, S_i of LAI seems to be in the lower range (<7%).

8. Calibration

Our model was calibrated using data of the years 2006–2009 and validated using the data of the years 2010–2011. Based on the results of the sensitivity analysis, the hydraulic conductivity for each zone, the van-Genuchten parameters and the porosity were the only parameters modified during calibration. The calibration was performed in five steps:

- First, we tested 200 randomly-chosen parameters sets using the coarse grid and artificial initial conditions to explore the most sensitive parameters space. In this first calibration step, we chose the best parameter set by comparing the modeled and measured mean hydraulic heads and the low flow of the hydrograph. Low flow was simply defined as the total flow on days without precipitation at that day and the day before, as explained in Section 6.1.
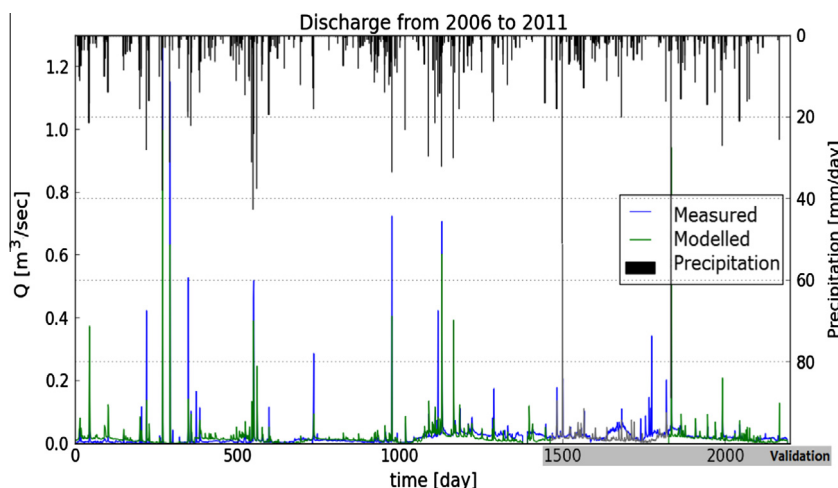

Fig. 10. Measured and modeled hydrograph for 2006–2011. Please notice the missing data at the end of 2009. Because of snow and breakage of the irrigation pipe, 2010 is not taken into account in our analysis.
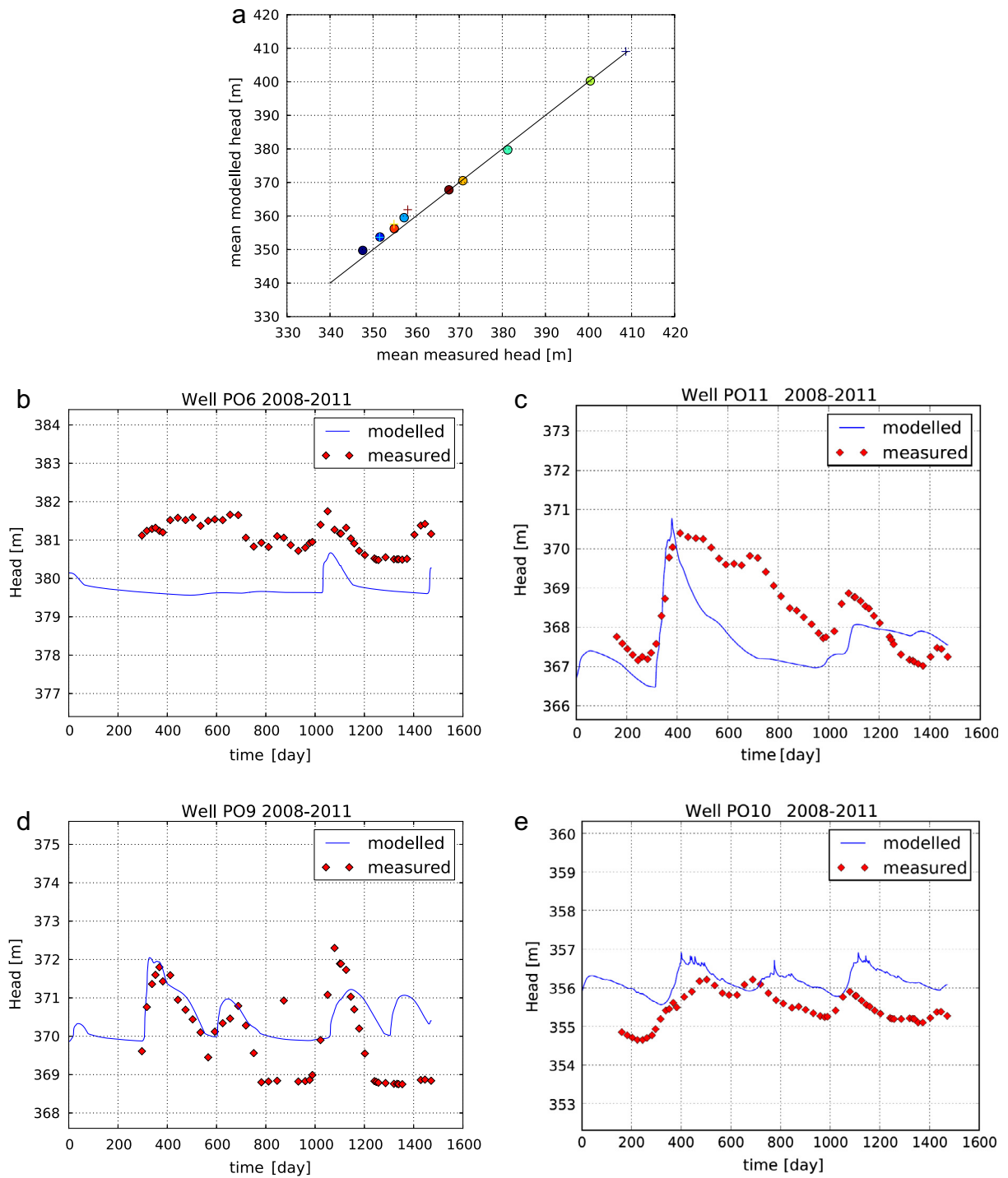
Fig. 11. Average modeled and measured value for all wells and transient hydraulic head for the wells P06, P09, P010 and P011. On the figure at the top, the wells are from the lowest to the highest hydraulic head: P01, P02, P03, P010, P04, P05, P012, P011, P09, P06, P08, P07. The mean modeled heads are the averages of the daily values from October 1, 2007 to September 30, 2011. The mean measured heads are the averages of the measured monthly values for the years 2008–2011.

- Using the selected best parameter set, we updated the initial condition by running the intermediate grid 100 times with the meteorological input of the year 2005 to reach dynamical steady state.
- Then, we manually calibrated the intermediate grid by trial and error, using the daily hydraulic heads and the full hydrograph. We tested about 70 parameter sets and we selected the parameter set which resulted in the highest NSE value and lowest

Table 6
Goodness-of-fit measure for calibration and validation periods.

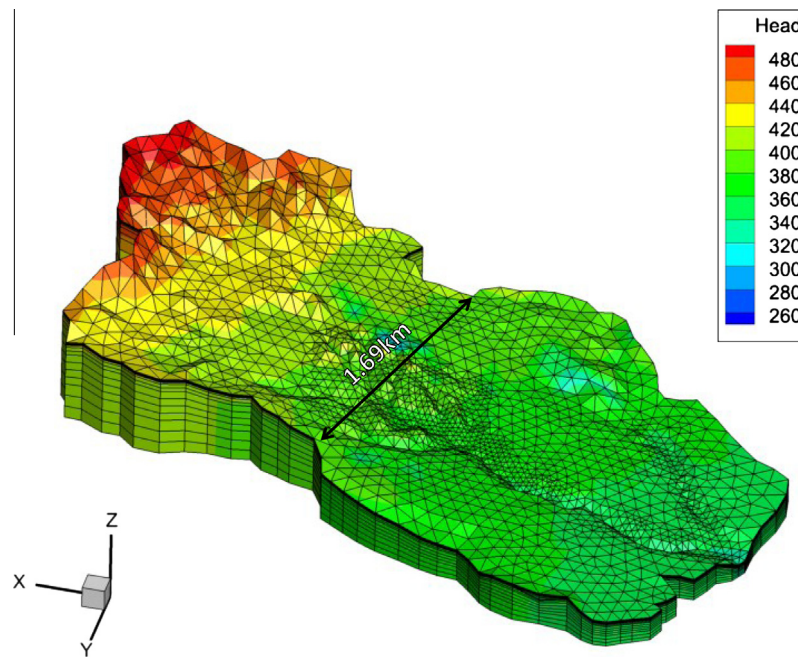|	2006–2009	2011
NSE	0.74	0.92
RMSE (%)	3.16	1.36

Fig. 12. Calibrated hydraulic head in m.a.s.l. for the Lerma catchment on the 4th November 2009. Vertical exaggeration is 5:1.

RMSE for the outflow. We estimated the quality of the modeled hydraulic heads by visually comparing this output with the measurements.

- Subsequently, the initial conditions were updated on the intermediate grid with the best parameter set found. The initial conditions were then transferred to the fine grid, using a linear interpolation scheme. The final model with the fine grid was then run three times with the meteorological input from 2005 and the parameters from the intermediate grid to finalize the initial conditions.
- Afterwards, we finished the calibration on the fine grid by manually adjusting the surface hydraulic conductivity to better match the peak flows at the outlet.

Fig. 10 shows the calibrated hydrograph and Fig. 11 the calibrated hydraulic heads. Table 6 lists the values of NSE and RMSE. Hydraulic-head values for the whole catchment are presented in Fig. 12 for the 4th November 2009. The calibrated parameters are listed in Table 7. All other parameters are identical to those given in Tables 4 and 5.

Based on the high NSE value of 0.74 and the low RMSE of 3.16%, we assess that our model can reproduce the flow hydrograph and the hydraulic heads well. Visual examination also confirms that the hydrograph is reproduced well even if the model has a tendency to underestimate discharge during the irrigation period (July–September), notably in 2009. Modeled mean hydraulic heads are close to the measured ones. Indeed, there is less than 2 m of difference between calibrated and measured mean hydraulic heads. This is on the same order of magnitude than the annual variability in most wells. In addition, the model simulations capture most of the variability of the hydraulic head measurements, even though a tendency to underestimate it was observed, notable for well P09 (Fig. 11). This might be explained by the position of well P09, situated close to a road whose filling material might disturb groundwater flow. Overall, we judged that the calibration was successful.

However, in 2010, the modeled hydrograph differs significantly from the measured one. An explanation may be that 2010 is one of the rare years in which snow was present in the Lerma catchment. Unfortunately, our model does not account for snow. In addition,

Table 7
Calibrated parameters for hydraulic conductivity, porosity and van-Genuchten parameters. See Table 4 for the definition of the parameters.

Parameter	Units	Calibrated Value
K_{bs1}	m/s	$3 * 10^{-6}$
K_{bs2}	m/s	10^{-6}
K_{cs}	m/s	$8 * 10^{-5}$
K_{be}	m/s	$3 * 10^{-6}$
K_{g1}	m/s	$1.7 * 10^{-4}$
K_b	m/s	10^{-7}
α_{bs1}	1/m	4.95
α_{bs2}	1/m	4
α_{cs}	1/m	4
α_{g1}	1/m	4
β_{bs1}	–	1.35
β_{bs2}	–	1.4
β_{cs}	–	1.35
β_{g1}	–	2
$\theta_{s,bs1}$	–	0.25
$\theta_{s,bs2}$	–	0.25
$\theta_{s,cs}$	–	0.25
$\theta_{s,g1}$	–	0.2

the main irrigation pipe broke in spring. This event caused a flood in this relatively small catchment, which is not captured by the model simulations. The year 2010 was therefore omitted from our analysis. However, the model was able to reproduce the following year adequately, with a NSE value 0.92 and a RSME of 1.36%. In addition, the model satisfactorily reproduces hydraulic heads during the whole validation period in all observation wells, including the wells drilled in 2010 which were not included in the model calibration.

During calibration, working with different grids was very useful. To quantify this advantage, we may examine the number of years that the model needs to run during calibration. We tested 200 parameter sets during two years for our first estimation. Then, we simulated 2×100 years for the initial condition and approximately 70 parameter sets over four years for manual calibration. To finish the calibration, three parameter sets over four years were tested on the fine grid, after a final update to the initial conditions.

Consequently, the equivalent of approximately 890 years were computed during model calibration. With the fine grid, this would have taken us more than two years of computational time. The creation of the initial conditions alone would have lasted more than 3 months. With our choice of grids, the simulation time was greatly reduced. We needed about ten days on one computational core to process the 200 first simulations, about six days to create the initial conditions and between five and eight hours to manually test one parameter set. Consequently, the calibration would last approximately a month if no adjustments to the model were needed.

9. Conclusions

To simulate hydrological processes at catchment scale, coupled *pde*-based models have the advantage that they simulate spatially distributed, measurable state variables such as hydraulic heads, while accounting for explicit coupling between surface and subsurface processes, thus allowing to predict changes of fluxes at compartmental interfaces. However, calibration of large distributed models is time-consuming and difficult, which limits their usefulness.

The method presented here is a significant step toward solving this problem. Using grid coarsening is a practical solution which reduces the time needed to test simulations with various parameter sets. Hence, it allows the modeler to better explore the parameter space in a shorter amount of time. We tested this approach under realistic conditions, using a catchment-scale case study, and we showed that this method has decreased calibration time. We suggest that our method can successfully be applied to other catchments as well. However, guidelines for the choice of the grid precision should be investigated further, as it is now principally based on empirical knowledge.

In addition, the proposed method could be easily modified to perform an automatic calibration. In addition, it can be extended to allow for simple uncertainty analysis similar to the one presented in Wildemeersch et al. (2014). Reactive transport modeling could also profit from a coarser grid for calibration of flow, as a finer spatial discretization is usually needed to resolve transport than flow (Chaubey et al., 2005).

Acknowledgments

References

Abrahao, R., Causapé, J., García-Garizábal, I., Merchán, D., 2011. Implementing irrigation: water balances and irrigation quality in the Lerma basin (Spain). Agric. Water Manage. 102, 97–104.

Allen, R., Pereira, L., Raes, D., Smith, M., 1998. Crop evapotranspiration (guidelines for computing crop water requirements). FAO Irrigation and Drainage Paper 56.

Beltrán, A., 1986. Estudio de los suelos de la zona regable de Bardenas II. Sectores VIII, IX, X, XII y XIII. Instituto Nacional de Reforma y Desarrollo Agrario, Ministerio de Agricultura, Pesca y Alimentación.

Beven, K., Binley, A., 1992. The future of distributed models: model calibration and uncertainty prediction. Hydrol. Process. 6, 279–298.

Blasone, R.S., Madsen, H., Rosbjerg, D., 2008. Uncertainty assessment of integrated distributed hydrological models using GLUE with Markov chain Monte Carlo sampling. J. Hydrol. 353, 18–32.

Bonton, A., Bouchard, C., Rouleau, A., Rodriguez, M.J., Therrien, R., 2012. Calibration and validation of an integrated nitrate transport model within a well capture zone. J. Contam. Hydrol. 128, 1–18.

Boone, A., Wetzel, P.J., 1996. Issues related to low resolution modeling of soil moisture: experience with the PLACE model. Global Planet. Change 13, 161–181.

Breuer, L., Eckhardt, L., Frede, H., 2003. Plant parameter values for models in temperate climates. Ecol. Modell. 169, 237–293.

Bruneau, P., Gascuel-Odoux, C., Robin, P., Merot, P., Beven, K., 1995. Sensitivity to space and time resolution of a hydrological model using digital elevation data. Hydrol. Process. 9, 69–81.

Calderhead, A., Therrien, R., Rivera, A., Martel, R., Garfias, J., 2011. Simulating pumping-induced regional land subsidence with the use of insar and field data in the Toluca valley, Mexico. Adv. Water Resour. 34, 83–97.

Canadell, J., Jackson, R., Ehleringer, J., Mooney, H., Sala, O., Schulze, E., 1996. Maximum root depth of vegetation types at global scale. Oecologia 108, 583–595.

Carrera-Hernandez, J., Smerdon, B., Mendoza, C., 2012. Estimating groundwater recharge through unsaturated flow modelling: sensitivity to boundary conditions and vertical discretization. J. Hydrol. 452, 90–101.

Chaplot, V., 2005. Impact of DEM mesh size and soil map scale on SWAT runoff, sediment, and NO3-N loads predictions. J. Hydrol. 312, 207–222.

Chaplot, V., 2014. Impact of spatial input data resolution on hydrological and erosion modeling: recommendations from a global assessment. J. Phys. Chem. Earth 69, 23–35.

Chaubey, I., Cotter, A.S., Costello, T.A., Soerens, T.S., 2005. Effect of DEM data resolution on SWAT output uncertainty. Hydrol. Process. 19, 621–628.

Christiaens, K., Feyen, J., 2002. Use of sensitivity and uncertainty measures in distributed hydrological modeling with an application to the MIKE-SHE model. Water Resour. Res. 38, 1169–1185.

Condon, L.E., Maxwell, R.M., Gangopadhyay, S., 2013. The impact of subsurface conceptualization on land energy fluxes. Adv. Water Resour. 60, 188–203.

Cotter, A.S., Chaubey, I., Costello, T.A., Soerens, T.S., Nelson, M.A., 2003. Water quality model output uncertainty as affected by spatial resolution of input data. JAWRA – J. Am. Water Resour. Assoc. 39, 977–986.

Dutta, D., Nakayama, K., 2009. Effects of spatial grid resolution on river flow and surface inundation simulation by physically based distributed modelling approach. Hydrol. Process. 23, 534–545.

Gardiol, J., Serio, L., Maggiora, A.D., 2003. Modelling evapotranspiration of corn (zea mays) under different plant densities. J. Hydrol. 271, 188–196.

Gayler, S., Wöhling, T., Grzeschik, M., Ingwersen, J., Wizemann, H.D., Warrach-Sagi, K., Högy, P., Attinger, S., Streck, T., Wulfmeyer, V., 2014. Incorporating dynamic root growth enhances the performance of Noah-MP at two contrasting winter wheat field sites. Water Resour. Res. 50, 1337–1356.

van Genuchten, M., 1980. A closed-form equation for predicting the hydraulic conductivity of unsaturated soils. Am. Soc. Soil Sci. 44, 892–898.

Goderniaux, P., Brouyère, S., Blenkinsop, S., Burton, A., Fowler, H.J., Orban, P., Dassargues, A., 2011. Modeling climate change impacts on groundwater resources using transient stochastic climatic scenarios. Water Resour. Res., 47.

Goderniaux, P., Brouyère, S., Fowler, H., Blenkinsop, S., Therrien, R., Orban, P., Dassargues, A., 2009. Large scale-surface subsurface hydrological model to assess climate change impacts on groundwater reserves. J. Hydrol. 373, 122–138.

Hessel, R., 2005. Effects of grid cell size and time step length on simulation results of the Limburg soil erosion model (LISEM). Hydrol. Process. 19, 3037–3049.

Heuvelink, E., 1995. Growth, development and yield of a tomato crop: periodic destructive measurements in a greenhouse. Sci. Horticul. 61, 77–99.

Howell, T., Evett, S., Tolk, J., Schneider, A., Steiner, J., 1996. Evapotranspiration of corn – southern high plains. In: Evapotranspiration and Irrigation Scheduling, Proceedings of the International Conference, American Society of Agricultural Engineers.

I.G.N., 2012. Modelo Digital del Terreno, hoja 282 del Mapa Topográfico Nacional (in Spanish). Instituto Geográfico Nacional.

Koning, A., 1994. Development and dry matter distribution in glasshouse tomato: a quantitative approach. Ph.D. thesis, Agricultural University of Wageningen.

Kozak, J., Ahuja, L.R., Green, T., Ma, L., 2007. Modelling crop canopy and residue rainfall interception effects on soil hydrological components for semi-arid agriculture. Hydrol. Process. 21, 229–241.

Kristensen, K., Jensen, S., 1975. A model for estimating actual evapotranspiration from potential evapotranspiration. Nordic Hydrol. 6, 170–188.

Kuo, W.L., Steenhuis, T.S., McCulloch, C.E., Mohler, C.L., Weinstein, D.A., DeGloria, S.D., Swaney, D.P., 1999. Effect of grid size on runoff and soil moisture for a variable-source-area hydrology model. Water Resour. Res. 35, 3419–3428.

Lemieux, J.M., Sudicky, E.A., Peltier, W.R., Tarasov, L., 2008. Simulating the impact of glaciations on continental groundwater flow systems: 2. Model application to

the Wisconsinian glaciation over the Canadian landscape. J. Geophys. Res. 113, F03018.

Li, Q., Unger, A., Sudicky, E., Kassenaar, D., Wexler, E., Shikaze, S., 2008. Simulating the multi-seasonal response of a large-scale watershed with a 3D physically-based hydrologic model. J. Hydrol. 357, 317–336.

Mailhol, J.C., Olufayo, A., Ruelle, P., 1997. Sorghum and sunflower evapotranspiration and yield from simulated leaf area index. Agric. Water Manage. 35, 167–182.

McMichael, C., Hope, A., Loaiciga, H., 2006. Distributed hydrological modelling in California semi-arid shrublands: MIKE-SHE model calibration and uncertainty estimation. J. Hydrol. 317, 307–324.

Mehl, S., Hill, M.C., 2002. Development and evaluation of a local grid refinement method for block-centered finite-difference groundwater models using shared nodes. Adv. Water Resour. 25, 497–511.

Mehl, S., Hill, M.C., Leake, S.A., 2006. Comparison of local grid refinement methods for MODFLOW. Groundwater 44, 792–796.

Merchán, D., Causapé, J., Abrahao, R., 2013. Impact of irrigation implementation on hydrology and water quality in a small agricultural bassin in Spain. Hydrol. Sci. J. 58, 1400–1413.

Moglen, G., Hartman, G., 2001. Resolution effects on hydrologic modeling parameters and peak discharge. J. Hydrol. Eng. 6, 490–497.

Molnár, D., Julien, P., 2000. Grid-size effects on surface runoff modeling. J. Hydrol. Eng. 5, 8–16.

Moussa, R., Bocquillon, C., 2000. Approximation zones of the saint-venant equations for flood routing with overbank flow. Hydrol. Earth Syst. Sci. 4, 251–261.

Muleta, M., Nicklow, J., 2005. Sensitivity and uncertainty analysis coupled with automatic calibration for a distributed watershed model. J. Hydrol. 306, 127–145.

Nash, J., Sutcliffe, V., 1970. River flow forecasting through conceptual models, part I – A discussion of principles. J. Hydrol. 10, 282–290.

Panday, S., Huyakorn, P., 2004. A fully coupled physically-based spatially-distributed model for evaluating surface/subsurface flow. Adv. Water Resour. 27, 361–382.

Partington, D., Brunner, P., Simmons, C., Werner, A., Therrien, R., Maier, H., Dandy, G., 2012. Evaluation of outputs from automated baseflow separation methods against simulated baseflow from a physically based, surface water-groundwater flow model. J. Hydrol. 459, 28–39.

Pérez, A., 2011. Physics-based numerical modeling of surface-groundwater flow and transport at catchment scale. Ph.D. thesis, Universität Tübingen.

Pérez, A., Abrahao, R., Causapé, J., Cirpka, O., Bürger, C., 2011. Simulating the transition of a semi-arid rainfed catchment towards irrigation agriculture. J. Hydrol. 409, 663–681.

Plata-Torres, J., 2012. Informe sobre la campaña de sondeos eléctrico verticales efectuados en el barranco de Lerma (Zaragoza). Grupo de Geofísica del Instituto Geológico y Minero de España.

Rosário, M.D., Calado, A.M., Oliveira, G., Portas, C., 1996. Tomato root distribution under drip irrigation. J. Am. Hort. Soc. 121, 644–648.

Samaniego, L., Kumar, R., Attinger, S., 2010. Multiscale parameter regionalization of a grid-based hydrologic model at the mesoscale. Water Resour. Res., 46.

Schmitz, M., Sourell, H., 2000. Variability in soil moisture measurement. Irrigat. Sci. 19, 147–151.

Sciuto, G., Diekkrüger, B., 2010. Influence of soil heterogeneity and spatial discretization on catchment water balance modeling. Vadose Zone J. 9, 955–969.

Shao, H., Kosakowski, G., Berner, U., Kulik, D.A., Mäder, U., Kolditz, O., 2013. Reactive transport modeling of the clogging process at Maqarin natural analogue site. J. Phys. Chem. Earth 64, 21–31.

Skhiri, A., Dechimi, F., 2011. Irrigation return flows and phosphorus transport in the Middle Ebro River valley (Spain). Spanish J. Agric. Res. 9, 938–949.

Therrien, R., 2006. HydroGeoSphere – A Three-Dimensional Numerical Model Describing Fully-Integrated Subsurface and Surface Flow and Solute Transport. Ph.D. thesis, Université Laval and University of Waterloo.

Therrien, R., McLaren, R., Sudicky, E., Panday, S., 2010. HydroGeoSphere: A Three-dimensional Numerical Model Describing Fully-integrated Subsurface and Surface Flow and Solute Transport – User Manual, University of Waterloo.

Tiktak, A., Bouten, W., 1992. Modelling soil water dynamics in a forested ecosystem. III: Model description and evaluation of discretization. Hydrol. Process. 6, 455–465.

Tolk, J., 2003. Soils, permanent wilting points. Encycl. Water Sci., 927–929.

Urdanoz, V., Aragüés, R., 2011. Pre- and post-irrigation mapping of soil salinity with electromagnetic induction techniques and relationships with drainage water salinity. Am. Soc. Soil Sci. 75, 207–215.

Vazquez, R.F., Feyen, L., Feyen, J., Refsgaard, J.C., 2002. Effect of grid size on effective parameters and model performance of the MIKE-SHE code. Hydrol. Process. 16, 355–372.

Wildemeersch, S., Goderniaux, P., Orban, P., Brouyère, S., Dassargues, A., 2014. Assessing the effects of spatial discretization on large-scale flow model performance and prediction uncertainty. J. Hydrol. 510, 10–25.

Xevi, E., Christiaens, K., Espino, A., Sewnandan, W., Mallants, D., Sorensen, H., Feyen, J., 1997. Calibration, validation and sensitivity analysis of the MIKE-SHE model using the Neuenkirchen catchment as case study. Water Resour. Manage. 11, 219–242.

5 Second publication

Title

Estimating climate-change effects on a Mediterranean catchment under various irrigation conditions

Journal

Journal of Hydrology: Regional Studies (Volume 4, pages 550-570)

Year

2015

Highlights

- The hydrological response of the Lerma catchment is simulated under four different irrigation regimes.

- Climate change impacts in the study area are simulated for these irrigation scenarios.

- The interactions between irrigation and climate changes are investigated:

  - Hydraulic heads and base flow react more to climate change if irrigation is present.
  - Peak flow are more sensitive to future precipitation variability without irrigation.
  - Actual evapotranspiration increases in scenarios with irrigation, but it decreases in the scenario without irrigation.
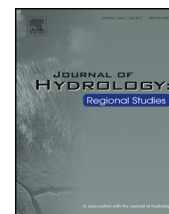
Estimating climate-change effects on a Mediterranean catchment under various irrigation conditions

D. von Gunten [a], T. Wöhling [a,c], C.P. Haslauer [a], D. Merchán [b], J. Causapé [b], O.A. Cirpka [a,*]

[a] *University of Tübingen, Center for Applied Geoscience, Hölderlinstr. 12, 72076 Tübingen, Germany*
[b] *Geological Survey of Spain – IGME, C/ Manuel Lasala no. 44, 9B, Zaragoza 50006, Spain*
[c] *Lincoln Agritech Ltd., Ruakura Research Centre, Hamilton, New Zealand*

A B S T R A C T

Study region: The Lerma catchment, a small ($7.3 \, \text{km}^2$) sub-catchment of the Ebro Basin in northern Spain.

Study focus: The Lerma catchment underwent a monitored transition to irrigated agriculture, using water from outside the catchment, between 2006 and 2008. This transition has successfully been simulated using the partial-differential-equation-based model HydroGeoSphere, simulating coupled evapotranspiration, surface water, and groundwater flow in the catchment. We use the calibrated model to study how irrigation practices influence the response of the Lerma catchment to the climate change projected for northern Spain. We consider four different irrigation scenarios: no irrigation, present irrigation, climate-adapted irrigation with current crops, and adapted irrigation for crops requiring less water. The climate scenarios are based on four regional climate models and two downscaling methods.

New hydrological insight: The simulated catchment responses to climate change show clear differences between the irrigation scenarios. In future climate, groundwater levels and base flows decrease more when irrigation is present than without irrigation, because groundwater levels and base flow in present climate are already at low levels without irrigation. In contrast, annual peak discharges increase more in non-irrigated cases than in irrigated cases. Irrigation increases water availability and an associated rise in potential evapotranspiration results in higher actual evapotranspiration during summer. In non-irrigated scenarios, by contrast, actual evapotranspiration in summer is controlled by precipitation and thus decreases in future climate.

1. Introduction

The increase in mean global air temperature over the past 30 years, linked to the anthropogenic increase of CO_2 emissions (e.g., Meehl et al., 2007), influences the global and regional water cycle and is expected to change future precipitation patterns (e.g., Sillmann and Roeckner, 2008). Particularly strong impacts are expected in semi-arid regions, such as the Ebro basin in north-east Spain (Vargas-Amelin and Pindado, 2014). The timing and magnitude of these impacts, however, are difficult to

* Corresponding author.
  E-mail address: olaf.cirpka@uni-tuebingen.de (O.A. Cirpka).

predict (Ghosh and Misra, 2010), a fact which complicates efficient mitigation. In the next century, less water will probably be available in the Ebro region (Bovolo et al., 2010; Buerger et al., 2007; Milano et al., 2013) as a result of increased potential evapotranspiration (Moratiel et al., 2010; García-Garizábal et al., 2014) and decreased precipitation in spring and summer (Blenkinsop and Fowler, 2007; Ribalaygua et al., 2013).

Various catchment-scale case-studies in north-east Spain forecast a decrease in runoff (Candela et al., 2012), streamflow (Ferrer et al., 2012; López-Moreno et al., 2014; Zambrano-Bigiarini et al., 2010), recharge (Candela et al., 2012), and water quality (Bovolo et al., 2010). Some recent observed changes, for example variations in run-off generation (Otero et al., 2011) and decrease in river flow (Milano et al., 2013), have already been linked to ongoing climate change. In addition, irrigation needs are likely to increase (e.g. Jorge and Ferreres, 2001; Rey et al., 2011; Iglesias and Minguez, 1997) because of the higher evaporative demand and possibly because of expanding irrigated areas (Scanlon et al., 2007; Bielsa and Cazcarro, 2015).

Changes in land use often interact with climate change and its impacts (e.g., Dale, 1997; Pielke, 2005). For example, predictions of stream-flow in the Pyrenean mountains indicate that reforestation and climate change together lead to a decrease stream-flow twice as much as climate change alone (López-Moreno et al., 2014). In the same region, the duration of snow cover is expected to decrease due to climate change, while reforestation influences the snow depth (Szczypta et al., 2015). Reforestation also impacts climate-change effects on erosion in semi-arid regions (Simonneaux et al., 2015) and on groundwater recharge (Montenegro and Ragab, 2012). In the semi-arid Upper Yellow River region of China, land-use changes, notably over-grazing and increased irrigation, result in a decrease of stream-flow at a similar magnitude than the one due to climate change (Cuo et al., 2013; Zhao et al., 2009; Zheng et al., 2009). In general, assessing the contribution of land-use and climate changes on streamflow changes is difficult and uncertainties are large (Cuo et al., 2013; Kling et al., 2014; Mehdi et al., 2015). In irrigated regions, the choice of irrigation techniques and cropping patterns can support the adaptation to climate change (Mehta et al., 2013; Woznicki et al., 2015). However, because of water-resources limitation and increasing irrigation needs, irrigation often worsens effects of climate change on hydrological processes in semi-arid climates (e.g., Candela et al., 2009).

Because of the interactions between climate and land-use changes, the increase in irrigation needs or in irrigated area, which might be as high as 50% of the current irrigated area in the Ebro region (Bielsa and Cazcarro, 2015), is likely to have impacts beyond the direct increase in water use. Apart from its importance for the regional water resources, irrigation management might influence the response of the catchment to climate change. An irrigated and a non-irrigated catchment might react differently to the same changes in climate. However, the extent and nature of these differences in climate sensitivity is unknown.

In this study, we analyze some of these differences to better understand the interactions between irrigation and climate change. We concentrate on a catchment-scale case study, situated in north-east Spain. The Lerma catchment experienced a monitored transition to irrigated agriculture in the years 2006–2008 allowing us to simulate the hydrological processes in this catchment, before and after the implementation of irrigation. Then, we model the studied catchment assuming different irrigation scenarios and a scenario without irrigation in present and future climate. The differences in the catchment responses to climate change can be linked to irrigation practices and used to improve the understanding of interactions between climate change and irrigation. Our comparison is centered on a specific case study. However, climate, geology, and agricultural practices in many catchments in the Ebro region are similar to those in the Lerma catchment. Hence, our results are relevant for the whole region, especially because of the planned expansion of irrigated agriculture.

The remainder of this paper is structured as follows: First, we review the study area and the hydrological model. Then, we describe the climate and the irrigation scenarios. Finally, we present our results about the impact of climate change on hydraulic heads, base flows, peak flows, and actual evapotranspiration assuming different irrigation scenarios.

2. Study area

The Lerma catchment ($\sim$42.06° N, $\sim$1.14° W, Fig. 1) is located in the central Ebro basin. Current climate is classified as semi-arid with a mean annual precipitation of 402 mm/year (2004–2011) and a mean reference evapotranspiration (ET_0) of 1301 mm/year (2004–2011) (Merchán et al., 2013). Daily precipitation and temperature have been measured since 1989 at the meteorological station of Ejea de los Caballeros, located $\sim$5 km to the north of the catchment. Wind speed, radiation and relative humidity have been measured there since 2003. Annual total precipitation has varied between 236 mm/year and 630 mm/year over that period of time. Most rains fall in autumn and spring, while summers are usually drier and characterized by long periods of anticyclonic conditions.

The catchment is about 7.3 km² large with elevation ranging between 330 meters above sea level (masl.) and 490 masl. Agriculture is currently the dominant land use (Pérez et al., 2011). However, prior to 2006, irrigated agriculture was not practiced in the catchment. Irrigation started in April 2006 and has been expanding since. Currently, the area of irrigated land is about half of the watershed. The volume of irrigation was 2.1×10^6 m³/year in 2011 (Merchán et al., 2013) and none prior to 2006 (Table 1). Irrigation is recorded daily in 52 zones, which are generally defined based on the limits of the fields owned by each farmer. The majority of irrigation is applied from April to September and the main cultivated crops are corn, winter cereal, and sunflower (Table 2). The irrigation water is provided from the Aragon river whose flow is stored in the Yesa reservoir, situated about 70 km to the north of the catchment in the Pyrenees. After being transported using the Bardenas irrigation canal, the irrigation water is distributed in the catchment using sprinklers in 86% of the irrigated area and drip irrigation otherwise (Abrahao et al., 2011). No groundwater is used for irrigation or for water supply within the catchment.
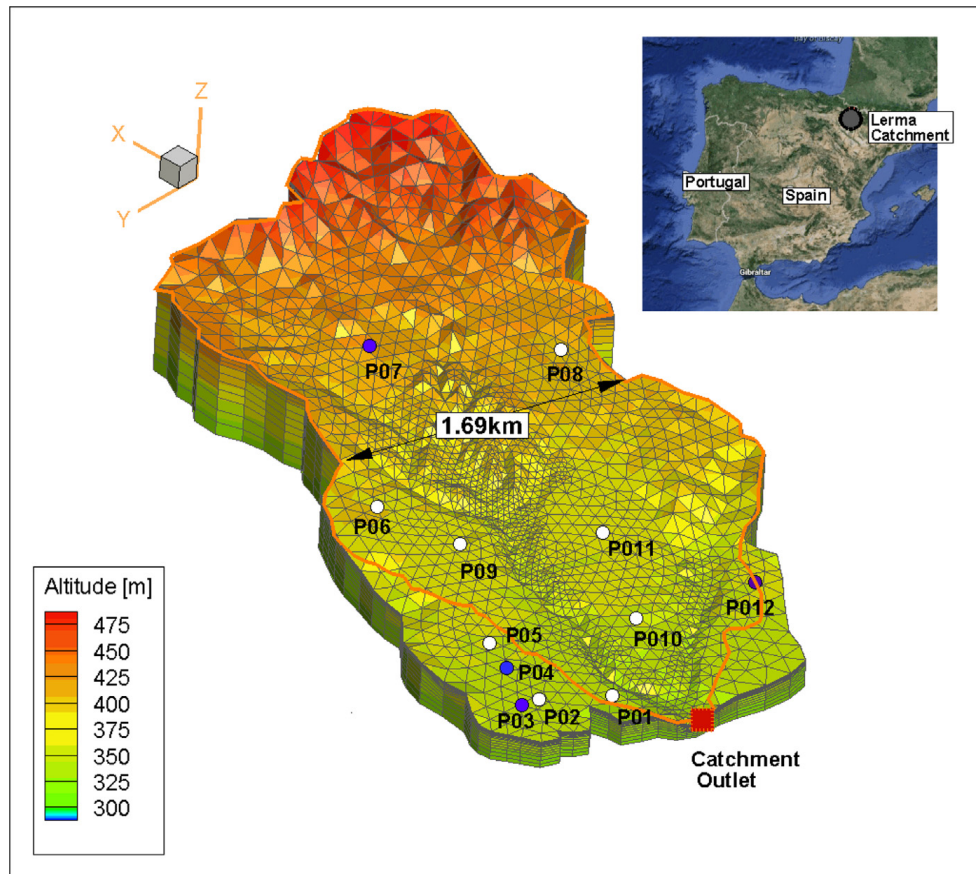
Fig. 1. Elevation of the Lerma catchment (masl.) and the computational grid of the hydrological model. Vertical exaggeration: 5:1. The catchment outlet is indicated by a red square, the wells installed in 2008 are indicated by white dots, and the ones installed in 2010 by blue dots. The orange line represents the limits of the surface-flow domain. (For interpretation of the references to color in this figure legend, the reader is referred to the web version of the article.)

Table 1
Yearly volume of irrigation – from Merchán et al. (2013).

Year	Irrigation [hm^3]
2005	0.00
2006	0.62
2007	1.59
2008	2.00
2009	2.01
2010	2.03
2011	2.07

Table 2
Area of cultivated crops in the Lerma catchment for 2009–2011, in % of total irrigated area (3.54 km^2). Year 1, 2, and 3 are used to define the 4th irrigation scenario. (Section 5).

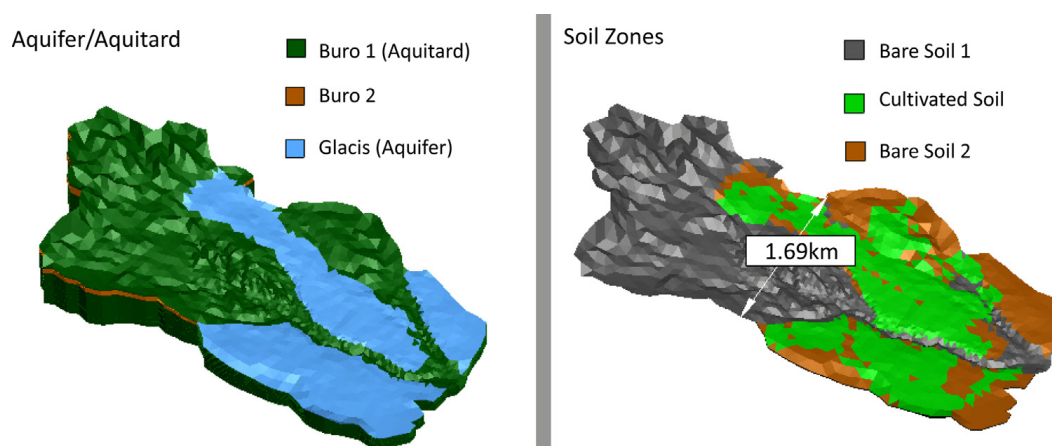| Crop type	Present			Future		
	2009	2010	2011	Year 1	Year 2	Year 3
Corn	39	36	47	15	13	20
Winter cereal	15	18	12	39	40	38
Tomato	8	5	0	8	5	0
Sunflower	13	3	8	0	0	0
Grass	4	3	4	17	6	12
Other crops	5	26	23	5	27	24
Fallow	16	9	6	16	9	6

Fig. 2. Conceptual model of the catchment: hydrogeological and soil units. Vertical exaggeration: 5:1. Extent of the cultivated soil is shown for the year 2009, present cropping pattern. Modified from von Gunten et al. (2014).

The subsurface of the catchment can be conceptualized as an unconfined aquifer lying above an aquitard. The aquifer, denoted glacis, is composed of permeable, clastic, and unconsolidated deposits from the Quaternary period. It covers about half of the surface of the catchment, in the regions where agriculture is the most intensive. The thickness of this aquifer (average thickness: 6.5 m, maximum thickness: 12.6 m) was measured at 12 observation wells and estimated at 63 other locations during an electrical sounding survey (Plata-Torres, 2012). The aquitard, denoted buro, is a Tertiary bedrock made of lutite and mudstones. The soil layer is shallow, 0.3-0.9 m deep (Beltrán, 1986), and composed of inceptisols (Pérez et al., 2011).

Many studies have been conducted in the Lerma catchment to explore the impacts on the catchment of the transition to irrigated agriculture (Abrahao et al., 2011; Merchán et al., 2013, 2014; Pérez et al., 2011; Skhiri and Dechimi, 2011; Urdanoz and Aragüés, 2011), and measurements are ongoing. Hydraulic heads in the glacis have been measured since March 2008 in eight wells, usually with a monthly frequency. In 2010, four additional observation wells were drilled (Fig. 1). Stream flow discharge at the catchment outlet has been measured since 2006 with a temporal resolution of 15 min. Crop types for each agricultural plot are recorded and planting dates for the region of Ejea de los Caballeros are obtained from Martínez-Cob (2004). A digital elevation model with a horizontal resolution of 5 m (IGN, 2012) was used.

3. Hydrological model

The model used in the study and its calibration have previously been described by von Gunten et al. (2014). Therefore, only a brief summary is given here.

3.1. Conceptual model

The subsurface of the Lerma catchment is separated into six zones, based on the local geology (Fig. 2). The deepest zone represents the buro (aquitard). The aquifer, denoted glacis, forms the second zone. In the parts of the domain where the buro is close to the ground surface, a thin layer exists that represents a weathered zone of the buro with an increased hydraulic conductivity. The soil layer is divided into three zones: the first represents the bare soil above the glacis, the second the bare soil above the buro, and the third the cultivated soil. All zones are considered internally homogeneous and anisotropic with the horizontal permeability being ten times larger than the vertical one.

The surface domain is separated into 55 zones representing fields of different crops (Table 2), described by a seasonal leaf area index and a constant root depth (as given by Pérez et al., 2011; von Gunten et al., 2014). These fields are very similar to the 52 zones used for irrigation inputs (Section 2). The difference between surface and irrigation zones is that three irrigation zones are separated in two halves each, representing areas with different crops. Manning's roughness coefficient n, and thus surface run-off, depends on the crop type and hence is assigned depending on the above described zones. Daily crop evapotranspiration under standard conditions (ET_c), corresponding to the maximum evapotranspiration of each crop without water limitation, is calculated using the FAO version of the Penman-Monteith equation (Allen et al., 2000). The spatial variability of the crops on the field scale is taken into account by multiplying the reference evapotranspiration by a time-varying crop coefficient. We use different crop coefficients, directly taken from Allen et al. (2000), for the 10 main crop types cultivated in the catchment. Precipitation inputs are described by daily values for mild precipitation events (less than 25 mm/day). During more intense precipitation events, the total daily precipitation is assumed to occur within 3 h during summer and spring, and within 9 h during autumn and winter. This procedure mimics intense convective precipitation events that frequently occur in this area, especially during summer (von Gunten et al., 2014).
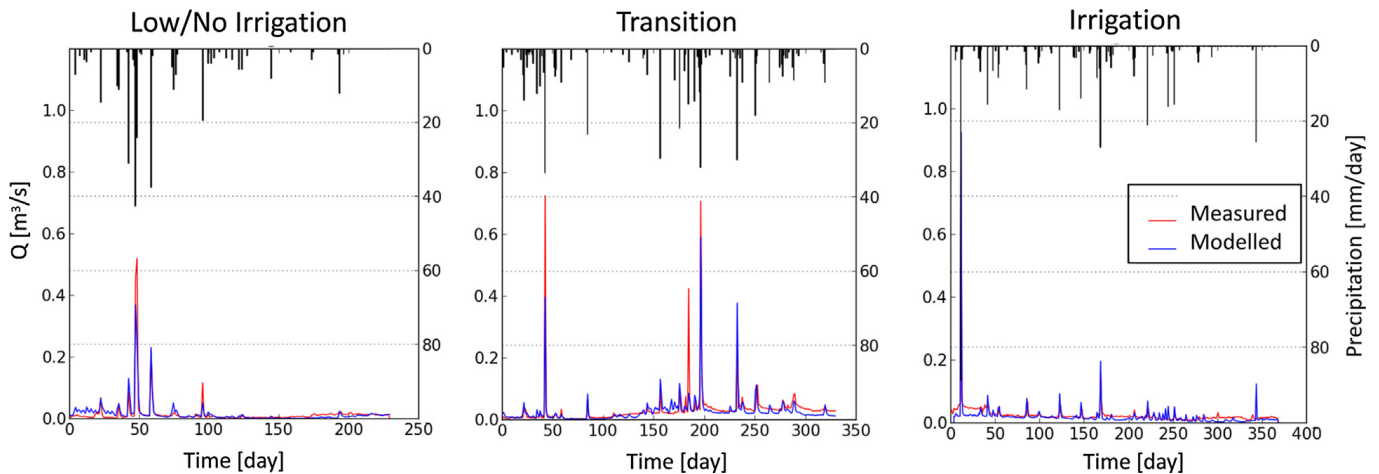
Fig. 3. Measured and modeled hydrograph for a period with no irrigation (start: 15th March 2007, left panel), a transition period (start: 18th May 2008, middle panel), and a period with large irrigation (start: 26th Oct. 2010, right panel). Modified from von Gunten et al. (2014).

A no-flow boundary condition is assumed at the bottom and the lateral sides of the sub-surface model domain. The boundaries of the model domain are based on the boundaries of the aquifer in the lower part of the catchment and on the surface catchment in the upper part of the domain, where there is no permeable layer (glacis). The boundaries of the aquifer are derived from an electrical sounding campaign (Plata-Torres, 2012) and the boundaries of the surface catchment are based on topography. The surface catchment is slightly smaller than the model domain. Hence, surface runoff outside the surface catchment is allowed to leave the model domain by assuming a critical-flow-depth boundary condition at the lateral boundaries of the domain. The computational grid is composed of ~80,000 elements separated in 22 horizontal layers. The mean surface area of the elements is about 0.2 ha and the thickness of the computational layers varies between 8 mm and 25 m, but is about 1–3 cm for the three first layers.

3.2. Numerical model

The hydrological model used in this study, HydroGeoSphere (Therrien, 2006; Therrien et al., 2010), is a well-established spatially distributed partial-differential-equation-based model. This type of model was more suitable than simpler conceptual models to simulate the hydrological changes due to the onset of irrigation (Pérez et al., 2011). In addition, the impacts of climate change on surface and subsurface water bodies can jointly be studied. Moreover, the coupling between surface and subsurface, and the low reliance of this kind of model on empirical relationships might improve its predictive power (Goderniaux et al., 2009).

In HydroGeoSphere, variably-saturated subsurface water flow is modeled using the three-dimensional Richards' equation (Richards, 1931). To solve the Richards' equation, a constitutive relationship between water saturation, relative permeability, and hydraulic heads is needed. In this study, we use the well-known Mualem-van-Genuchten parametrization (van Genuchten, 1980). The surface flow is simulated using the diffusive-wave approximation of the two-dimensional Saint Venant equations (Moussa and Bocquillon, 2000). The calculation of actual evapotranspiration depends on ET_c, soil–water saturation, and crop types (Therrien et al., 2010). Surface and subsurface flow are coupled by the dual-node approach (Therrien et al., 2010). Infiltration and exfiltration are conceptualized using an approach adapted from Darcy's law. The flow between the surface and the subsurface domains is a function of the head differences between the two domains, the relative permeability, and the coupling length, which is a parameter describing the connectivity between the surface and the subsurface. Irrigation and precipitation are implemented as a prescribed volume flux per area to each element. Precipitation is applied to the whole model domain, while irrigation is assigned to the area of each individual field.

3.3. Model calibration

von Gunten et al. (2014) presented the calibration of the model using a hierarchy of grids. Hydraulic heads in 12 observations wells and the hydrograph at the catchment outlet for the years 2006–2009 were used to calibrate the model parameters which had been identified as the most sensitive ones with respect to the calibration targets (i.e., the hydraulic conductivity in all model zones, except from the zone representing the weathered buro, the porosity, and the van-Genuchten parameters in the soil zones). Model validation was performed using the same data types for the years 2010–2011. More details on the calibration have been reported by von Gunten et al. (2014) and are not repeated here. The result of the calibration for the hydrograph and the observation wells are reproduced in Figs. 3 and 4. The Nash-Sutcliffe efficiency (NSE, Nash and Sutcliffe, 1970) is larger than 0.7 for discharge (Table 3), and the difference between measured and modelled mean hydraulic heads is less than 2 m, which is close to the annual variability in most wells. Moreover, the variability of the hydraulic heads is
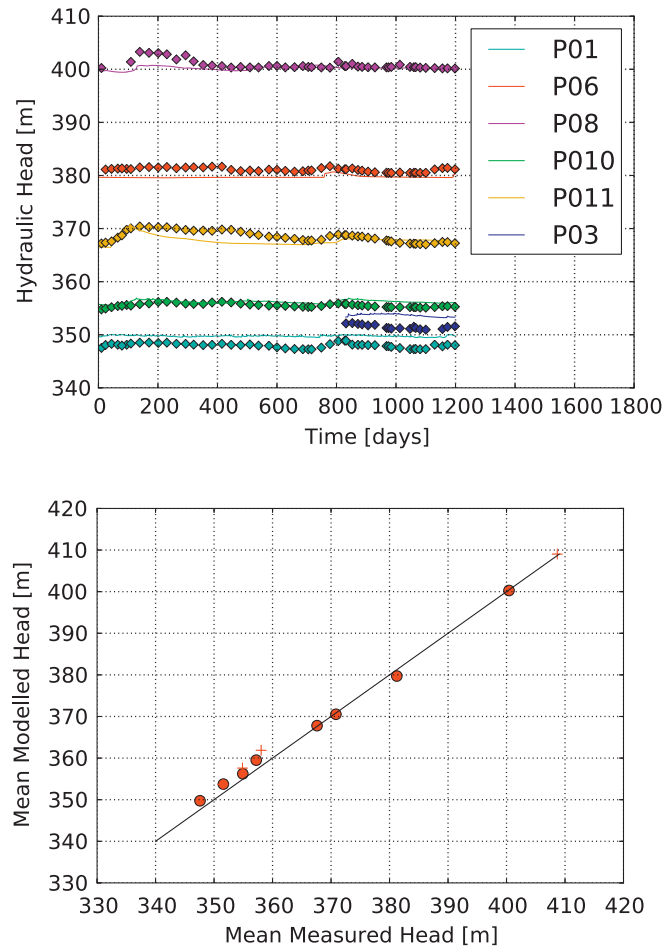
Fig. 4. Left panel: Measured (squares) and modeled (solid lines) transient hydraulic head for selected wells (start: 1st October 2008). Right panel: Average modeled and measured hydraulic-head values for all wells (2008–2011). The wells are from the lowest to the highest hydraulic head: PO1, PO2, PO3, PO10, PO4, PO5, PO12, PO11, PO9, PO6, PO8, PO7. Modified from von Gunten et al. (2014).

Table 3
Goodness-of-fit measures for calibration and validation periods. Spring of 2010 is excluded from the analysis because of strong snow events and because of the breakage of the main irrigation pipe, causing a flooding in the study area. From von Gunten et al. (2014).

	2006–2009	2010–2011
NSE	0.74	0.92
RMSE [%]	3.16	1.36

Table 4
Calibrated parameters for hydraulic conductivity, porosity and van Genuchten parameters. From von Gunten et al. (2014).

Parameter	Units	Calibrated value	Parameter role
K_{bs1}	m/s	$3*10^{-6}$	Hydraulic conductivity – Bare soil 1
K_{bs2}	m/s	10^{-6}	Hydraulic conductivity – Bare soil 2
K_{cs}	m/s	$8*10^{-5}$	Hydraulic conductivity – Cultivated soil
K_{g1}	m/s	$1.7*10^{-4}$	Hydraulic conductivity – Glacis
K_b	m/s	10^{-7}	Hydraulic conductivity – buro
α_{bs1}	1/m	4.95	van Genuchten parameter – Bare soil 1
α_{bs2}	1/m	4	van Genuchten parameter – Bare soil 2
α_{cs}	1/m	4	van Genuchten parameter – Cultivated soil
n_{bs1}	–	1.35	van Genuchten parameter – Bare soil 1
n_{bs2}	–	1.4	van Genuchten parameter – Bare soil 2
n_{cs}	–	1.35	van Genuchten parameter – Cultivated soil
$\theta_{s,g1}$	–	0.2	Porosity – Glacis

Table 5
Name and acronym of the analyzed regional climate model from the ENSEMBLES project. Adapted from (Herrera et al., 2010).

Acronym	RCM	GCM	References
ETHZ	CLM	HadCM3	Jaeger et al. (2008)
METO	HadRM3	HadCM3	Collins et al. (2006)
MPI	M- REMO	ECHAM5	Jacob et al. (2001)
UCLM	PROMES	HadCM3	Sánchez et al. (2004)
METNO	HIRHAM	HadCM3	Haugen and Haakensatd (2005)
KNMI	RACMO	ECHAM5	van Meijgaard (2008)
CNRM	ALADIN-Climat	ARPEGE	Radu et al. (2008)
ICTP	RegCM3	ECHAM5	Pal et al. (2007)
SMHI	RCA	ECHAM5	Kjellström et al. (2005)
DMI	HIRHAM	ARPEGE	Christensen et al. (2006)

generally reproduced by the model, even if annual variability is sometimes underestimated in the wells close to the aquifer boundary (such as PO1, PO8 or PO9). Calibrated parameters are presented in Table 4.

4. Climate scenarios

In this study, future CO_2 emissions follow the IPCC scenario A1B (Nakićenović et al., 2000), which consists of a generally large CO_2 flux and rapid economic growth, consistent with an increase in irrigated agriculture. Climate predictions resulting from this emission scenario are based on the ENSEMBLES project (Hewitt and Griggs, 2004 http://www.ensembles-eu.org), which proposed future climate scenarios for Europa, based on ten regional climate models (RCM) driven by three global climate models (GCM). Table 5 lists the different RCMs and GCMs used in this study.

4.1. Choice of regional climate model

Because the various climate models are constructed differently, notably in the representation of cloud physics (van der Linden and Mitchell, 2009) and of land surface/atmosphere interactions (Flato et al., 2013), a relatively large inter-model variability can be observed in the ENSEMBLES forecast (van der Linden and Mitchell, 2009). For example, predicted changes in mean winter precipitation for 2050 on the Iberian Peninsula vary between −30% and +20% of the present precipitation (van der Linden and Mitchell, 2009). Estimation of future climate impacts is therefore usually based on the output of more than one combination of regional and global climate models (Tebaldi and Knutti, 2007). Nevertheless, incorporating the outputs from regional climate models that poorly reproduce the measured local meteorological variables during the control simulation most likely deteriorates the quality of the prediction (Herrera et al., 2010). Therefore, in order to create meaningful climate scenarios, it is necessary to choose the more suitable regional climate models. While precipitation is especially important for hydrological catchment responses, it is difficult to predict (Ghosh and Misra, 2010). The reproduction of local and regional precipitation is therefore used in this study to select regional climate models for future climate predictions. This analysis is based on the assumption, commonly applied in environmental modeling, that reproducing the observed time series is a pre-requisite to predict future conditions (e.g., Hill and Tiedeman, 2007). However, reproducing the observations alone does not insure an adequate prediction, which depends on the skill of the model to reproduce changes, such as an increase in temperature. Regional and global climate models are, however, generally based on conservation principles, which hold in all climates. Moreover, they have been validated by testing their ability to reproduce climate change of the past, such as cooling caused by historical volcano eruptions (Yokohata et al., 2005) or the last glacial maximum (Kubatzki et al., 2006). Hence, we assume that the selected regional climate models will predict the future climate adequately.

To perform the model selection, we compare the precipitation output of the control simulation of the 10 regional climate models listed in Table 5 and the measured precipitation at the station of Ejea de los Caballeros. The RCM cell containing the Lerma catchment and the mean of the 8 cells of the RCM surrounding the study area were considered to rank the performance of each regional climate model. We compared monthly mean and standard deviation of the precipitation, the number of dry days in each month, and the root mean square error between the frequency distributions of modeled and measured daily precipitation. For each tested statistic, a rank was given to each model and all the ranks were added to find the most suitable models (Table 6). Four RCMs (ETHZ, METO, MPI, and UCLM) outperform the other regional climate models, based on the considered statistics.

Because of the small number of computational cells involved, the comparison described above can be misleading. Measurements and RCM outputs might be similar at a local level even though they do not reproduce the regional climate well. Consequently, we checked our results using a study of Herrera et al. (2010) who compared measured precipitation and output from the ENSEMBLES project across Spain. In this study, five regional climate models (MPI, ETHZ, UCLM, METO, and KNMI) are found to have a noticeably higher spatial correlation (between 0.7 and 0.8) with the measurements than the four other (The ICTP model was not considered by Herrera et al. (2010)). Because their ability to reproduce the local and regional precipitation, we use the MPI, ETHZ, UCLM, and METO regional climate models to create climate scenarios for the Lerma catchment.

Table 6
Ranks of the RCM for the reproduction of mean monthly precipitation (Mean), monthly standard deviation (Std), frequency distribution (Freq), number of dry days (Dry) in the Lerma catchment and the spatial correlation between the Spanish yearly climatology and the different RCMs from Herrera et al. (2010) (Corr). The ranks ranges from 1 (best) to 10 (worst). Hence, the better models have the smaller marks. The models selected for the production of the climate scenarios are indicated in bold fonts. Days are considered dry if less than 1 mm/day of precipitation is recorded.

RCM	Mean	Std	Freq	Dry	Corr	Total
ETHZ	2	2	2	2	3	11
METO	1	5	1	1	5	13
MPI	3	1	3	5	4	16
UCLM	6	4	5	3	2	20
METNO	5	7	4	4	6	26
KNMI	7	8	7	6	1	29
CNRM	4	3	6	7	9	29
ICTP	9	9	10	10	–	(38)
SHMI	8	6	8	9	8	39
DMI	10	10	9	8	7	44

4.2. Downscaling of the climate scenarios

Because of the mismatch between the scale of the outputs of the RCM ($625 \, \text{km}^2$) and of the study area ($7.3 \, \text{km}^2$) and because of the modeling uncertainties related to the climate models, RCM outputs cannot directly be used as input for the hydrological simulations (van Roosmalen et al., 2011). Instead, it is necessary to downscale the raw climate scenarios to the catchment scale. There are different methods to downscale climate inputs (Wilby and Wigley, 1997) which may result in significantly different scenarios. While no downscaling method has been univocally identified as superior over all others (Fowler et al., 2007), stochastic methods based on weather generators are often considered advantageous (Goderniaux et al., 2011; Holman et al., 2009) as they consider natural climate variability. We have used this approach as the main method to downscale the outputs of the regional climate models. To test the consistency of our results, we additionally used a quantile-based bias-correction method. Both downscaling methods are briefly presented here.

4.2.1. Downscaling by a weather generator

A weather generator is a statistical model that generates artificial time series of meteorological variables with a set of defined statistical properties that are identical to those of a reference time series. In this study, we use the RainSim weather generator (Burton et al., 2008) for precipitation and the EARWIG weather generator (Kilsby et al., 2007) for temperature, radiation, relative humidity and ET_0. RainSim is based on a Neyman-Scott rectangular pulses stochastic model (Burton et al., 2008) while EARWIG is based on first-order autoregressive processes, separating dry and wet periods (Kilsby et al., 2007). Both weather generators have been used for downscaling purposes before (e.g. Burton et al., 2010; Goderniaux et al., 2011).

The weather generators are calibrated using 24 years of daily precipitation (1989–2012) and 8 years of daily radiation, relative humidity, maximum, and minimum temperature (2004–2012) from the station of Ejea de los Caballeros. After the calibration, the RainSim performance has been evaluated by the following statistical properties of precipitation: Monthly mean, monthly variance, number of dry days, monthly skewness, frequency distribution of dry spells, frequency distribution of wet spells, annual daily maximum, and the length of longest period of the year without precipitation. Afterwards, the performance of EARWIG has been evaluated by the monthly mean of minimum and maximum daily temperature, sunshine hours, and relative humidity as well as the mean and the variance of the reference evapotranspiration. Fig. 5 presents the results of the weather-generator evaluation for the mean and skewness of precipitation, the mean, and variance of evapotranspiration and the length of dry spells. The other tested variables are not shown here for brevity, but results are similar. For each variable, the difference between the modeled and measured yearly average is less than 8%, except for the difference in the mean ET_0 variance which is 10.6%. The variables which are not directly used to calibrate the weather generators, such as the skewness of the precipitation or the frequency of dry spells, perform similarly (less than 8% of difference) as the calibrated ones.

To downscale future precipitation using RainSim, monthly change factors are extracted from the regional climate models, following the approach of Burton et al. (2010). Monthly mean rainfall, duration of dry spells, mean monthly variance and 1-day auto-correlation from the 1990 to 2000 decade are compared to the 2040–2050 decade in each regional climate model. Statistical properties of the calibrated weather generators are corrected using these change factors to calibrate RainSim for the future climate. For ET_0, a similar procedure is carried out in EARWIG. In this case, we use the mean monthly temperature, the variance of daily temperature, the mean and variance of the daily temperature range, the monthly mean of relative humidity, and the sunshine hours as target properties. We use 30 realizations of the weather generators, i.e., 30 modeled time series of daily precipitation and ET_c with a duration of 8 years each, for each group of hydrological simulations. The number of realizations was chosen by running the hydrological model with 100 realizations of the present climate without irrigation. We compared hydraulic heads in four observations wells (PO8, PO9, PO10, PO11), actual evapotranspiration (AET), and the yearly maximum and mean discharge at the outlet. The average value and variance of these hydrological variables over all realizations is very similar when more than 20 simulations were considered. We use 30 realizations, a number that was also considered to be sufficient in a case study in Belgium (Goderniaux et al., 2011).
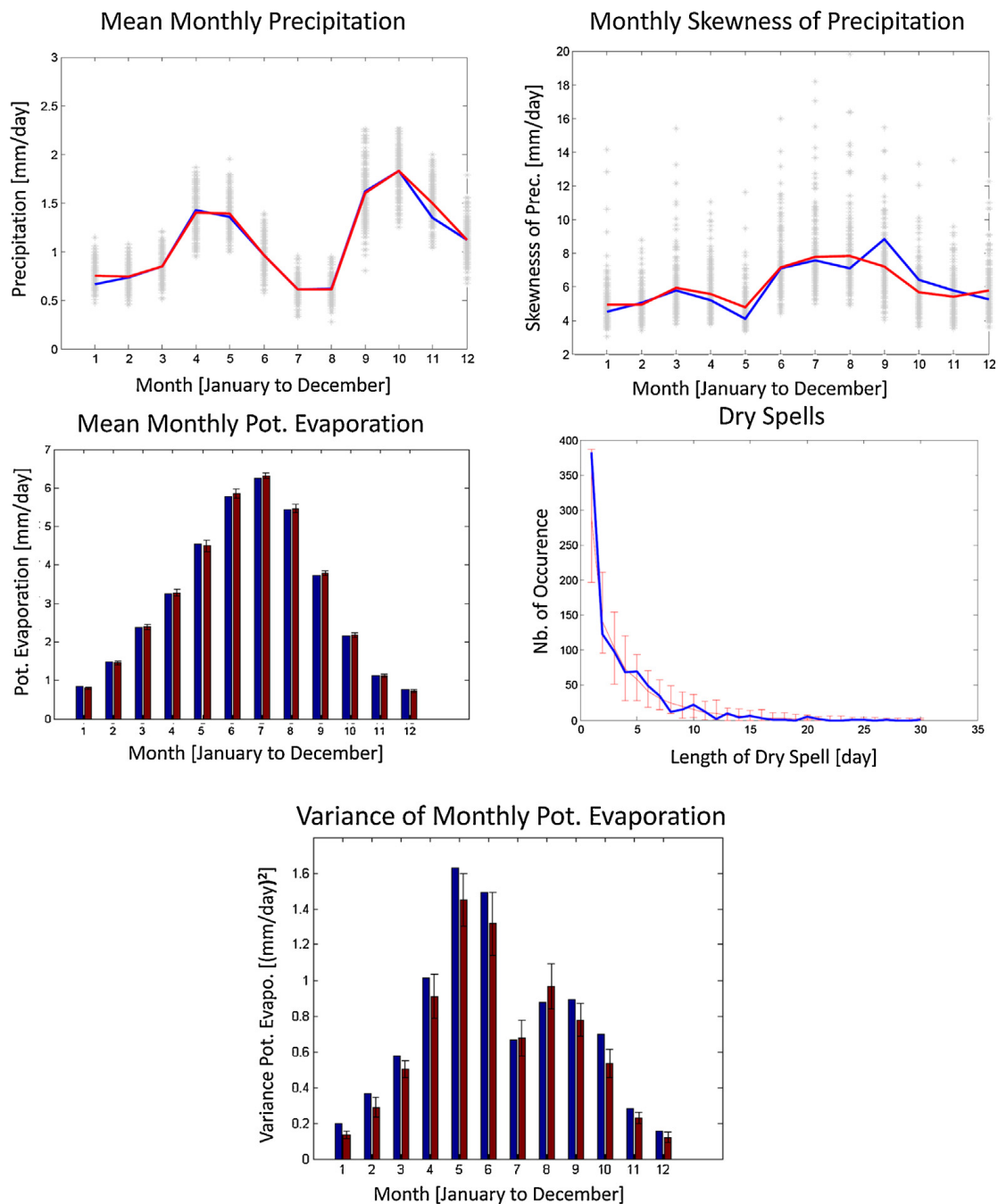
Fig. 5. Validation of the weather generator: mean and skewness of precipitation, length of dry spell, and mean and variance of reference evapotranspiration. The measured data are shown in blue and the model results in red. The error bar (bottom figures) and the gray stars (top figure) are showing the spread of the different realizations of the weather generator. (For interpretation of the references to color in this figure legend, the reader is referred to the web version of the article.)

4.2.2. Bias correction based on the mapping of quantiles

The quantile-map approach, summarized in Eq. (1), is a downscaling method which compares the frequency distribution of measured and modeled meteorological variables (Li et al., 2009). It is assumed that the computed differences are stable over time. Practically, for each value x_i of a meteorological variable for the future climate, the corresponding percentile of this variable is found in the modeled simulation for the present climate, given by the frequency distribution F_{crtl}. The bias corrected value x_{corr} of this variable for the future climate is then found in the inverse of the frequency distribution of the measured data F_{mes}.

$$x_{corr} = F_{mes}^{-1}(F_{crtl}(x_i)) \qquad (1)$$

Using this method, the RCM output in a future climate can be corrected to create future climate scenarios, which are consistent with measurements and predictions from the regional climate models. We use outputs of the regional climate models from 1990 to 2000 to compare the measured and modeled frequency distribution of daily precipitation, minimum
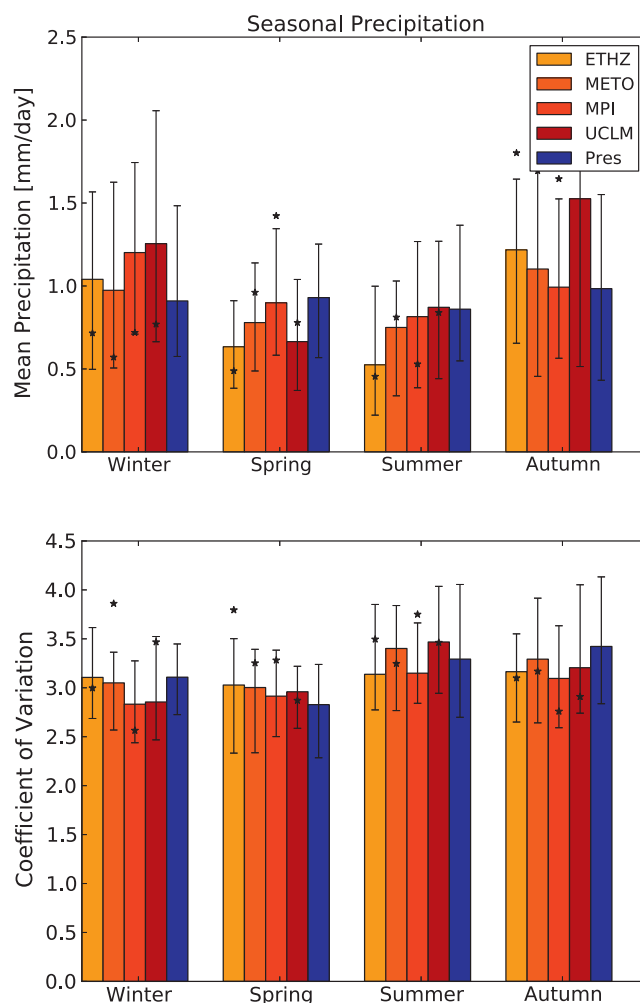
Fig. 6. Monthly mean and coefficient of variation for present and future precipitations. Based on IPCC A1B emission scenarios for 2040–2050. The error bars represent the span of the 30 realizations of the weather generator. The scenarios that are downscaled using the quantile–quantile transformation are indicated by stars. Meteorological seasons are used.

and maximum daily temperature, relative humidity, and short-wave radiation. This method produces daily time series, but the frequency distribution is based on monthly data to better reproduce the temporal auto-correlation (e.g., Ntegeka et al., 2014). The RCM outputs for the years 2040–2050 are used to create the scenarios for future climate.

4.3. Results from the climate projections

4.3.1. Precipitation

The RCM predictions for changes in mean annual precipitation differ among each other. The MPI and UCLM models forecast an increase in precipitation while the two other RCMs (ETHZ and METO) forecast a decrease. We aggregated the average predicted precipitation and the variance by season (Fig. 6) for comparison purposes. All regional climate models predict an increase in precipitation in winter and autumn (between 1% and 55%) and most models predict a decrease in summer and spring precipitation (between 3% and 39%). UCLM predicts a small precipitation increase (1.3%) during summer, which is probably not significant. Blenkinsop and Fowler (2007) found a similar seasonal pattern for the Ebro region, using regional climate models from the PRUDENCE project (Christensen and Christensen, 2007) for 2070–2100 and the A2 emission scenarios (Nakićenović et al., 2000).

Considering precipitation variability, the coefficient of variation decreases in autumn and winter (between −0.1 and −10%) and increases in spring (between +3 and +6%). Results are not unequivocal for summer (between −5% and +5%). Overall, the precipitation results from the quantile-mapped downscaling method are in agreement with those from the weather generator, i.e., the results from the quantile-mapped method fall into the spread of the realizations of the weather generator.

4.3.2. Reference evapotranspiration

Reference evapotranspiration (ET_0) increases in all RCM predictions (Fig. 7) because of the predicted increase in temperature and because of the predicted changes in relative humidity and solar radiation. The increase in total annual ET_0 ranges
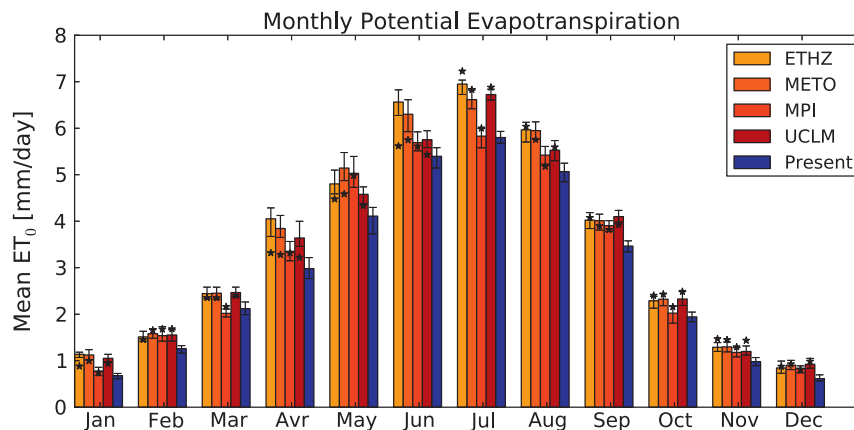
Fig. 7. Comparison of present and future ET_0. IPCC A1B emission scenarios for 2040–2050. The error bars represent the span of the 30 realizations of the weather generator. The scenarios downscaled using the quantile mapped method are indicated by stars.

from 9% in UCLM to 22% in ETHZ, and is higher in summer than in winter. A small decrease in the coefficient of variation of ET_0 is predicted, for example, from 0.3 under current conditions to 0.28 under future conditions in the ETHZ case. Variations between the realizations of the weather generator for ET_0 are low, compared to the differences between the realizations of the weather generator for precipitation.

The climate scenarios for ET_0 downscaled with the quantile mapped methods are in general similar to those using the weather generator (Fig. 7). However, ET_0 predictions based on the weather generator for ETHZ and METO between April and June are larger than the results based on the quantile-mapped method, i.e., the results from the quantile-mapped method fall under the spread of the realizations of the weather generator in these cases.

4.4. Length of observation time series and hydrological simulations

Climate change should not be confused with weather variability. Long time series are therefore necessary to create stable averages, which do not depend on short-term weather variations. This is especially important when considering precipitation. In our case, precipitation has been measured for 24 years, which was found to be sufficient to validate the weather generator. Shorter precipitation measurement time series have been used successfully in other climate-impact studies (e.g., Bouraoui et al., 1999; Fujihara et al., 2008). The time series of relative humidity, temperature, and short-wave radiation used in the present study have a duration of 8 years only, but these variables exhibit a lower variability. Therefore, we assume that the computed averages are meaningful. It is further assumed that the weather generator reproduces the general characteristics of the measured ET_0 time series (Section 4.2.1 and Fig. 5), even if the measured time series are relatively short.

We chose a length of 8 years for each of the 30 hydrological simulations (Section 4.2.1). We did not model the 240 years consecutively to reduce simulation time. In each hydrological simulation, the first two years were found to be sufficient to let the model equilibrate to the new climatic conditions ("spin-up"). These years are not considered in the analysis. While surface water reacts quickly, usually in less than a day, groundwater responds more slowly, but the aquifer is shallow (maximum depth: 12.6 m) and has a relatively large hydraulic conductivity, with a calibrated value of 1.7×10^{-4} m/s, consistent with local observations (Pérez, 2011). In addition, we found similar results for the cumulated distribution function of discharge and hydraulic head in observation wells for the scenarios without irrigation and with present irrigation when we used three or four years as spin-up periods. Consequently, we produced 30 realizations with a duration of 8 years each with the weather generator. The total length of the simulated time series is therefore $(8-2)$ years $\times 30 = 180$ years for each climate and irrigation scenario. The results using meteorological forcings that were downscaled with the quantile mapped method are used to validate the simulations whose forcings were based on the weather generators.

5. Irrigation scenarios

5.1. Methodology

To compare the impact of climate change under different agricultural managements, we considered four irrigation scenarios, representing potential agricultural practices. These scenarios were combined with the climate predictions presented above.

1. No irrigation: In this scenario, the catchment is not used for agriculture. This reflects the situation in the Lerma catchment in the years 2003–2005 and in many catchments in the Ebro region. Currently, only about 11% of the Ebro region is irrigated (Milano et al., 2013).

2. Present irrigation: Observed irrigation and crop types of the years 2009, 2010, and 2011 (Table 2) are used in the following order: 2009, 2010, 2009, 2010, 2011, 2009, 2010, 2011, with the two first years used for model spin-up. Daily distribution of irrigation at field scale is identical to the measured one.

3. Future irrigation and present cropping pattern: We use the same crop types as in scenario 2, but the irrigation volume is increased to adapt to the higher evaporative demand. Future irrigation I_{fut} [mm/day] is calculated using the following estimate (Towes and Allen, 2009):

$$I_{fut} = R_I \cdot ET_c - P_{eff} \tag{2}$$

in which ET_c is the daily crop evapotranspiration under standard condition during the irrigation season [mm/day] and P_{eff} the seasonal effective precipitation [mm/day], which is the infiltrating portion of precipitation, estimated as all precipitation under 25 mm/day, based on the definition of mild precipitation in Section 3.1. The excess precipitation (>25 mm/day) is assumed not to contribute to crop growth. R_I [-] represents the effectiveness of irrigation, which is assumed to be identical to the present one. It is calculated to be 1.06, based on data from 2009, 2010, and 2011. Values of $R_I > 1$ indicate that irrigation is larger than ET_c. However, because of surface run-off, infiltration, and soil salinisation risks due to poor irrigation practices, this value is small and shows, on average over the catchment, a well-managed irrigation or even a deficit in the total irrigation. For comparison, Towes and Allen (2009) obtained an R_I between 1.2 and 2.2 in a case study in the Okanagan basin in Canada. A similar observation about irrigation volume has been made by Abrahao et al. (2011) who note that the agricultural production did not reach the maximum potential of the area, possibly because of a water deficit.

Daily distribution of irrigation is identical in our hydrological simulation under present and future climate to reflect the local irrigation management. Under current irrigation management practices, the farmers have to order irrigation water some days before it is available. In addition, there is no precipitation in about 90% of the days in present and future climate during the irrigation period. Therefore, the amount of irrigation water is only weakly linked with daily precipitation and daily precipitation cannot be used to determine the temporal distribution of future irrigation. The spatial and temporal distribution of measured irrigation is used as model input in future climate to reflect growth distribution, crop growth, and irrigation variability between the farms. However, the total amount of irrigation depends on seasonal precipitation, a behavior reproduced by Eq. (2).

4. Future cropping pattern: Predicting the response of the farmers to climatic changes is difficult as their decision is influenced by uncertain social and economic factors in addition to climatic conditions. Their future choice of cropping patterns/crops is therefore unknown. However, we can use their response to recent weather variability as an estimate for future cropping patterns. García-Garizábal and Causapé (2010) record crop types in 2000 and 2007 in the Bardenas Canal Irrigation District no.V, a catchment close to the Lerma catchment with a similar geology and climate. In 2000, water in the Yesa reservoir, which supplies both this irrigation district and the Lerma catchment, was sufficient to meet the irrigation demand. However, in 2007, the water in the reservoir was low and usage had to be restricted. The farmers responded by decreasing the area of their corn fields by about 50% and of their sunflower fields by 90%. Instead, they increased the proportion of winter cereal and grass by 50%. Based on these observations, we assume the following changes in our scenarios with the cropping patterns:

• Sunflowers fields are replaced by grass fields.
• Half of the corn fields are replaced by fields of winter cereal. The modified fields are selected so that about half of the area planted with corn is covered by winter cereal.

These changes are summarized in Table 2. The created cropping patterns were used in the following order: Year 1, Year 2, Year 1, Year 2, Year 3, Year 1, Year 2, Year 3 (Table 2), with the two first years used for model spin-up.

In our analysis, we did not consider any change in plant physiology or plant reaction to increased CO_2 availability. Planting dates are assumed to be identical in present and future climate. These dates are actually influenced by climate but determined by the farmer's management choices. Consequently, a determination of the planting dates based only on temperature changes (as by Serrat-Capdevila et al., 2011) would be inconsistent with actual management practices. We did not consider any change in the length of the growing season.

In all our hydrological simulations, we use the same model parameters as described by von Gunten et al. (2014) (Table 4). When parameters depend on the crop type, as it is the case for Manning's n, the leaf area index, and the rooting depth, they are updated to be consistent with the irrigation scenario. No cultivated zone (indicated in light green in Fig. 2) is present in Scenario 1, in which agriculture is absent.

5.2. Projected irrigation demand

Based on Eq. (2), we predict an increase in irrigation demand of 9.2% on average under future climatic conditions with the present-day cropping pattern. Our results are consistent with earlier studies for the Ebro region (Table 7). Three studies out of five (Fischer et al., 2007; Rey et al., 2011; Jorge and Ferreres, 2001) predict an increase in irrigation demand between 6% and 11%. Two other studies (Döll, 2002; Iglesias and Minguez, 1997) indicate a larger range (3–20%) of future irrigation

Table 7
Predicted irrigation changes in the Ebro region and comparison with literature.

Study	Crops	Model[a]	CO_2-related plant change	Emission scenario[b]	Irrigation increase
This study – ETHZ	Various	ET_c – P	No	A1B/2050	10.3%
This study – METO	Various	ET_c – P	No	A1B/2050	10.6%
This study – MPI	Various	ET_c – P	No	A1B/2050	6.6%
This study – UCLM	Various	ET_c – P	No	A1B/2050	9.3%
Döll (2002)	Various	ET_c – P	No	IS92a/2020	+5-20%
Fischer et al. (2007)	Various	AEZ	Yes	A2/2040	+10%
Iglesias and Minguez (1997)	Corn	CERES	Yes	+600 μmol^{-1}	+3 to +8%
Rey et al. (2011)	Corn	CERES	Yes	A2 /2070	−3%[c]
Jorge and Ferreres (2001)	Corn and Sunflower	CropWat	No	A/2050	+7.5%

^a The method used in this paper "ET_c – P" is described in Section 5. Döll (2002) uses a similar method, described in their paper. CERES is described in Jones and Kiniry (1986), CropWat in Smith (1993) and AEZ in Fischer et al. (2005).

^b The emission scenarios A1B, A2 and A are presented in Nakićenović et al. (2000) and IS92a in Leggett et al. (1992). Scenarios in Iglesias and Minguez (1997) are defined by an increase in temperature (1 or 3 °C) or CO_2 concentration (+600 μmol^{-1}).

^c Before impact of precipitation changes. Precipitation decreases of about 14% in summer (based on the average of the four RCM), which results in an irrigation increase of about 6% with an irrigation of 200 mm/year in present climate.

needs. In the fourth scenario, when expanding crops with a lower water use, the decrease in irrigation needs is between 12% and 15% in the future climate, compared to the current situation.

6. Results from the hydrological simulations

In this section, we analyze the outputs of the different hydrological simulations. These results are based on the hydrological model presented in Section 3. Climate and irrigation inputs are discussed in Sections 4 and 5. Our comparison concentrates on the differences in the hydrological responses of the catchment to climate change, distinguishing between the four irrigation scenarios. We investigate the responses of hydraulic head, base flow, peak flow, and actual evapotranspiration.

6.1. Overview of the water balance

In Fig. 8, we briefly present the yearly water balance of the catchment in scenario 1 (non-irrigated) and scenario 2 (present irrigation) in the present climate. We analyze the individual parts of the water balance in the subsequent sections. Hence, this section only gives a general introduction.

In the Lerma catchment, precipitation is the main water input to the catchment, closely followed by irrigation (350 mm/year and 222 mm/year, respectively). In the lower portion of the catchment, where most of the irrigation is applied, irrigation input exceeds precipitation.

Actual evapotranspiration is the main water loss (about 261 mm/year in Scenario 1 without irrigation) and it increases by 56% if irrigation is present. Discharge is a small part of the water balance in this catchment. It increases in the irrigated cases, reaching 110 mm/year, but it stays noticeably under the actual evapotranspiration volume in all scenarios. Because of the critical depth boundary condition in the surface catchment, precipitation and irrigation which fall outside of the surface catchment but inside the boundary of the aquifer can freely leave the domain (see Section 3.1). This water volume
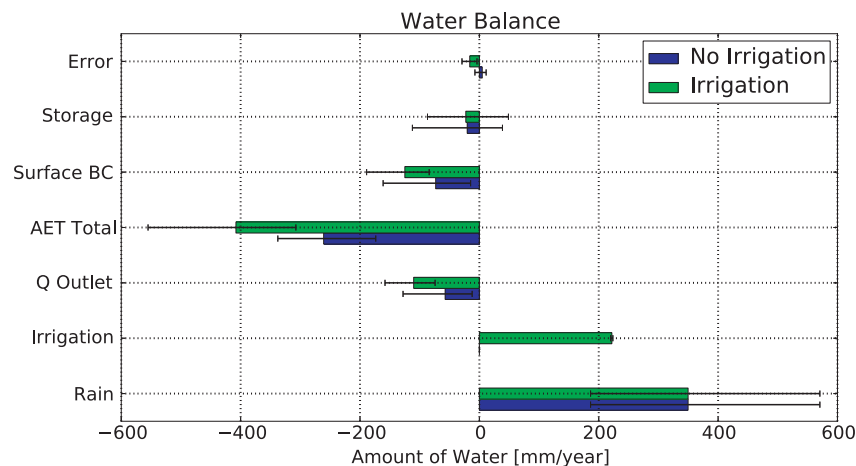

Fig. 8. Water balance of the catchment in the irrigated (Scenario 2) and non-irrigated cases (Scenario 1) for the present climate. See Section 6.1 for the definition of the "Surface BC" component. The error bars represent the spread of the 30 realizations created with the weather generator.
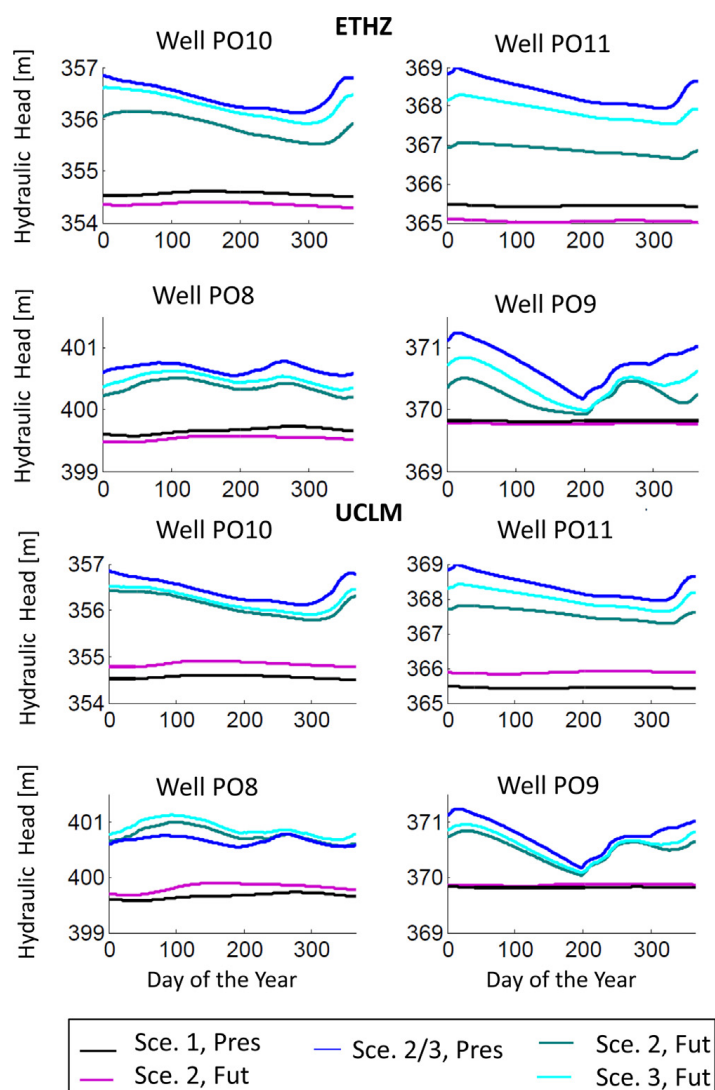
Fig. 9. Daily hydraulic heads in four wells for the scenarios 1 (no irrigation), 2 (present irrigation), and 3 (future irrigation) for the 30 realizations of the weather generator. Average over the 6 hydraulic years and over the 30 realizations (Start: 1st of October).

is indicated by the name "Surface BC" in Fig. 8 and it increases in scenario 2 (with irrigation) because of the additional water volume which enters the fields which are outside of the surface catchment.

Storage is similar with and without irrigation (about −20 mm/year). This storage is not the storage change from the "non-irrigated" (scenario 1) to the "irrigated" (scenario 2) stage. The latter would be larger and positive. The storage indicated in Fig. 8 would be zero on average if the catchment was at steady state. However, the meteorological measurements which inform the weather generator end in 2011. This means that parts of the measurements show a small but noticeable increase in temperature, consistent with the current climate change in the region. Hence, the current climate has a small drying effect on the catchment because of the increase in reference evapotranspiration. However, the storage change is small and close to the model error.

6.2. Hydraulic heads

Fig. 9 shows yearly time series of predicted hydraulic heads (i.e., groundwater level) in four observation wells for the scenarios with no irrigation, present, and future irrigation (scenarios 1, 2, and 3 from Section 5) for the regional climate models ETHZ and UCLM. Hydraulic heads driven by the climate scenarios based on MPI are showing similar results to those based on UCLM and hydraulic heads driven by the climate scenarios based on METO are similar to those based on ETHZ. Consequently, the results of the MPI and METO regional climate models are not shown here for brevity.

Under present climate conditions, predicted groundwater levels are higher when the catchment is irrigated than when it is not. The maximum mean difference is 2.7 m in the observation well PO11 (Fig. 1) but is about 1m for most observation wells, which is consistent with the observed changes during the transition to irrigation. Each observation well responds differently to the irrigation onset. Generally, irrigation seems to strongly affect the wells which are located in the thickest
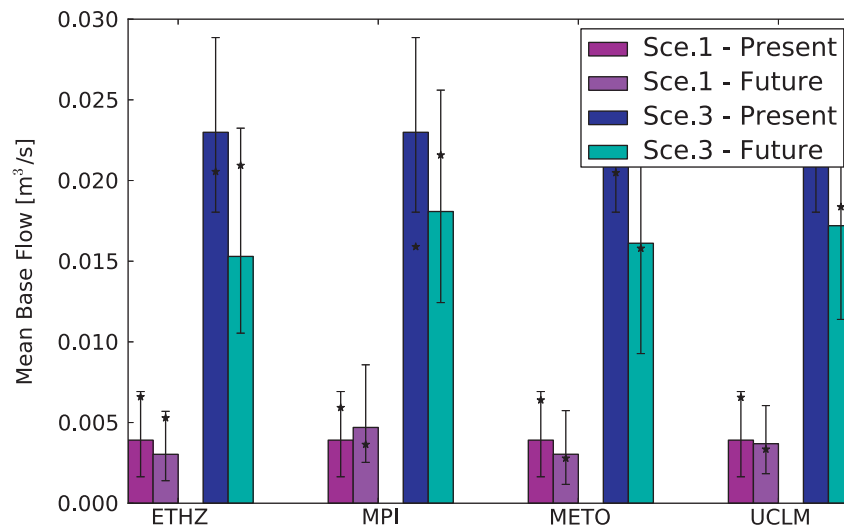
Fig. 10. Present and future base flow in the scenarios without irrigation (Scenario 1) and with future irrigation (Scenario 3). The error bars represent the spread of the 30 scenarios created with the weather generators. The stars indicate the results using the quantile mapped downscaling method.

part of the aquifer (e.g, PO11). Moreover, if a well is close to the aquifer boundaries (such as PO9), its response to irrigation is often less directly related to this impulse because the groundwater flow is affected by the aquifer boundaries.

Hydraulic heads generally decline from present to future climate. The extent of the decrease in hydraulic heads depends on the precipitation outputs of the regional climate models. Two regional climate models (ETHZ and METO) predict a decrease in annual precipitation and two regional climate models (MPI and UCLM) predict an increase in annual precipitation, when compared to the present situation. If the annual precipitation is predicted to decrease, hydraulic heads strongly decrease in all wells. If the annual precipitation is predicted to increase, hydraulic heads often decrease nonetheless, because of the increased ET_c and changes in precipitation seasonality. However, if annual precipitation is predicted to increase, the decrease in hydraulic head is smaller and even an increase in hydraulic head is observed in some wells. In the observation wells PO9, PO10, and PO11 for scenario 2, future hydraulic heads decrease (between 1.3 m and 0.13 m, depending on the wells), regardless of the regional climate model. Nevertheless, the decrease is about 2 times smaller when UCLM or MPI is used instead of ETHZ or METO. Moreover, the predicted mean hydraulic head in the observation well PO8 in scenario 2 (present irrigation) is 0.1 m higher in the UCLM climate scenario than in the present climate. The hydraulic head in this well decreases by 0.25 m when the ETHZ climate scenario is compared to the present level (average of daily data, based on the 30 hydrological simulations). The weaker response of well PO8 to climate change (when compared to other observation wells) may be an artifact of the hydrological model as it underestimates the variability of hydraulic head in this well already under current climate conditions (see the corresponding results of the calibration and validation periods in Fig. 4).

Generally, the impacts of climate change on groundwater levels are larger in the scenarios with irrigation (scenarios 2, 3 and 4) than in the scenario without irrigation (scenario 1). This is particularly true for scenario 2 (present irrigation) because the higher irrigation demand, lower precipitation, and higher ET_c result in a generally decreasing water table. Differences between present and future groundwater levels are nevertheless larger in scenario 3 (future climate and irrigation) than in the scenario 1 (without irrigation). In general, in scenario 1, hydraulic heads decrease only little (about 0.18 m with the ETHZ or METO climate scenarios) or increase only slightly (about 0.15 m, when using MPI or UCLM climate scenario). When irrigation is present, the decrease can be about 1.3 m in Scenario 2 or about 0.4 m in scenario 3 (observation well PO11 in the ETHZ climate scenario).

The increased sensitivity of groundwater levels to climate change in the scenarios with irrigation (2 and 3) is probably a consequence of the higher water table, increased transpiration, soil moisture, and deeper root depth, which are a result of the irrigation onset. The dependence between groundwater levels and climate processes increases when the water table is closer to the surface, especially if the root depth is close to the water level (Kollet and Maxwell, 2008). The mean depth to groundwater in the north of the domain decreased from about 3.7 m prior to irrigation (2005) to about 2.6m after the transition to irrigation (2011). The model considers the root depth (the maximum depth at which plants extract water for transpiration), as a spatially distributed parameter. It is chosen to be 1m for corn (which is the main crop in the catchment) and 0.1 m for uncultivated soil. Hence, the mean distance from the water table to the bottom of the root zone passes from 3.6 m to 1.6 m after irrigation started in the catchment, resulting in a better connection between the water table and the root zone. This range is within the critical depth identified by Kollet and Maxwell (2008) where evapotranspiration is sensitive to the water-table depth. In addition to the decreased depth to the water table, the larger soil moisture results in a higher sensitivity of actual evapotranspiration to ET_c, resulting in a higher sensitivity of recharge to ET_c-changes, and therefore of the groundwater levels to climate change.

6.3. Base flow

In this study, we define base flow as total discharge in days with no precipitation on this day and the previous day. Because of the large hydraulic conductivity of the aquifer and the small size of the Lerma catchment, discharge peaks generally recess in less than a day. Therefore, the total discharge during the periods with no precipitation largely depends on subsurface flow and is a good estimation of base flow. Base flow has similar responses to changes in irrigation and climate as groundwater levels (Fig. 10). In present climate, average daily base flow is 5.8 times higher in presence of irrigation than without. This is similar to the measured response of discharge to irrigation onset. Measured base flow was about 5.2 times larger in the hydrological year 2011 (after the implementation of irrigation) than in 2006 (before the start of irrigation), corresponding to an increase in flow of about 0.015 m³/s. The measured annual precipitation was lower in 2011 (365 mm) than in 2006 (459 mm).

When comparing present and future climate, base flow decreases more in scenarios with irrigation, i.e., scenarios 2, 3, and 4, than in scenario 1 without irrigation. In scenario 3 (with future irrigation), the decrease of mean daily base flow due to climate change is between 33% and 21% of the present base flow, or −0.008 m³/s and −0.005 m³/s, depending on the used regional climate model (average on all hydrological simulations). In scenario 1 (without irrigation), future daily base flow decreases between -9×10^{-4} m³/s and -2×10^{-4} m³/s for the ETHZ, UCLM, and METO climate scenarios and increases of 8×10^{-4} m³/s in the MPI climate scenario. Fig. 10 shows the mean base flow using the four regional climate models for the scenario with no irrigation and future irrigation (Scenarios 1 and 3).

6.4. Peak discharge

On the regional scale, flood risk is low in the Ebro region because of the various reservoirs, that control river flows and cap peak flows (Bovolo et al., 2010). However, flood protection might fail if intense precipitation events occur in rapid succession (López-Moreno et al., 2002) and is not always effective on a local scale, where streamflow depends more on local precipitation events. Moreover, the variability of precipitation is predicted by all regional climate models to increase moderately in the spring and possibly during summer (UCLM and METO, see Fig. 6). This higher variability might increase future peak discharges.

However, the relation between precipitation events and corresponding discharge responses is not linear and depends notably on prior soil moisture conditions (Hill et al., 2010). In the Lerma catchment, before the introduction of irrigation, the soil was generally relatively dry and covered by sparse vegetation. Consequently, during intense convective rainfall events, run-off generation was primarily controlled by the infiltration rate (Pérez et al., 2011). When irrigation was introduced in the Lerma catchment, soil moisture increased and cultivation changed the soil characteristics. These transformations had a strong influence on the run-off generation mechanisms and annual peak discharge decreased. When considering the average of all hydrological simulations in present climate, mean annual maximum daily discharge is 1.42 m³/s in scenario 1, without irrigation, and 0.55 m³/s in the scenarios with irrigation, a 61% decrease. A similar behavior is observed in the measured time series of discharge and has often been noticed in catchments with a semi-arid climate (e.g., Berndtsson and Larson, 1987).

After calibration, our model is able to adequately reproduce these changes. Indeed, because of the fine vertical layering (about 1–3 cm close to the surface), the model allows for a rapid saturation of the surface and shallow subsurface zones (during an event with a large precipitation intensity) and a delayed vertical water movement under low-saturation conditions. Additionally, soil parameters are different for each soil zone, influencing infiltration and peak discharges (Fig. 2). Finally, surface flow velocities are faster when crops are absent because of a lower surface roughness, resulting in a shorter contact time and a lower infiltration in the scenario without irrigation.

Fig. 11 presents the annual daily maximum flow, based on the present and future climate predicted by all regional climate models. Annual maximum flows increase when the coefficient of variation of precipitation is predicted to increase in summer (UCLM and METO), a period of frequent intense precipitation events. The increase is relatively small when comparing the median annual maximum flow over all hydrological simulations. For example, in scenario 1, the median annual peak discharge shows an increase of 0.12 m³/s (8.7%) in the METO case. However, when considering the years with an annual maximum discharge in the higher quartile, the increase is more important, especially in scenario 1 (without irrigation). In this scenario, when considering the years with an annual maximum peak flow in the higher quartile, the annual maximum discharges show an increase of 0.5 m³/s (29%) in the METO climate scenario and of 1.24 m³/s (68%) in the UCLM climate scenario. In scenario 3 (future irrigation), the annual maximum flows in the higher quartile increase, but only moderately. In the METO climate scenario, the increase amounts to 0.13 m³/s. Therefore, without irrigation, changes in precipitation variability in summer, which are linked with an increase in intense precipitation events, have a large impact on peak discharge. When changes in precipitation variability is unclear or when precipitation variability decreases in summer (MPI and ETHZ), annual maximum flow is not showing a clear trend (Fig. 11). Results are similar for all irrigation scenarios (2, 3, and 4).

6.5. Actual evapotranspiration

All regional climate models predict an increase in ET_c. However, because of soil-moisture limitations, this does not automatically imply an increase in actual evapotranspiration (AET). For example, in scenario 1 (without irrigation), future
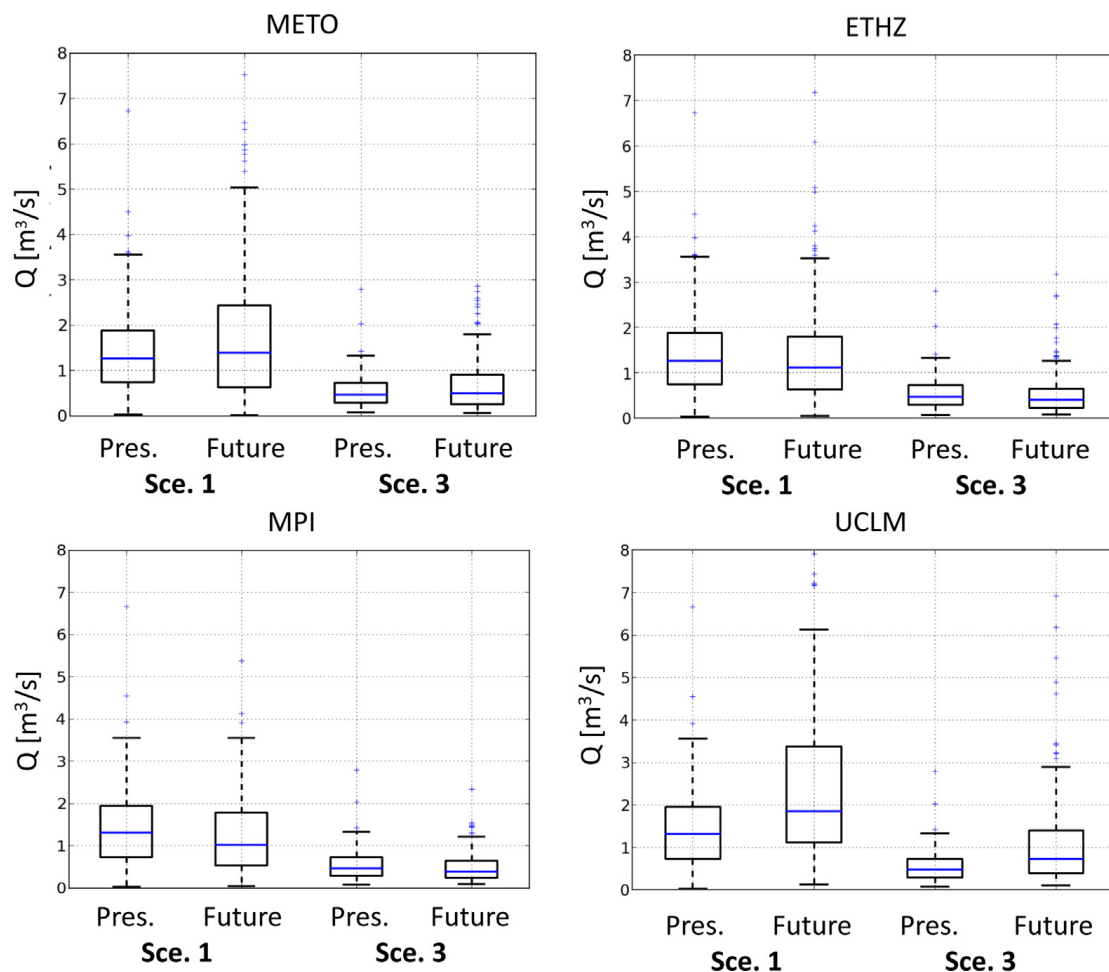
Fig. 11. Annual maximum outflow for the four regional climate models. Scenario 1 (with no irrigation) and 3 (future irrigation).

AET decreases during summer for all climate scenarios (Fig. 12). In general, in scenario 1 (no irrigation), changes in ET_c have a small impact and changes in AET follow the precipitation changes. Climate scenarios based on regional climate models predicting a large decrease in summer precipitation as ETHZ (−36% of present precipitation) forecasts a relatively large decrease in AET (−27% of present AET). On the contrary, if the regional climate model predicts only small changes in summer precipitation (e.g., MPI with −6% of present precipitation), AET does not decrease as much (−3.3% of present AET).
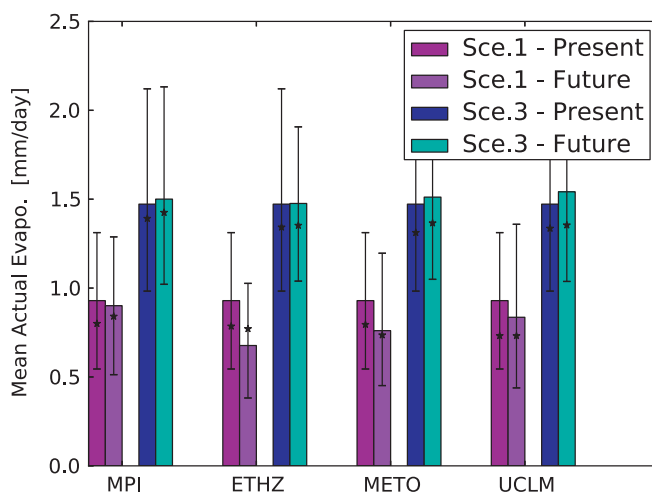

Fig. 12. Present and future AET in the scenarios without irrigation and with future irrigation during the irrigation period (15th April to 30th September). The error bars represent the spread of the 30 scenarios created with the weather generators. The stars indicate the results using the quantile mapped downscaling method.

On the contrary, with irrigation, soil moisture increases and AET increases during summer because of the higher water availability (Fig. 12). When comparing the situation in present climate, AET is 56% larger when fields are irrigated compared to a situation without irrigation. In future climate with irrigation, especially in scenario 3, AET increases, contrarily to the results based on scenario 1 (without irrigation). In scenarios 2 and 3, the future increase in ET_0 has more impact on AET than in scenario 1 because of the generally larger soil moisture. However, the differences in AET between future and present climate are still relatively small (between 0.003 mm/day and 0.07 mm/day).

In the scenario with future cropping patterns (scenario 4), yearly AET is predicted to decrease by 8% in the ETHZ case, when compared to the present cropping pattern and climate (scenario 2, present). AET is strongly impacted by water availability in semi-arid climates and total irrigation volume in scenario 4 is about 15% smaller (Section 5.2) than in the present case. However, the decrease of AET in this scenario is predicted to occur mainly in summer, during the vegetative period, when AET has its seasonal peak. Future AET in winter increases of 20%, due to the higher irrigation, precipitation and transpiration during this period. Indeed, in scenario 4, the area where winter cereal is cultivated increases, resulting in an overall higher transpiration in the catchment during the cultivation period of this crop.

7. Discussion and conclusion

Water availability will likely decrease in the Ebro region (Bovolo et al., 2010) as a result of climate change. An increase of the irrigation demands by about 10% (Table 7 and Section 5.2) is predicted in the next 40 years in the Ebro region, based on current cropping practices. In addition, the volume of water available for storage in the Yesa reservoir, which is the water source for irrigation in the Lerma catchment, will probably decrease. For example, López-Moreno et al. (2014) modeled a 30% decrease of streamflow to the Yesa reservoir, because of land-use and climate change. Moreover, an expansion of the irrigated area (between 30% and 50% of the present irrigated area) is currently planned by the local irrigation authority in the region (Bielsa and Cazcarro, 2015; Milano et al., 2013). Consequently, efficient mitigation strategies for climate change impacts are needed. These strategies should consider land-use changes and future agricultural practices. As demonstrated by this study, the impact of climate change will be different for irrigated and non-irrigated areas. For example, annual maximum peak flow could increase more in non-irrigated regions compared to irrigated regions. Consequently, flood risk increases more in non-irrigated areas than in irrigated areas, even with identical changes in precipitation variability.

In contrast, base flow rates are more impacted by climate change in streams which are heavily influenced by irrigated agriculture. In the Lerma catchment, the transition from rain-fed to irrigation agriculture has resulted in larger flows in the streams during dry periods because of higher groundwater levels. However, stream flows are expected to decrease under future climate scenarios. Base flows in irrigated catchments might therefore rapidly change. This change is expected to impact, for example, stream ecology, as rapid changes of flow rate are difficult to overcome by ecological communities (e.g Sandel et al., 2011; Bradford and Heinonen, 2008), or on water quality as lower outflows might results in an increase of nutriment and pollutant concentrations (Whitehead et al., 2009), because of the lacking dilution.

In semi-arid climates, the actual evapotranspiration (AET) on the catchment scale depends on water availability in the soil zone, among other factors. In the Lerma basin, climate change is predicted to result in a decrease of AET in our scenario without irrigation but in an increase of AET in the scenarios where the catchment is irrigated in summer, especially for scenarios with increased irrigation volume. In this case, irrigation influences the gradient of air humidity, creating a feed-back loop between irrigation management and atmospheric conditions. Hence, impact of water management, as irrigation management, and climate changes are strongly interlinked and feed-backs between them should be analyzed and understood in climate-change impact studies (Holman, 2005).

Appendix A. Supplementary Data

Supplementary data associated with this article can be found, in the online version, at http://dx.doi.org/10.1016/j.ejrh.2015.08.001.

References

Abrahao, R., Causapé, J., García-Garizábal, I., Merchán, D., 2011. Implementing irrigation: water balances and irrigation quality in the Lerma basin (Spain). Agric. Water Manage. 102, 97–104.

D. von Gunten et al. / Journal of Hydrology: Regional Studies 4 (2015) 550–570

Allen, R., Pereira, L., Raes, D., Smith, M., 2000. Crop evapotranspiration (guidelines for computing crop water requirements). FAO irrigation and drainage paper 56.

Beltrán, A., 1986. Estudio de los suelos de la zona regable de Bardenas II. Sectores VIII, IX, X, XII y XIII. Instituto Nacional de Reforma y Desarrollo Agrario, Ministerio de Agricultura, Pesca y Alimentación.

Berndtsson, R., Larson, M., 1987. Spatial variability of infiltration in a semi-arid environment. J. Hydrol. 90, 117–133.

Bielsa, J., Cazcarro, I., 2015. Implementing integrated water resources management in the Ebro river basin: from theory to facts. Sustainability 7, 441–464.

Blenkinsop, S., Fowler, H., 2007. Changes in European drought characteristics projected by the PRUDENCE regional climate models. Int. J. Climatol. 27, 1595–1610.

Bouraoui, F., Vachaud, G., Li, L., le Treut, H., Chen, T., 1999. Evaluation of the impact of climate changes on water storage and groundwater recharge at the watershed scale. Clim. Dyn. 15, 153–161.

Bovolo, C., Blenkinsop, S., Majone, B., Zambrano-Bigiarini, M., Fowler, H., Bellin, A., Burton, A., Barceló, D., Grathwohl, P., Barth, J., 2010. Climate change, water resources and pollution in the Ebro basin: Towards an integrated approach. In: Barceló, D., Petrovic, M. (Eds.), The Ebro River Basin. Springer-Verlag.

Bradford, M., Heinonen, J., 2008. Low flows, instream flow needs and fish ecology in small streams. Can. Water Resour. J. 33, 165–180.

Buerger, C., Kolditz, O., Fowler, H., Blenkinsop, S., 2007. Future climate scenarios and rainfall-runoff modelling in the Upper Gallego catchment (Spain). Environ. Pollut. 148, 842–854.

Burton, A., Fowler, H., Blenkinsop, S., Kilsby, C., 2010. Downscaling transient climate change using a Neyman-Scott rectangular pulses stochastic rainfall model. J. Hydrol. 381, 18–32.

Burton, A., Kilsby, C., Fowler, H., Cowpertwait, P., O'Conell, P., 2008. RainSim: a spatial-temporal stochastic rainfall modelling system. Environ. Model. Softw. 23, 1356–1369.

Candela, L., von Igel, W., Elorza, F.J., Aronica, G., 2009. Impact assessment of combined climate and management scenarios on groundwater resources and associated wetland (Majorca, Spain). J. Hydrol. 376, 510–527.

Candela, L., Tamoh, K., Olivares, G., Gomez, M., 2012. Modelling impacts of climate change on water resources in ungauged and data-scarce watersheds. Application to the Siurana catchment (NE Spain). Sci. Total Environ. 440, 253–260.

Christensen, J., Christensen, O., 2007. A summary of the PRUDENCE model projections of changes in European climate by the end of this century. Clim. Change 81, 7–30.

Christensen, O., Drews, M., Christensen, J., Dethloff, K., Ketelsen, K., Hebestadt, I., Rinke, A., 2006. The HIRHAM regional climate model version 5 (b), tech. rep. 06-17. Dan. Meteorol. Inst., Copenhagen.

Collins, M., Booth, B., Harris, G., Murphy, J., Sexton, D., Webb, M., 2006. Towards quantifying uncertainty in transient climate change. Clim. Dyn. 27, 127–147.

Cuo, L., Zhang, Y., Gao, Y., Hao, Z., Cairang, L., 2013. The impacts of climate change and land cover/use transition on the hydrology in the upper Yellow River Basin, China. J. Hydrol. 502, 37–52.

Dale, V., 1997. The relationship between land-use change and climate change. Ecol. Appl. 7, 753–769.

Döll, P., 2002. Impact of climate change and variability on irrigation requirements: a global perspective. Clim. Change 54, 269–293.

Ferrer, J., Pérez-Martín, M.A., Jiménez, S., Estrela, T., Andreu, J., 2012. GIS-based models for water quantity and quality assessment in the Júcar river basin, Spain, including climate change effects. Sci. Total Environ. 440, 42–59.

Fischer, G., Shah, M., Tubiello, F., van Velhuizen, H., 2005. Socio-economic and climate change impacts on agriculture: an integrated assessment, 1990–2080. Philos. Trans. R. Soc. 360, 2067–2083.

Fischer, G., Tubiello, F., van Velthuizen, H., Wiberg, D., 2007. Climate change impact on irrigation water requirements. effects of mitigation, 1990–2080. Technol. Forecast. Soc. Change 74, 1083–1107.

Flato, G., Marotzke, J., Abiodun, B., Braconnot, P., Chou, S., Collins, W., Cox, P., Driouech, F., Emori, S., Eyring, V., Forest, C., Gleckler, P., Guilyardi, E., Jakob, C., Kattsov, V., Reason, C., Rummukainen, M., 2013. Evaluation of climate models. In: Climate change 2013: The physical science basis. Contribution of working group I to the fifth assessment report of the intergovernmental panel on climate change. Cambridge University Press, Cambridge, United Kingdom and New York, NY, USA.

Fowler, H., Blenkinsop, S., Tebaldi, C., 2007. Linking climate change modelling to impacts studies: recent advances in downscaling techniques for hydrological modelling. Int. J. Climatol. 27, 1547–1578.

Fujihara, Y., Tanaka, K., Watanabe, T., Nagano, T., Kojiri, T., 2008. Assessing the impacts of climate change on the water resources of the Seyhan river basin in Turkey: use of dynamically downscaled data for hydrologic simulations. J. Hydrol. 353, 33–48.

García-Garizábal, I., Causapé, J., 2010. Influence of irrigation water management on the quantity and quality of irrigation return flows. J. Hydrol. 385, 36–43.

García-Garizábal, I., Causapé, J., Abrahao, R., Merchán, D., 2014. Impact of climate change on Mediterranean irrigation demand: Historical dynamics of climate and future projections. Water Resour. Manage. 28, 1449–1462.

Ghosh, S., Misra, C., 2010. Assessing hydrological impacts of climate change: modeling techniques and challenges. Open Hydrol. J. 4, 115–121.

Goderniaux, P., Brouyère, S., Blenkinsop, S., Burton, A., Fowler, H.J., Orban, P., Dassargues, A., 2011. Modeling climate change impacts on groundwater resources using transient stochastic climatic scenarios. Water Resour. Res. 47, W12516.

Goderniaux, P., Brouyère, S., Fowler, H., Blenkinsop, S., Therrien, R., Orban, P., Dassargues, A., 2009. Large scale surface-subsurface hydrological model to assess climate change impacts on groundwater reserves. J. Hydrol. 373, 122–138.

Haugen, J., Haakenstad, H., 2006. Validation of HIRHAM version 2 with 50 km and 25 km resolution. RegClim Phase III – Gen. Tech. Rep. 9. Norw. Meteorol. Inst., Oslo.

Herrera, S., Fita, L., Fernández, J., Gutiérrez, J.M., 2010. Evaluation of the mean and extreme precipitation regimes from the ENSEMBLES regional climate multimodel simulations over Spain. J. Geophys. Res. 115, D21117.

Hewitt, C., Griggs, D., 2004. Ensembles-based predictions of climate changes and their impacts. Trans. Am. Geophys. Union (EOS) 85, 556.

Hill, C., Verjee, F., Barrett, C., 2010. Flash flood early warning system reference guide. National Oceanic and Atmospheric Administration, U.S. Department of Commerce.

Hill, M., Tiedeman, C., 2007. Effective Groundwater Model Calibration: With Analysis of Data, Sensitivities, Predictions, and Uncertainty. John Wiley and Sons, Inc.

Holman, I., 2005. Climate change impacts on groundwater recharge-uncertainty, shortcomings, and the way forward? Hydrogeol. J. 14, 637–447.

Holman, I., Tascone, D., Hess, T., 2009. A comparison of stochastic and deterministic downscaling methods for modelling potential groundwater recharge under climate change in East Anglia, UK: implications for groundwater resource management. Hydrogeol. J. 17, 1629–1641.

Iglesias, A., Minguez, M., 1997. Modelling crop-climate interactions in Spain: vulnerability and adaptation of different agricultural systems to climate change. Mitig. Adapt. Strateg. Glob. Changes 1, 273–288.

I.G.N., 2012. Modelo Digital del Terreno, hoja 282 del Mapa Topográfico Nacional (in Spanish). Instituto Geográfico Nacional.

Jacob, D., Van den Hurk, B., Andrae, U., Elgered, G., Fortelius, C., Graham, L.P., Jackson, S.D., Karstens, U., Köpken, C., Lindau, R., Podzun, R., Rockel, B., Rubel, F., Sass, B.H., Smith, R.N.B., Yang, X., 2001. A comprehensive model inter-comparison study investigating the water budget during the BALTEX-PIDCAP period. Meteorol. Atmos. Phys. 77, 19–43.

Jaeger, E., Anders, I., Lüthi, D., Rockel, B., Schär, C., Seneviratne, S., 2008. Analysis of ERA40-driven CLM simulations for Europe. Meteorol. Ztg. 17, 349–367.

Jones, C., Kiniry, J., Dyke, P., 1986. CERES-maize: A simulation model of maize growth and development. Texas A. and M. University Press, pp. 194.

Jorge, J., Ferreres, E., 2001. Irrigation scenario vs climate change scenario. In: India, M., Bonillo, D. (Eds.), Detecting and Modelling Regional Climate Change. Springer, Berlin/Heidelberg, pp. 581–592.

Kilsby, C., Jones, P., Burton, A., Ford, A., Fowler, H., Harpham, C., James, P., Smith, A., Wilby, R., 2007. A daily weather generator for use in climate change studies. Environ. Model. Softw. 22, 1705–1719.

Kjellström, E., Bärring, L., Gollvik, S., Hansson, U., Jones, C., Samuelsson, P., Rummukainen, M., Ullerstig, A., Willén, U., Wyser, K., 2005. A 140-year simulation of European climate with the new version of the Rossby Centre regional atmospheric climate model (RCA3). Rep. Meteorol. Climatol. Swed. Meteorol. and Hydrol. Inst., Norrköping, Sweden, pp. 54.

Kling, H., Stanzel, P., Preishuber, M., 2014. Impact modelling of water resources development and climate scenarios on Zambezi River discharge. J. Hydrol. Reg. Stud. 1, 17–43.

Kollet, S., Maxwell, R., 2008. Capturing the influence of groundwater dynamics on land surface processes using an integrated, distributed watershed model. Water Resour. Res. 44, W02402.

Kubatzki, C., Claussen, M., Calov, R., Ganopolski, A., 2006. Sensitivity of the last glacial inception to initial and surface conditions. Clim. Dyn. 27, 333–344.

Leggett, J., Pepper, W., Swart, R., 1992. Emission scenarios for the IPCC: An update – the supplementary report to the IPCC scientific assessment. Cambridge University Press.

Li, H., Sheffield, J., Wood, E., 2009. Bias correction of monthly precipitation and temperature fields from intergovernmental panel on climate change AR4 models using equidistant quantile matching. J. Geophys. Res. 115, D10101.

van der Linden, P., Mitchell, J., 2009. ENSEMBLES: climate change and its impact: summary of research and results from the ENSEMBLES project. Met Office Hadley Centre, UK, pp. 1–160.

López-Moreno, J., Beguería, S., García-Riuz, J., 2002. Influence of the Yesa reservoir on floods of the Aragón river, central Spanish Pyrenees. Hydrol. Earth Sys. Sci. 6, 753–762.

López-Moreno, J., Zabalza, J., Vicente-Serrano, S., Revuelto, J., Gilaberte, M., Azorin-Molina, C., Morán-Tejeda, E., García-Ruiz, J., Tague, C., 2014. Impact of climate and land use change on water availability and reservoir management: Scenarios in the Upper Aragón river, Spanish Pyrenees. Sci. Total Environ. 493, 1222–1231.

Martínez-Cob, A., 2004. Revisión de las necesidades hídricas netas de los cultivos de la cuenca del Ebro. Confederación Hidrográfica del Ebro.

Meehl, G.A., Stocker, T.F., et al., 2007. Global climate projections. In: Climate Change 2007: The Physical Science Basis. Contribution of Working Group I to the Fourth Assessment Report of the Intergovernmental Panel on Climate Change. Cambridge University Press, Cambridge.

Mehdi, B., Ludwig, R., Lehner, B., 2015. Evaluating the impacts of climate change and crop land use change on streamflow, nitrates and phosphorus: a modeling study in Bavaria. J. Hydrol. Reg. Stud. Part B 4, 60–90.

Mehta, V.K., Haden, V.R., Joyce, B.A., Purkey, D.R., Jackson, L.E., 2013. Irrigation demand and supply, given projections of climate and land-use change, in Yolo County, California. Agr. Water Manage. 117, 70–82.

van Meijgaard, E., van Ulft, L., van de Berg, W., Bosveld, F., van den Hurk, B., Lenderink, G., Siebesma, A., 2008. The KNMI regional atmospheric climate model RACMO, version 2.1, KNMI – tech. rep. 302.

Merchán, D., Causapé, J., Abrahao, R., 2013. Impact of irrigation implementation on hydrology and water quality in a small agricultural basin in Spain. Hydrolog. Sci. J. 58, 1400–1413.

Merchán, D., Otero, N., Soler, A., Causapé, J., 2014. Main sources and processes affecting dissolved sulphates and nitrates in a small irrigated basin (Lerma basin, Zaragoza, Spain): isotopic characterization. Agr. Ecosyst. Environ. 195, 127–138.

Milano, M., Ruelland, D., Dezetter, A., Fabre, J., Ardoin-Bardin, S., Servat, E., 2013. Modeling the current and future capacity of water resources to meet water demands in the Ebro basin. J. Hydrol. 500, 114–126.

Montenegro, S., Ragab, R., 2012. Impact of possible climate and land use changes in the semi arid regions: a case study from North Eastern Brazil. J. Hydrol. 434–435, 55–68.

Moratiel, R., Durán, J., Snyder, R., 2010. Responses of reference evapotranspiration to changes in atmospheric humidity and air temperature in Spain. Clim. Res. 44, 27–40.

Moussa, R., Bocquillon, C., 2000. Approximation zones of the Saint-Venant equations for flood routing with overbank flow. Hydrol. Earth Syst. Sci. 4, 251–261.

Nakićenović, N., Davidson, O., Davis, G., Grübler, A., Kram, T., Rovere, E.L.L., Metz, B., Morita, T., Pepper, W., Pitcher, H., Sankovski, A., Shukla, P., Swart, R., Watson, R., Dadi, Z., 2000. Emissions scenarios – summary for policymakers. A special report of working group III of the Intergovernmental Panel on Climate Change.

Nash, J., Sutcliffe, V., 1970. River flow forecasting through conceptual models, part I – a discussion of principles. J. Hydrol. 10, 282–290.

Ntegeka, V., Baguis, P., Roulin, E., Willems, P., 2014. Developing tailored climate change scenarios for hydrological impact assessments. J. Hydrol. 508, 307–321.

Otero, I., Boada, M., Badia, A., Pla, E., Vayreda, J., Sabaté, S., Gracia, C.A., Peñuelas, J., 2011. Loss of water availability and stream biodiversity under land abandonment and climate change in a Mediterranean catchment (Olzinelles, NE Spain). Land Use Policy 28, 207–218.

Pal, J., Giorgi, F., Bi, X., Elguindi, N., Solmon, F., Rauscher, S.A., Gao, X., Francisco, R., Zakey, A., Winter, J., Ashfaq, M., Syed, F.S., Sloan, L.C., Bell, J.L., Diffenbaugh, N.S., Karmacharya, J., Konaré, A., Martinez, D., da Rocha, R.P., Steiner, A.L., 2007. Regional climate modeling for the developing world: the ICTP regCM3 and regCNET. Bull. Am. Meteorol. Soc. 88, 1395–1409.

Pérez, A., 2011. Physics-based numerical modeling of surface-groundwater flow and transport at catchment scale. University of Tübingen (Ph.D. thesis).

Pérez, A., Abrahao, R., Causapé, J., Cirpka, O., Bürger, C., 2011. Simulating the transition of a semi-arid rainfed catchment towards irrigation agriculture. J. Hydrol. 409, 663–681.

Pielke, R., 2005. Land use and climate change. Science 310, 1625–1626.

Plata-Torres, J., 2012. Informe sobre la campaña de sondeos eléctrico verticales efectuados en el barranco de Lerma (Zaragoza). Grupo de Geofísica del Instituto Geológico y Minero de España.

Radu, R., Déqué, M., Somot, S., 2008. Spectral nudging in a spectral regional climate model. Tellus Ser. A 60, 898–910.

Rey, D., Garrido, A., Mínguez, M., Ruiz-Ramos, M., 2011. Impact of climate change on maize's water needs, yields and profitability under various water prices in Spain. Span. J. Agric. Res. 9, 1047–1058.

Ribalaygua, J., Pino, M., Pórtoles, J., Roldán, E., Gaitán, E., Chinarro, D., Torres, L., 2013. Climate change scenarios for temperature and precipitation in Aragón (Spain). Sci. Total Environ. 463–464, 1015–1030.

Richards, L., 1931. Capillary conduction of liquids through porous mediums. J. Appl. Phys. 1, 318–333.

Sánchez, E., Gallardo, C., Gaertner, M., Arribas, A., Castro, M., 2004. Future climate extreme events in the Mediterranean simulated by a regional climate model: a first approach. Glob. Planet. Change 44, 163–180.

Sandel, B., Arge, L., Dalsgaard, B., Davies, R.G., Gaston, K.J., Sutherland, W.J., Svenning, J.C., 2011. The influence of late quaternary climate-change velocity on species endemism. Science 334, 660–664.

Scanlon, B.R., Jolly, I., Sophocleous, M., Zhang, L., 2007. Global impacts of conversions from natural to agricultural ecosystems on water resources: quantity versus quality. Water Resour. Res. 43, W03437.

Serrat-Capdevila, A., Scott, R., Shuttleworth, J., Valdés, J., 2011. Estimating evapotranspiration under warmer climates: insights from a semi-arid riparian system. J. Hydrol. 399, 1–11.

Sillmann, J., Roeckner, E., 2008. Indices for extreme events in projections of anthropogenic climate change. Clim. Change 86, 83–104.

Simonneaux, V., Cheggour, A., Deschamps, C., Mouillot, F., Cerdan, O., Le Bissonnais, Y., 2015. Land use and climate change effects on soil erosion in a semi-arid mountainous watershed (High Atlas, Morocco). J. Arid Environ. 122, 64–75.

Skhiri, A., Dechmi, F., 2011. Irrigation return flows and phosphorus transport in the Middle Ebro River valley (Spain). Span. J. Agric. Res. 9, 938–949.

Smith, M., 1993. CLIMWAT for CROPWAT: Climatic database for irrigation planning and management. FAO Irrigation and Drainage Paper 49.

Szczypta, C., Gascoin, S., Houet, T., Hagolle, O., Dejoux, J.F., Vigneau, C., Fanise, P., 2015. Impact of climate and land cover changes on snow cover in a small Pyrenean catchment. J. Hydrol. 521, 84–99.

Tebaldi, C., Knutti, R., 2007. The use of the multi-model ensemble in probabilistic climate projections. Philos. Trans. R. Soc. 365, 2053–2075.

Therrien, R., 2006. HydroGeoSphere – A Three-Dimensional Numerical Model Describing Fully-Integrated Subsurface and Surface Flow and Solute Transport. Université Laval and University of Waterloo (Ph.D. thesis).

Therrien, R., McLaren, R., Sudicky, E., Panday, S., 2010. HydroGeoSphere: A Three-dimensional Numerical Model Describing Fully-integrated Subsurface and Surface Flow and Solute Transport – User Manual. University of Waterloo.

Toews, M., Allen, D., 2009. Evaluating different GCMs for predicting spatial recharge in an irrigated arid region. J. Hydrol. 374, 265–281.

Urdanoz, V., Aragüés, R., 2011. Pre- and post-irrigation mapping of soil salinity with electromagnetic induction techniques and relationships with drainage water salinity. Soil Sci. Soc. Am. J. 75, 207–215.

van Roosmalen, L., Sonnenborg, T., Jensen, K., Chistensen, J., 2011. Comparison of hydrological simulations of climate change using perturbation of observations and distribution-based scaling. Vadose Zone J. 10, 136–150.

van Genuchten, M., 1980. A closed-form equation for predicting the hydraulic conductivity of unsaturated soils. Soil Sci. Soc. Am. J. 44, 892–898.

von Gunten, D., Wöhling, T., Haslauer, C., Merchán, D., Causapé, J., Cirpka, O., 2014. Efficient calibration of a distributed pde-based hydrological model using grid coarsening. J. Hydrol. 519, 3290–3304.

Vargas-Amelin, E., Pindado, P., 2014. The challenge of climate change in Spain: Water resources, agriculture and land. J. Hydrol. 518, 243–249.

Whitehead, P.G., Wilby, R., Battarbee, R., Kernan, M., Wade, A., 2009. A review of the potential impacts of climate change on surface water quality. Hydrol. Sci. 54, 101–123.

Wilby, R., Wigley, T., 1997. Downscaling general circulation model output: a review of methods and limitations. Prog. Phys. Geogr. 21, 530–548.

Woznicki, S., Nejadhashemi, A., Parsinejad, M., 2015. Climate change and irrigation demand: uncertainty and adaptation. J. Hydrol. Reg. Stud. 3, 247–264.

Yokohata, T., Emori, S., Nozawa, T., Tsushima, Y., Ogura, T., Kimoto, M., 2005. Climate response to volcanic forcing: validation of climate sensitivity of a coupled atmosphere-ocean general circulation model. Geophys. Res. Lett. 32, L21710.

Zambrano-Bigiarini, M., Majone, B., Bellin, A., Bovolo, C.I., Blenkinsop, S., Fowler, H., 2010. Hydrological impact of climate change on the Ebro river basin. In: The Ebro River Basin. Springer-Verlag.

Zhao, F., Xu, Z., Zhang, L., Zuo, D., 2009. Streamflow response to climate variability and human activities in the upper catchment of the Yellow River Basin. Sci. China Ser. E: Technol. Sci. 52, 3249–3256.

Zheng, H., Zhang, L., Zhu, R., Liu, C., Sato, Y., Fukushima, Y., 2009. Responses of streamflow to climate and land surface change in the headwaters of the Yellow River Basin. Water Resour. Res. 45, W00A19.

6 Third publication

Title

Using an integrated hydrological model to estimate the usefulness of meteorological drought indices in a changing climate

Journal

Hydrological and Earth System Science

Year

2015-2016 (Submitted 2015)

Highlights

- We compare seven different drought indices with three simulated hydrological variables (mean annual discharge, hydraulic heads and water deficit).

- The correlation coefficients between these drought indices and hydrological variables are similar in all irrigation scenarios for present and future climate.

- Assumed linear relationships are different in present and future climate.

- Drought intensity and frequency will likely increase in north-east Spain.

Using an integrated hydrological model to estimate the usefulness of meteorological drought indices in a changing climate

Diane von Gunten[1], **Thomas Wöhling**[1,2,3], **Claus P. Haslauer**[1], **Daniel Merchán**[4], **Jesus Causapé**[4], **and Olaf A. Cirpka**[1]

[1]University of Tübingen, Center for Applied Geoscience, Hölderlinstr. 12, 72076 Tübingen, Germany
[2]Technische Universität Dresden, Department of Hydrology, Bergstr. 66, 01069 Dresden, Germany
[3]Lincoln Agritech Ltd., Ruakura Research Centre, Hamilton, New Zealand
[4]Geological Survey of Spain – IGME, C/ Manuel Lasala no. 44, 9B, Zaragoza, 50006, Spain

Correspondence to: Olaf A. Cirpka (olaf.cirpka@uni-tuebingen.de)

Abstract. Droughts are serious natural hazards, especially in semi-arid regions. They are also difficult to characterize. Various summary metrics representing the dryness level, denoted drought indices, have been developed to quantify droughts. They typically lump meteorological variables and can thus directly be computed from the outputs of regional climate models in climate-change assessments. While it is generally accepted that drought risks in semi-arid climates will increase in the future, quantifying this increase using climate model outputs is a complex process which depends on the choice and the accuracy of the drought indices, among other factors. In this study, we compare seven meteorological drought indices that are commonly used to predict future droughts. Our goal is to assess the reliability of these indices to predict hydrological impacts of droughts under changing climatic conditions. We simulate the hydrological responses of a small catchment in northern Spain to droughts in present and future climate, using an integrated hydrological model, calibrated for different irrigation scenarios. We compute the correlation of meteorological drought indices with the simulated hydrological times series (discharge, groundwater levels, and water deficit), and we compare changes in the relationships between hydrological variables and drought indices. While correlation coefficients are similar for all tested land-uses and climates, the relationship between drought indices and hydrological variables often differs between present and future climate. Drought indices based solely on precipitation often underestimate the hydrological impacts of future droughts, while drought indices that additionally include potential evapotranspiration sometimes overestimate the drought effects. In this study, the drought indices with the smallest bias were: the rainfall anomaly index, the reconnaissance drought index, and the standardized precipitation evapotranspiration index. However, the efficiency of these drought indices depends on the hydrological variable of interest and the irrigation scenario. We conclude that meteorological drought indices are able to identify the timing of hydrological impacts of droughts in present and future climate. However, these indices are not capable of estimating the severity of hydrological impacts of droughts in future climate. A well-calibrated hydrological model is necessary in this respect.

1 Introduction

In semi-arid regions, droughts are a serious natural hazard, often causing tens of millions of euros of damage (Gil et al., 2011). In northern Spain, for example, drought severity has increased in the last decades (Hisdal et al., 2001) and is expected to increase further in the next 50 years (Bovolo et al., 2010), as a result of the ongoing increase in global mean temperature (e.g., Meehl et al., 2007). More severe droughts will negatively impact the region, notably the agricultural sector (Stahl et al., 2015).

Droughts have a wide range of impacts, and are often difficult to define. They have been classified in four main categories (Mishra and Singh, 2010; Samaniego et al., 2013; Wilhite and Glantz, 1985):

- *meteorological* droughts defined by a lack of precipitation over a certain period of time for a certain region,

- *hydrological* droughts defined by a reduced surface and subsurface water availability for a given water resource,

- *agricultural* droughts defined by a period of declining soil moisture and reduced crop yields,

– and *socio-economical* droughts defined by a failure of water-resources management to meet the supply and demand of water (taken as an economic good).

In order to quantitatively describe drought levels, about 150 different drought indices have been developed (Zargar et al., 2011). A drought index is a scalar composed of one or more measured variables affected by dry and wet periods. In the case of meteorological drought (which is the focus of this study), typical variables considered for the calculation of drought indices are precipitation and potential evapotranspiration.

In addition to the identification of drought periods, these meteorological drought indices are also good indicators for various droughts impacts in present climate, based on the results of a range of studies. For example, text-recollection of droughts, such as newspaper articles, are linked with different drought indices, indicating a relationship between the social impacts of droughts and drought-index values (Bachmair et al., 2015). Crop yields are also correlated with drought indices in different climatic regions (e.g., Quiring and Papakryiakou, 2003; Mavromatis, 2007). Moreover, Vicente-Serrano et al. (2012a) analyzed the correlation between six drought indices and environmental variables, such as stream flow, tree rings widths, and soil moisture. A significant correlation between the studied environmental variables and the drought indices was found. The correlation between groundwater levels and drought indices seems to be smaller than for other drought impacts, but it was still noticeable (Kumar et al., 2015).

Hence, meteorological drought indices are correlated with hydrological and agricultural impacts of meteorological droughts. Consequently, they are also correlated with hydrological or agricultural droughts. Many of the drought impacts cited above, such as changes in groundwater levels or discharge, could also be conceptualized as an indicator of hydrological or agricultural droughts. For example, groundwater levels could be transformed to a drought indicator such as the standardized groundwater level index (SGI, Bloomfield and Marchant (2013)) to identify hydrological droughts (Kumar et al., 2015). Indeed, hydrological impacts of drought and hydrological drought indices are often two perspectives of the same drought event. The viewpoint of this study is that changes in environmental variables are introduced by non-stationary meteorological forcings, i.e., that hydrological changes are a consequence of meteorological droughts. Therefore, we will not use hydrological variables to define droughts. We explain our motivations for this choice in Sect. 2.1.

The relationship between meteorological drought indices and drought impacts is valid for many drought indices in present climate, including simpler indices using one input variable, such as precipitation. However, the suitability of drought indices has not been tested under a changing climate. The ongoing increase in air temperature was not taken into account. Because climate change will probably impact drought intensity and frequency (e.g., Dai, 2011), various studies have aimed at predicting future changes in dry periods using drought indices based on the output of regional or global climate models. An assumption of these studies is that drought indices perform similarly in present and future climate. Our aim is to test this hypothesis. That is, we will test the capability of meteorological drought indices to predict hydrological impacts of drought under a changing climate.

A large number of drought indices have been used in recent climate-impact studies. For instance, the standardized precipitation index was often used to study future droughts (e.g., Leng et al., 2015; Masud et al., 2015; Tue et al., 2015; Zarch et al., 2015). However, several studies used other indices, as the reconnaissance drought index (e.g., Kirono et al., 2011; Zarch et al., 2015), the standardized precipitation evapotranspiration index (e.g., Kim et al., 2014; Masud et al., 2015), the effective drought index (e.g, Park et al., 2015), or the Palmer drought severity index (e.g., Burke et al., 2006), among others. The choice of the drought index can have an important impact on the results. For example, Kim et al. (2014) and Park et al. (2015) predicted future droughts over Korea in the next century using very similar climate scenarios. While Kim et al. (2014) projected an increase in the severity of droughts in this region, Park et al. (2015) projected a more complex spatial pattern and a possible decrease in drought severity in coastal regions. A possible reason for these contradictory results is that Park et al. (2015) used a drought index based on precipitation only, while Kim et al. (2014) used an index which considers both potential evapotranspiration and precipitation. Precipitation-based drought indices, such as the effective drought index (EDI) or the standardized precipitation index (SPI), tend to work well in present climate. However, they may be inadequate to predict climate-change effects because they neglect the increase in potential evapotranspiration, resulting in a possible underestimation of the intensity of future droughts (Dubrovsky et al., 2009; Vicente-Serrano et al., 2009, 2015; Zarch et al., 2015).

To study the validity of drought indices in future climate, we chose seven well-known drought indices, which can be computed from the output of climate models, such as precipitation, temperature or potential evapotranspiration. We investigate the ability of these indices to predict hydrological variables under drought conditions: groundwater heads, discharge at the catchment outlet, and water deficit of the crops, under present and (projected) future climate conditions. These three metrics address different hydrological effects of droughts of high ecologic and/or economic relevance. Reduced stream discharge can deteriorate the ecological status of the stream because the stream temperature and the concentrations of contaminants increase with decreasing discharge. In the most extreme case, the stream falls dry. The drawdown of groundwater heads is of high economic relevance when groundwater is pumped for water supply and ir-

rigation which, however, is not the case in the studied catchment. Groundwater levels also control low flows in gaining streams. Finally, the water deficit of the crops, that is, the difference between transpiration under conditions when enough water is available and the actual transpiration, is a simple metric of water stress experienced by the crops, which may diminish crop yields.

A fully-integrated hydrological model of a small catchment, the Lerma catchment, in north-east Spain, is used to simulate the hydrological responses to the meteorological forcing. This catchment has recently undergone a monitored transition from rainfed to irrigated agriculture, in which the irrigation water is imported from the Yesa reservoir located outside of the catchment (Merchán et al., 2013). The model was calibrated under different irrigation conditions (von Gunten et al., 2014), which increases our confidence in its ability to predict the hydrological responses to changes in (meteorological and land-use) forcing. We use these different land-use/irrigation schemes to test the different drought indices. The outputs from a weather generator, representing present and future climate, are used as meteorological inputs to the model and for the computation of the drought indices.

The remainder of this paper is structured as follows: First, we present the methodology used in this study. Specifically, we briefly describe the study area, the hydrological model, the climate scenarios, the irrigation scenarios, and the drought indices. Secondly, we compare the frequency distribution of drought indices computed from measurements and based on the outputs of the weather generator. Next, we summarize an analysis of the correlation coefficients between hydrological variables and drought indices for two different land-uses (with/without irrigation), and for present and future climate scenarios. Afterwards, we investigate changes in the relationship between these drought indices and the hydrological variables. We then use these results to predict relevant changes in drought risks in the study area in future climate. Finally, we discuss the usefulness of drought indices in climate-impact studies.

2 Methods

2.1 Overview

The main objective of this paper is to test the suitability of several meteorological drought indices to estimate the impacts of climate change on the water cycle of a small catchment. Seven drought indices, described in Sect. 2.6, are investigated. The information on drought severity (as computed by these indices) is compared to three simulated hydrological impacts of drought: (1) the mean annual discharge at the outlet, (2) the mean annual hydraulic heads in 12 observations wells of the local aquifer, and (3) the water deficit

(WD), which is a simplified representation of how well the water demand of the crops can be met (Abrahao et al., 2011):

$$WD\,[\%] = 100 \times \frac{ET_c - AET}{ET_c} \qquad (1)$$

where ET_c is the annual crop evapotranspiration under standard conditions (Allen et al., 2000), and AET is the simulated actual evapotranspiration, calculated on the yearly time scale.

The time series of the drought impacts listed above are obtained using the outputs from a calibrated, integrated, pde-based, hydrological model (Sect. 2.3) forced by present and future meteorological time series (Sect. 2.4), and daily irrigation scenarios (Sect. 2.5). Five climate scenarios (one based on present climate and four based on the projections of regional climate models) and three irrigation scenarios are constructed and combined with each other in our simulations. The length of the simulation is 180 years for each combination of (present and future) climate and irrigation scenarios. This is equivalent to a total 2700 simulated years. From these 2700 simulated years, we extract time series of discharge, hydraulic heads, and water deficit.

In this study, the time series of these three hydrological variables are directly used to represent the drought impacts on hydrology. We do not consider indicators of hydrological droughts such as the standardized groundwater level index (SGI, Bloomfield and Marchant (2013)) or the standardized streamflow index (SSI, Vicente-Serrano et al. (2012b)). SGI and SSI are hydrological drought indices representing drought events using the normalized changes in hydraulic heads and discharge, respectively. We decided not to use these indices here because the focus of this study is on meteorological droughts. In this context, changes in hydrological variables during dry periods are the consequence of a drought and not an indicator of a drought situation. Moreover, we restrict our investigation to drought indices which can be computed from the outputs of regional or global climate models (precipitation, temperature, etc.), which would not be possible for SGI and SSI. Finally, no drought indices similar to SSI or SGI exist for water deficit. Therefore, a transformation from time series inputs to drought indices would not have been easily possible for this variable. For these reasons, only time series of the hydrological variables are investigated in this study.

The three hydrological time series are compared to the time series of meteorological drought indices (Sect. 2.8): We first compute the Peason correlation coefficient between the drought indices and the hydrological variables. Next, we analyze changes in the (assumed) linear relationship between hydrological variables and drought indices. These comparisons are repeated in present and future climate for the different irrigation scenarios. A suitable drought index for climate-change studies would have a large correlation coefficient with all hydrological variables and the relationships between this index and the hydrological variables would be identical

in present and future climate. The results of these quantitative studies are presented in Sect. 3, while we discuss additional aspects of using meteorological drought indices in climate-impact studies in Sect. 4.

2.2   Study area

The Lerma catchment is situated within the Ebro basin in Spain with an altitude varying between 330 and 490 masl., and an area of ~7.3 km^2 (Fig. 1). Its climate is classified as semi-arid, with a mean precipitation of ~400 mm/year (2004-2011) and a mean potential evapotranspiration rate of ~1300 mm/year (2004-2011) (Merchán et al., 2013). Precipitation and temperature have been measured since 1988 at the meteorological station of Ejea de los Caballeros (~5 km north of the study area). Radiation, wind, and relative humidity have been measured since 2003. Annual precipitation is highly variable, ranging from 268 mm/year to 558 mm/year (2004-2011). Because of the limited water resources, drought is a serious natural hazard in the region (Bovolo et al., 2010).

The catchment underwent a rapid transition from non-irrigated to irrigated agriculture between 2006 and 2008. The majority of the fields within the catchment are now irrigated, with an irrigation water volume of $2.1 \cdot 10^6$ m^3 in 2011 (Merchán et al., 2013). This transition was closely monitored and monthly hydraulic head data, daily discharge, crop types, and daily irrigation volume are available. In addition, a vertical-electrical-sounding campaign (Plata-Torres, 2012) was conducted to better understand the local geology. Two main hydrologically relevant layers were identified: The top layer is composed of clastic and unconsolidated Quaternary deposits and forms a shallow aquifer. Underneath lies an aquitard composed of lutite and marlstones (Fig. 2). Soils are relatively shallow, with depths below ground surface ranging between 0.3 and 0.9 m (Beltrán, 1986), and are classified as inceptisols.

2.3   Hydrological model

To simulate the hydrological response of the Lerma catchment, we use HydroGeoSphere (Therrien, 2006), a three-dimensional, fully-coupled, integrated hydrological model, based on partial differential equations. In HydroGeoSphere (Therrien et al., 2010), water flow in the variably-saturated sub-surface is modelled using the three-dimensional Richards' equation, while overland flow is simulated by the diffusive-wave approximation of the Saint-Venant equations. We use the Mualem-van Genuchten parametrization (van Genuchten, 1980) to relate relative permeability and water saturation to capillary pressure in the vadose zone. The surface and subsurface domains are coupled using a dual-node approach, where the coupling between the domains is conceptualized as a virtual thin layer of porous material. The model choice is based on the necessity to model the transition to irrigation, which has a large impact

on the hydrology of the catchment. Moreover, HydroGeoSphere allows to simultaneously study the impact of droughts on the surface and subsurface components of water flow. The underlying equations have been reviewed by von Gunten et al. (2014, 2015) and are not repeated here.

The conceptual model of our study area and its calibration have also been presented by von Gunten et al. (2014) and thus are only presented here briefly. We divide the sub-surface catchment in six zones, two zones representing the aquitard, one representing the aquifer, and three representing the different soil zones (Fig. 2). The model parameters are homogeneous in each zone and the saturated hydraulic conductivity is one order of magnitude smaller in the vertical direction than in the horizontal one. The surface domain is divided into 55 zones, representing the different farm fields. Daily irrigation volume, Manning's parameters, seasonal leaf area index, and rooting depth are specified separately for each surface zone, based on crop types and irrigation data. Precipitation is given as daily input, apart from days with intense rainfall (>25mm/day). In this case, precipitation data is given as a 3-hour mean during summer and spring, and as a 9-hour mean during autumn and winter, to mimic intense convection events (von Gunten et al., 2014), which are frequent in the region. A no-flow boundary condition is assumed at the lateral and the bottom boundaries of the sub-surface domain. Critical flow depth is used for the lateral boundaries of the surface flow domain.

We calibrated the parameters of the model using three computational grids of increasing resolution (von Gunten et al., 2014). The calibrated parameters are the hydraulic conductivity in all zones, apart from the "weathered aquitard" zone (Fig. 2), the porosity of the aquifer, and the van-Genuchten parameters of the soil zones. The calibration period is from 2006 to 2009 and the validation period is from 2010 to 2011. The model is calibrated on the measured discharge at the outlet and on the hydraulic heads in eight observation wells (twelve observation wells were used during validation). The model reproduces the measurements satisfactorily (von Gunten et al., 2014). For example, the Nash-Sutcliffe efficiency (Nash and Sutcliffe, 1970) of discharge is of 0.74 during the calibration period and of 0.92 during the validation period. The model performs similarly well under all irrigation conditions. Because the model was able to reproduce the response in both discharge and groundwater tables to the changes in irrigation practice, we are confident that it can also predict the response to changes in meteorological forcing projected by climate models.

2.4   Climate scenarios

The climate scenarios used in this study have been presented by von Gunten et al. (2015) and are thus only summarized here.

Our future climate scenarios cover the time period of 2040-2050, using the A1B IPCC emission scenario

(Nakićenović et al., 2000). They are based on 4 regional climate models from the ENSEMBLES project (van der Linden and Mitchell, 2009) driven by two global climate models (Table 2). As it is not advisable to use the direct outputs from climate models as input for a small-scale hydrological model (Prudhomme et al., 2002), we have downscaled the outputs from the climate models using a weather generator, i.e., a statistical model reproducing the characteristics of the observed climatic time series (Srikanthan and McMahon, 2001). We calibrated the weather generator using the observed time series of the closest meteorological station (Ejea de los Caballeros). Then, the parameters of the weather generator were modified using the differences between the control and future simulations of the regional climate models. These change factors, described in Burton et al. (2010), are an indication of future changes of the mean and variability of precipitation, temperature, radiation, and relative humidity. The weather generator is run using the updated parameters to create the future climate scenarios. In this study, we use the RainSim weather generator for precipitation (Burton et al., 2008) and the EARWIG weather generator for potential evapotranspiration (Kilsby et al., 2007).

The downscaling of climate model outputs is a complex task and the choice of a particular downscaling method can have a large impact on the results (Holman et al., 2009). Our study is not an exception and the downscaling process presented here might introduce uncertainties in the climate scenarios. We have mitigated this issue using three different approaches: a) We prepared both present and future time series of meteorological inputs using the weather generator. Hence, the potential bias resulting from the weather generator is reproduced in the present and future time series. b) The time series of present precipitation and potential evapotranspiration have been extensively tested against measurements to control the quality of the weather generator outputs (von Gunten et al., 2015). c) We compared the future time series of precipitation and potential evapotranspiration downscaled with the weather generator with the corresponding time series downscaled with a simpler bias correction method (Li et al., 2009). The time series were found to be generally similar regardless of the downscaling method (von Gunten et al., 2015). Hence, we consider that the quality of the climate downscaling in our study is acceptable.

The chosen downscaling procedure has the advantage of producing longer time series, compared to the relatively short (23 years) climate record in the Lerma catchment. Moreover, it reproduces future changes in the precipitation variability, and not only in the precipitation mean, which is an important criterion when studying future droughts.

Future precipitation (Fig. 3) is predicted to decrease in summer and spring (between 3% and 39% of the current precipitation, depending on the regional climate model). In winter and autumn, an increase in precipitation is predicted (between 1% and 55%). Change in total annual precipitation depends on the regional climate model. MPI and UCLM predict a wetter future, while ETHZ and METO predict a dryer one (see Table 2 for the references of the regional climate models). The coefficients of variation increase in spring (between +3% and +6%), decrease in winter and autumn (between -0.1% and -10%), and do not show a clear trend in summer (between +5% and -5%).

Because of the higher temperature, potential evapotranspiration increases (between 9% and 22% in the annual average) in all regional climate models for all months. This increase might impact droughts, regardless of the precipitation changes.

2.5 Irrigation scenarios

Consistent with our earlier study (von Gunten et al., 2015), we use three irrigation (or land-use) scenarios that can be summarized as follows:

– scenario NOIRR: without irrigation and without agriculture.

– scenario PIRR: with present cropping patterns and present irrigation.

– scenario FUTIRR: with present cropping pattern, but with an updated irrigation volume to account for future climatic conditions. To create this scenario, we assume that the irrigation efficiency will not change in future climate. In addition, we assume that the increase in irrigation will only depend on the increase in potential evapotranspiration and changes in precipitation amount (see Toews and Allen, 2009).

2.6 Drought indices

More than 150 drought indices have been developed in the past (Zargar et al., 2011) and it would be unrealistic to include all of them in this study. Therefore, we have selected seven well-known and commonly-used drought indices, based on the reviews by Agwata (2014), Hayes and Lowrey (2007), Heim (2002), Niemeyer (2008), and Zargar et al. (2011). Our choice was guided by the required data input and the popularity of the indices in recent studies related to climate change. We present the selected indices briefly below and provide a summary in Table 1.

In this study, we generally consider meteorological drought indices that aggregate data annually. The only exceptions are the Palmer drought indices (PDSI and PHDI) whose time length depends on an empirical estimation of the start and the end of drought periods (Szép et al., 2005). We chose an annual time scale because it is often used when predicting future droughts (e.g., Kirono et al., 2011; Park et al., 2015) and because it is the most dominant precipitation cycle worldwide (Park et al., 2015).

Our definition of a drought is identical for present and future climate. Practically, we standardize the drought indices

in the present climate and keep the same standardization (explained below) in the future climate. From a conceptual point of view, this is unexpected as meteorological droughts can be defined as a period of exceptionally dry conditions. If the average precipitation changes, the definition of a meteorological drought should also be changed. However, from a practical point of view, drought severity depends on the water needs and on the vulnerabilities of the social and agricultural structures. Hence, the definition of future droughts is linked to current conditions. From this perspective, using the same standardization in present and future climate is logical. Moreover, this procedure has been applied in the majority of studies on future droughts (e.g., Zarch et al., 2015).

2.6.1 Standardized precipitation index (SPI)

SPI (McKee et al., 1993; Svoboda et al., 2012) is a widely-used drought index (Zargar et al., 2011). To compute this index, precipitation data is first fitted to a probability distribution. We use a gamma distribution with the shape parameter α and the scale parameter β (Wu et al., 2005). The fitted parameters $\hat{\alpha}$ and $\hat{\beta}$ are then used to find the cumulative probability $G(P)$ of the precipitation amount P (Edwards, 1997):

$$G(P) = \int_0^P g(x)dx = \frac{1}{\hat{\beta}^{\hat{\alpha}}\Gamma(\hat{\alpha})} \int_0^P x^{\hat{\alpha}-1}e^{\frac{-x}{\hat{\beta}}}dx \qquad (2)$$

where Γ is the gamma function or $\Gamma(\alpha) = \int_0^\infty x^{\alpha-1}e^{-x}dx$. The probability of null precipitation q is estimated by dividing the number of dry months by the length of the monthly time series. It is accounted for by:

$$H(P) = q + (1-q)G(P) \qquad (3)$$

To compute the value of SPI, an equiprobability transformation is made from the cumulative probability $H(P)$, i.e., $H(P)$ is transferred to a standard normal random variable with a mean of zero and a variance of unity:

$$SPI = \Phi^{-1}(H(P)) \qquad (4)$$

where Φ is the standard normal cumulative distribution function. SPI takes monthly precipitation as input and can be computed at various time scales, from 1 month to 24 months. In this study, we use a 12-months time scale. An SPI-value smaller than -1 indicates a dry period, and an SPI-value larger than +1 a wet period (Svoboda et al., 2012).

2.6.2 Standardized precipitation evapotranspiration index (SPEI)

SPEI (Vicente-Serrano et al., 2009) has been developed to account for the impact of potential evapotranspiration on droughts, especially in a changing climate. Its computation

is similar to SPI. For SPEI, the difference between precipitation and potential evapotranspiration, rather than only precipitation, is used in the index computation. This time series is fitted to a probability distribution as described for SPI. A log-logistic distribution (e.g., Ashkar and Mahdi, 2006) is used here, following Vicente-Serrano et al. (2009). The sensitivity of SPEI to potential evapotranspiration is higher than other drought indices (Vicente-Serrano et al., 2015), such as PDSI or RDI (defined in Sect. 2.6.5 and 2.6.6).

2.6.3 Rainfall anomaly index (RAI)

RAI can be used to analyze dry or wet periods. When used to study droughts, RAI (e.g., Keyantash and Dracup, 2002) represents a ranking of yearly precipitation, compared to the most negative precipitation anomalies recorded. It is defined as follows:

$$RAI = -3\frac{P - \bar{P}}{\bar{E} - \bar{P}} \qquad (5)$$

where P is the annual precipitation, $\bar{P}$ the mean annual precipitation and $\bar{E}$ is the precipitation average of the ten driest years. Negative values of RAI indicate dry periods.

2.6.4 Effective drought index (EDI)

In contrast to the other drought indices, EDI (Byun and Wilhite, 1999) is computed using daily precipitation to better take into account the effect of precipitation variability on droughts. The effective precipitation EP is calculated first:

$$EP = \sum_{n=1}^i \frac{\sum_{d=1}^n P_d}{n} \qquad (6)$$

where i is the summation period and P_d is the precipitation of d days before the end of the period i. We choose $i = 365$ days in our application, i.e., annual averages. EP is then normalized to calculate the EDI:

$$EDI = \frac{EP - \overline{EP}}{\sigma_{EP}} \qquad (7)$$

where $\overline{EP}$ is the mean of the effective precipitation (EP) and σ_{EP} its standard deviation.

2.6.5 Palmer drought severity index (PDSI) and Palmer hydrological drought index (PHDI)

PDSI was developed by Palmer (1965) to better consider the role of evapotranspiration on droughts and to "measure the cumulative departure of moisture supply" during dry periods. This index is composed of a simplified water balance of a basic two-layer soil model which is then compared to

a reference water balance time series. It is a dimensionless number, usually ranging between -4 and +4, with negative values indicating dry periods (Keyantash and Dracup, 2002). It is widely used, especially in the United States, but it is relatively involved to calculate (Jacobi et al., 2013). In addition, it assumes a homogeneous soil type and the time window considered by the index varies depending on the weather.

PHDI (Palmer, 1965) is a variation of the previous index which has been developed to better represent hydrological droughts. To achieve this, PHDI applies the same simplified soil model as PDSI, but stricter criteria are used to define the limits of the wet and dry periods. This results in an index which reacts more gradually than the original Palmer index (Keyantash and Dracup, 2002).

In this study, we use the Matlab tool developed by Jacobi et al. (2013) to calculate PDSI and PHDI.

2.6.6 Reconnaissance drought index (RDI)

The RDI (Tsakiris and Vangelis, 2005) is based on the FAO aridity index α_i, defined as:

$$\alpha_i = \frac{\sum_{j=1}^{12} P_{ji}}{\sum_{j=1}^{12} PET_{ji}} \tag{8}$$

where P_{ji} is the monthly precipitation of the year i and PET_{ji} is the monthly potential evapotranspiration. The standardized RDI is computed as followed (Tsakiris and Vangelis, 2005):

$$RDI = \frac{ln(\alpha_i) - \overline{ln(\alpha_i)}}{\sigma_{ln(\alpha_i)}} \tag{9}$$

where $\sigma_{ln(\alpha_i)}$ is the standard deviation of the natural logarithm of the aridity index and $\overline{ln(\alpha_i)}$ its mean.

2.7 Computation of potential evapotranspiration

SPEI, PDSI, PHDI, and RDI are calculated using the same expression for potential evapotranspiration (ET_0), sometimes referred to as reference evapotranspiration. We use the well-known FAO Penman-Monteith equation (Allen et al., 2000) in all our calculations. Some indices, for example PDSI, are often computed using simpler expressions for potential evapotranspiration that are based only on temperature, such as the Thornthwaite equation (Jacobi et al., 2013). However, we compute all indices with identical ET_0 to avoid an undue influence on the performance of the drought indices by the choice of ET_0.

The hydrological model, described in Sect. 2.3, also uses daily inputs of reference evapotranspiration as estimated by the FAO Penman-Monteith equation (Allen et al., 2000). ET_0 is then multiplied by a time-varying crop coefficient to account for the different crop types and their spatial distribution in the catchment. Hence, the final model input is the spatially-explicit daily crop evapotranspiration under standard conditions (ET_c), corresponding to the maximum evapotranspiration of each crop without water limitation. The crop coefficients are taken from Allen et al. (2000). Although ET_c is used to simulate hydrological impacts, it is not used in the computation of drought indices. Here, we use ET_0 in all calculations. This is consistent with the approaches used in other studies. We want to mimic the typical utilization of drought indices, which are usually computed directly from meteorological data (e.g., Zarch et al., 2015). To test the impact of our assumption, we repeated the analysis presented in this paper using ET_c instead of ET_0 (results not shown) and found very similar correlations and relationships between drought indices and hydrological variables.

The potential evapotranspiration used by the hydrological model and in the computation of drought indices is calculated from the outputs of a weather generator (Sect. 2.4). To validate the outputs of the weather generator (Sect. 3.1), time series of potential evapotranspiration are prepared, based on measured time series. More precisely, we use 23 years of precipitation and temperature (1988-2011) measured at the meteorological station of Ejea de los Caballeros (Sect. 2.2). Time series of radiation, wind, and relative humidity are also needed to calculate ET_0. However, these variables are only measured for the last 9 years. For the 14 years with missing data, ET_0 is calculated using the daily mean radiation, wind, and relative humidity averaged over the last 9 years and on the actual measurement of temperature. Differences between the usual calculation of ET_0 and the calculation based on averaged radiation, relative humidity, and wind are small. The Nash-Sutcliffe efficiency (Nash and Sutcliffe, 1970) between the ET_0 using the full data set and the ET_0 based on averaged data is above 0.85 for the 9 last years.

2.8 Methods of comparing the drought indices to predict hydrological variables

To compare how well the drought indices can predict the chosen hydrological variables in present and future climate, we use two approaches. First, we compute the Pearson's linear correlation coefficient r between the time series of meteorological drought indices and the hydrological variables. Secondly, we compute changes in the coefficients of the (assumed) linear regressions between the time series in present and future climate and the drought indices.

2.8.1 Pearson's correlation coefficient

The Peason's linear correlation coefficient quantifies how well the variability in one time series can be explained by the variability of another time series, assuming a linear relationship between the two variables. In the context of this study, it indicates if the drought indices have the capability of finding periods with a discharge or hydraulic heads lower than usual and periods with water deficit higher than usual.

It is defined as follows:

$$r = \frac{cov(DI, x)}{\sigma_{DI}\sigma x} \qquad (10)$$

in which cov is the covariance, DI is the value of the drought index and x is the hydrological variable under consideration. The range of r is -1 to +1, where +1 indicates a perfect positive correlation, -1 is a perfect negative correlation, and a value of zero signifies no correlation.

2.8.2 Linear regression

The Pearson's correlation coefficient indicates the degree of linear dependence between two variables. However, if this correlation coefficient is calculated under different climatic conditions, it does not indicate possible changes in the coefficients of the (assumed) linear dependencies. To investigate the changes in the linear dependency between the two climates, we perform a linear regression between a drought index and a hydrological variable in the present climate. Then, we use this linear relationship to predict the hydrological variables from the same drought indices in future climate. We conduct this analysis for each combination of drought index and hydrological impact in all irrigation scenarios. By this, we aim to investigate if drought indices in future climate represent on average a similar drought (i.e., a drought with similar hydrological impacts) than in present climate. This is important because many drought studies (e.g., Kirono et al., 2011) only report changes in drought indices, implicitly assuming identical drought impacts for identical drought-index values in present and future climate. However, a drought described by a SPI-value of -1, for example, may have different consequences on discharge and water deficit in projected future climate than under current climate conditions (see Sect. 3.3).

To quantify the changes in the linear dependencies between hydrological variables and drought indices, two performance metrics were selected: The model bias B and the normalized root mean square error ($NRMSE$). The model bias is the sum of the differences between the predicted and the actual values of the hydrological variable:

$$B = \sum_{i=1}^{n} V_{stat,i} - V_{mod,i} \qquad (11)$$

where $V_{stat,i}$ indicates the predicted value of discharge or water deficit based on the linear regression, $V_{mod,i}$ represents the value of the same variable predicted by the hydrological model and n is the length of the time series.

The $NRMSE$ is the root mean square error divided by the standard deviation of the least-square regression in present climate σ_{pres}:

$$NRMSE = \frac{1}{\sigma_{pres}}\sqrt{\frac{\sum_{i=1}^{n}(V_{stat,i} - V_{mod,i})^2}{n}} \qquad (12)$$

In present climate, the variability of the differences between the outputs from the hydrological model and the linear regression is smaller than 12% of the average difference between model outputs and the linear regression. Hence, the error of the linear model in the present climate can be considered homoscedastic, i.e, σ_{pres} is considered constant in the subsequent analysis.

3   Results

3.1   Validation of the weather generator outputs

Because the outputs from the weather generator are used to compute the drought indices and to force the hydrological model, the weather generator must reproduce the observed characteristics of the meteorological variables. The calibration and validation of the weather generator for the statistics of precipitation and potential evapotranspiration has been presented by von Gunten et al. (2015). We extend this work by comparing the frequency distribution of the studied drought indices in the observed climate record with the corresponding frequency distribution computed from the weather generator outputs in the current climate.

All seven drought indices used in our study are normalized (Sect. 2.6) so that they can be used in different regions. If the normalization would have been carried out separately in the observed and simulated data, the frequency distributions of the drought indices would be similar, regardless of the similarity of the time series. To provide a meaningful comparison, we compute the normalization on the simulated data (weather generator) and we use the same normalization for the observed data (current climate record).

To compute each drought index, we use the measured time series, which has a length of 23 years (1988-2011). In addition, we compute the drought indices using the simulated data. To get a comparable length between measured and modeled data, the time series of drought indices based on the weather generator are separated into 15 periods with a duration of 23 years each (totaling 354 years). The final length of this time series is chosen such that it is about twice the length of the hydrological simulations (180 years). We then prepare 15 empirical cumulative distribution functions (*ecdf*) based on the outputs of the weather generator and compare them with the *ecdf* based on the current observed climate record (Fig. 4).

The *ecdf* of all drought indices based on measurements fall into the region defined by the 15 modeled *ecdf*. Hence, differences between the observed and simulated data were small, compared to the difference between the 15 modeled *ecdf*. In addition, we used a 2-sided Kolmogorov-Smirnov test to compare the time series based on modeled and measured data. This test (e.g., Hazewinkel, 2001) is a non-parametric statistical test which quantifies the maximum distance in cumulative probability between two distributions and tests how

likely it is that the two samples are drawn from the same distribution. All drought indices pass this test, i.e., the null hypothesis of identical *ecdf* between measured and simulated data is not rejected at a 5% significance level. Therefore, the drought indices based on the time series of the weather generator outputs are showing a reasonable agreement with the observed time series to be used in present climate. Weather generators are commonly operated to produce time series of future hydro-meteorological variables (e.g., Burton et al., 2010) and we are also confident to use the weather generator to produce future time series of drought indices.

3.2 Correlation coefficients between drought indices and hydrological variables

In this section, we analyze the correlation between the different drought indices for the 180 years of each scenario and the corresponding simulated mean annual discharge, water deficit, and hydraulic heads. For this purpose, we use the Pearson's linear correlation coefficient r between the drought indices and the hydrological variables (Sect 2.8.1). We conduct the same analysis for present and future climate, and for the different irrigation scenarios. Here, we present only the main results of this comparison (details are available in the supplementary material).

In summary, the correlation coefficients between the hydrological variables and the drought indices are similar for all irrigation scenarios in present and future climate. For example, let us consider the correlation coefficients between drought indices and discharge (Fig. 5). In present climate, SPEI, RDI, and RAI have the highest correlation with discharge in the PIRR scenario ($0.77 < r < 0.80$) as well as in the NOIRR scenario ($0.81 < r < 0.83$). These indices also have similar correlation coefficients in future climate ($0.79 < r < 0.84$). If we consider the correlation of a particular drought index with discharge over all climate/irrigation scenarios, the differences in r is < 0.1.

Water deficit exhibits a similar behavior as discharge when correlation coefficients are examined. When the absolute values of correlation coefficients are large in present climate, they will be similarly large in future climate or in another irrigation scenario. SPEI, RDI, and RAI have the largest correlation coefficients with water deficit in all scenarios ($0.78 < |r| < 0.81$).

Correlation coefficients between drought indices and groundwater heads in a particular observation well are similar for all drought indices considered. However, the correlation coefficients are very different from one observation well to another (see supplementary material for more information).

3.3 Linear regressions between hydrological variables and drought indices

The previous section has shown that the linear correlation between drought indices and hydrological variables is relatively similar under all climatic and irrigation conditions. Hence, a particular drought index is able to identify the dry periods in present and future climate. However, this does not indicate whether the droughts in future climate have similar hydrological impacts than those in present climate. Correlation coefficients quantify how well a relationship between two variables can be expressed by an (assumed) linear equation, without considering the actual coefficients of the linear equation. The latter are commonly evaluated by linear regression.

Identifying changes in the regression coefficients of the relationships between drought-indices and hydrological variables is important when making hydrological predictions based on meteorological drought indices in a changing climate. Only when the regression coefficients do not change, the same value of a drought index has the same hydrological impact. Towards this end, we compare changes in the (assumed) linear regressions between drought indices, and discharge or water deficit (Sect. 2.8.2). In the subsequent analysis, we do not consider hydraulic heads because the results almost entirely depend on the position of the observation well.

The stability of the relationship between drought indices and hydrological variables strongly depends on the chosen drought index and the irrigation scenario. In Fig. 6, we exemplify the relationship between SPEI and discharge for two irrigation scenarios in present and future climate. On the right panel of Fig. 6 (scenario FUTIRR), the relationship between SPEI and discharge is relatively stable in different climates. A drought with a similar intensity (as defined by SPEI) has similar impacts on discharge in present and future climate. On the left panel, the bias is larger. In this case, a drought with a particular SPEI-value results in a different annual mean discharge in present and future climate.

As outlined above, we use two different performance metrics to quantify this bias, the model bias B and the $NRMSE$ (Sect 2.8.2). Fig. 7 shows these two metrics for all indices and the two hydrological variables (discharge and water deficit) as bar plots. Overall, our results suggest that the relationships between the chosen meteorological drought indices and hydrological variables are not stable under a changing climate. The computed model biases between drought indices in present and future climate appear important. In the scenario without irrigation, the largest observed model bias is 0.012 m³/s for discharge and 3.1% for the water deficit (mean discharge in present climate: 0.015 m³/s, mean annual water deficit: 80%). With irrigation, the largest bias for discharge is 0.006 m³/s for the RAI drought index and 9% for water deficit (mean discharge: 0.03 m³/s, mean annual water deficit for irrigated and non-irrigated zones: 52%). In the worst case described above (discharge without irrigation),

the model bias can reach 80% of the value of the hydrological variable, which is a significant difference. For certain conditions, however, the bias is low. For example, water deficit in the scenario without irrigation is predicted well by the linear model (the largest bias is equivalent to only 3.9% of the present water deficit).

For discharge, model bias depends strongly on the irrigation scenario (Fig. 7, top panels). With irrigation, the drought indices often underestimate the changes in discharge, especially if the indices are based on precipitation only. For example, in the case of SPI, the model bias for discharge is -0.006 m^3/s with irrigation (and 0.001 m^3/s without irrigation). On the contrary, drought indices which are based on ET$_0$ and precipitation have a lower bias in the scenario with irrigation than in the scenario without irrigation. For example, SPEI has a model bias of 0.001 m^3/s with irrigation and of 0.012 m^3/s without irrigation. In the Lerma catchment, discharge is more sensitive to climate change when irrigation is present (von Gunten et al., 2015). Hence, drought indices which are more sensitive to climate change, notably to changes in ET$_0$, predict changes in discharge better in irrigated cases. The discharge in the scenario without irrigation does not change significantly and drought indices with a smaller reaction to climate change are better predictors for hydrological impacts than those with a stronger reaction (Fig. 7, top panels).

For the water deficit (Fig. 7, bottom panels), drought indices which include ET$_0$ have a lower model bias than indices which only include precipitation. In the case of SPI with irrigation, the model bias is 8.5%. In the case of RDI, which includes ET$_0$, the model bias is 3.3%. The lower bias for drought indices containing ET$_0$ can be explained because ET$_0$ is directly influencing the water-deficit calculation.

The drought indices with the lowest model bias and a correlation coefficient $r > 0.6$ are: RAI for discharge in NOIRR scenario, RDI for the water deficit in FUTIRR/PIRR scenario, and SPEI for the water deficit in the NOIRR scenario and discharge in FUTIRR/PIRR scenario.

3.4 Future droughts

In Sect. 3.2 and Sect. 3.3, we explored the relationships between the different drought indices and the selected hydrological variables in present and future climate. In the present section, we compare the drought indices in present climate to those in future climate. This is a step forward compared to previous studies because we use the information of Sect. 3.2 and Sect. 3.3 to improve the predictions of future droughts, notably to interpret differences between the predictions based on different drought indices. Fig. 8 shows the changes between present and future climate in the seven drought indices based on the outputs of the four regional climate models. Note that a decrease in the values of the drought indices indicates an increase in drought intensity.

When we compare the changes in drought indices between present and future climate, significant differences can be ob-

served between the different climate scenarios (based on the 4 regional climate models). Indices which only contain precipitation (RAI, SPI, and EDI) predict a small increase in droughts or a small decrease depending on the climate scenario (Fig. 8, top panels). For example, the average SPI decreases by -0.4 when using the ETHZ climate scenario and increases by 0.2 when using the MPI scenario (for comparison, an SPI of -3 would be an extreme drought). The MPI and UCLM regional climate models predict an increase in annual precipitation for the Lerma catchment (von Gunten et al., 2015). Hence, the climate scenarios based on these regional climate models result in a decrease in drought events (i.e., an increase in the drought index value) when indices are only based on precipitation. Indices which also consider ET$_0$ (Fig. 8, bottom panels) indicate an increase in droughts in all analyzed future climates. However, this increase is smaller when MPI and UCLM are used to construct the climate scenario. In the MPI case, a decrease of 1.1 in the mean value of SPEI is computed. When the ETHZ climate model is used, a decrease of 2.95 is computed (Fig. 8, bottom panel).

In addition to the differences related to the chosen climate scenario, the choice of the drought index has a large influence on the prediction of future droughts. These differences in drought prediction are largely the reflection of the differences in the linear relationships between drought indices and hydrological variables discussed in Sect. 3.3. If a drought index has a negative bias for discharge (as it is the case for indices which are based on precipitation only), small changes in future droughts are predicted. For example, when we average the four different climate scenarios, mean RAI in future climate shows a decrease of 0.02 when compared to RAI in present climate (Fig. 8, top panel, left column). Based on the linear model under present irrigation conditions, this can be translated to an increase in water deficit of 0.21 mm/year and a decrease in discharge of 8.7×10^{-5} m^3/s. These changes are unlikely to have consequential impacts on irrigation or on the hydraulic regime of the catchment. For the indices that depend on ET$_0$, the predicted increase in droughts becomes larger. For example, mean SPEI shows a decrease of -2.43 (average of four regional climate models). If we would use the linear model developed in present climate, the decrease in discharge in the scenario with irrigation would be of 0.01 m^3/s, which is one third of the annual mean discharge. Based on the hydrological model, the change in discharge in the FUTIRR scenario is 0.006 m^3/s (average of the four climate models). Large uncertainties linked with climate prediction and hydrological modeling still prevail in this estimation. However, the hydrological model generally reproduces discharge and hydraulic head measurements. Moreover, it simulates many relevant processes leading to discharge generation. Hence, we assess this model to be more reliable in predicting hydrological effects of climate change than a mere comparison of meteorological drought-index values.

4 Discussion

Outputs from global or regional climate models are often used to predict changes of droughts in future climates because these outputs are easy to obtain and relatively simple to analyze. In most cases, the analysis is based on the computation of meteorological drought indices. To use drought indices in climate-impact studies, it is necessary to choose a particular set of indices. Based on the assessment of correlation coefficients and stability of the relationships between hydrological variables and drought indices, the drought indices RDI, RAI, and SPEI are the most suitable indices in our case study. However, their performance strongly depends on the assumed irrigation scenarios and may thus be different in other climates and land-uses. Other drought indices might perform better in more humid or colder climates. However, based on this study, these three indices are the most suitable for climate-impact studies in Mediterranean climate.

On a broader level, we propose to use drought indices with a certain caution in climate-impact studies and advise against using a single drought index. A hydrological model is a more direct way to analyze hydrological drought impacts in future climate and it should be used whenever possible in such studies. Unfortunately, the development and the parameter calibration of hydrological models is a complicated task and depends on the availability of hydrological measurements such as discharge and hydraulic heads.

If the development of a hydrological model is not an option, our results suggest that outputs from drought indices should be analyzed in detail with respect to three issues, regardless of the set of the chosen drought indices:

1. The importance of potential evapotranspiration: Many meteorological drought indices only consider precipitation. Because these indices neglect the predicted increase in potential evapotranspiration, their uses could lead to an underestimation of future drought risks. This has been reported in previous studies, notably by Dubrovsky et al. (2009) and Zarch et al. (2015). Our study confirms that drought indices which neglect potential evapotranspiration predict smaller changes in droughts than those which include ET_0 (Sect. 3.4). However, we found that some indices that include ET_0, such as SPEI, predict larger changes in drought severity compared to the simulations with the hydrological model (Sect 3.3), especially in scenarios with low soil moisture (scenario NOIRR). This was not previously considered and it indicates that, under some circumstances, the influence of ET_0 can be overestimated.

2. Correlation coefficients are not always sufficient to compare drought indices: Our comparison of the correlation coefficients between hydrological variables and drought indices (Sect 3.2) leads to similar results than previous studies. For example, Vicente-Serrano et al. (2012a) compared the correlation between standardized

stream flow (SSI) at monthly time scale and 6 drought indices, including SPI, SPEI, PDSI, and PHDI. SPEI showed the best correlation with discharge - results that we could reproduce (Fig. 5). SPI has a lower correlation than SPEI, but the difference is relatively small in both studies. However, more detailed investigations of the relationships between the drought indices and hydrological variables provide new insights which are not possible to obtain by using correlation coefficients alone. For instance, the correlation coefficients between drought indices and annual mean discharge are similar in all scenarios and all climates within our study, while the regression coefficients change in future climate, and they do so differently in different irrigation scenarios. Hence, impacts of irrigation and climate on drought indices are better understood if we use analysis tools beyond correlation coefficients.

3. The hydrological impacts of drought depend on climate change: This has been previously explored in other studies, notably in studies focusing on hydrological droughts. For instance, Wanders et al. (2015) proposed a method to adapt the low-flow threshold defining the start of a hydrological drought as a function of the advance of climate change. The goal was to account for changes in the responses of low flows to droughts in a changing climate. However, these changes are also important when studying meteorological droughts. In this field, it is often assumed that the same lack of precipitation would have the same (hydrological) effects in present and future climate. However, this is not always the case (Sect 3.3). Investigating changes in frequency and intensity of meteorological droughts results in biased predictions of climate change impacts if changes in the hydrological processes are not considered.

5 Conclusions

The interpretation of changes in meteorological drought indices between future and present climates can be considerably compromised by the assumption that the relationship between the drought indices and the hydrological variables (which represent the effects of drought) is identical in present and future climate. The same drought-index value might lead to different drought consequences in present and future climate. Results can be further compromised by neglecting the increase in ET_0. In our case study, drought indices that take into account precipitation only (SPI, RAI, and EDI) underestimate the impact of droughts on water deficit and discharge often. By contrast, indices which give a high weight to ET_0 (as SPEI) sometimes overestimate the impact of future droughts on discharge, especially in the absence of irrigation.

As a summary, in the Lerma catchment, drought indices are useful indicators of dry periods in all tested climates and land-uses. However, a change in a particular drought

index in future climate cannot easily be transferred to hydrological effects of droughts. In a stationary climate, the relationships between drought impacts and drought indices are usually reliable and so the hydrological consequences of droughts can be assessed from the drought indices. However, these relationships may change in a non-stationary climate and their evolution strongly depends on the particular combination of drought index and land-use. Hence, projections of future droughts using only one drought index may results in misleading estimation of the possible drought impacts.

Because drought indices can be estimated directly from the outputs of climate models, they are popular metrics of droughts even though they cannot be related uniquely to hydrological or even ecological impacts of droughts. Rather than relying on these indices, we recommend using a hydrological model to study hydrological effects of future droughts whenever possible. If setting up a hydrological model is not feasible, we advise to consider more than a single drought index and choose drought indices that take both precipitation and ET_0 into account. We also advise to test the chosen drought indices against measured or modeled results.

Regardless of the chosen drought index or of the climate scenarios, this study, and many previous studies (e.g., Blenkinsop and Fowler, 2007), predict an increase in the severity of droughts in the next fifty years in northern Spain. Adaptation to the new climatic conditions will therefore be necessary. The complexity of hydrological predictions should not prevent a timely adjustment of the urban water and irrigation networks.

6   Data availability

Hydrological data from the Lerma catchment have been collected and is owned by the Spanish Geological Survey (e.g., Merchán et al., 2013). Meteorological data have been collected by the Spanish meteorological national agency (AEMET) and is currently proprietary. Data from the ENSEMBLES project is available at: http://ensemblesrt3.dmi.dk/.

References

Abrahao, R., Causapé, J., García-Garizábal, I., and Merchán, D.: Implementing irrigation: Water balances and irrigation quality in the Lerma basin (Spain), Agricul. Water Manag., 102, 97–104, 2011.

Agwata, J.: A review of some indices used for drought studies, Civil and Environmental research, 6, 14–21, 2014.

Allen, R., Pereira, L., Raes, D., and Smith, M.: Crop evapotranspiration (guidelines for computing crop water requirements), FAO irrigation and drainage paper, 56, 2000.

Ashkar, F. and Mahdi, S.: Fitting the log-logistic distribution by generalized moments, J. Hydrol., 328, 694 – 703, 2006.

Bachmair, S., Kohn, I., and Stahl, K.: Exploring the link between drought indicators and impacts, Nat. Hazard and Earth Sys., 15, 1381–1397, 2015.

Beltrán, A.: Estudio de los suelos de la zona regable de Bardenas II. Sectores VIII, IX, X, XII y XIII., Instituto Nacional de Reforma y Desarrollo Agrario, Ministerio de Agricultura, Pesca y Alimentación, 1986.

Blenkinsop, S. and Fowler, H.: Changes in European drought characteristics projected by the PRUDENCE regional climate models, Int. J. Climatol., 27, 1595 – 1610, 2007.

Bloomfield, J. and Marchant, B.: Analysis of groundwater drought building on the standardised precipitation index approach, Hydrol. Earth Syst. Sci., 17, 4769–4787, 2013.

Bovolo, C., Blenkinsop, S., Majone, B., Zambrano-Bigiarini, M., Fowler, H., Bellin, A., Burton, A., Barceló, D., Grathwohl, P., and Barth, J.: Climate change, water resources and pollution in the Ebro basin: towards an integrated approach, in: The Ebro River Basin, edited by Barceló, D. and Petrovic, M., Springer-Verlag, 2010.

Burke, E. J., Brown, S. J., and Christidis, N.: Modeling the recent evolution of global drought and projections for the twenty-first century with the Hadley Centre climate model, J. Hydrometeor., 7, 1113–1125, 2006.

Burton, A., Kilsby, C., Fowler, H., Cowpertwait, P. S. P., and O'Conell, P.: RainSim: A spatial-temporal stochastic rainfall modelling system, Environ. Mod. Software, 23, 1356–1369, 2008.

Burton, A., Fowler, H., Blenkinsop, S., and Kilsby, C.: Downscaling transient climate change using a Neyman-Scott Rectangular Pulses stochastic rainfall model, J. Hydrol., 381, 18–32, 2010.

Byun, H.-R. and Wilhite, D.: Objective quantification of drought severity and duration, J. Climate, 12, 2747–2756, 1999.

Collins, M., Booth, B., Harris, G., Murphy, J., Sexton, D., and Webb, M.: Towards quantifying uncertainty in transient climate change, Clim. Dyn., 27, 127–147, 2006.

Dai, A.: Drought under global warming: a review, Wiley Interdisciplinary Reviews: Climate Change, 2, 45–65, 2011.

Dubrovsky, M., Svoboda, M., Trnka, M., Hayes, M., Wilhite, D., Zalud, Z., and Hlavinka, P.: Application of relative drought indices in assessing climate-change impacts on drought conditions in Czechia, Theor. Appl. Climatology, 96, 155–171, 2009.

Edwards, D.: Characteristics of 20th century drought in the United States at multiple time scales, Ph.D. thesis, Colorado State University, 1997.

Gil, M., Garrido, A., and Gómez-Ramos, A.: Economic analysis of drought risk: An application for irrigated agriculture in Spain, Agr. Water Manage., 98, 823–833, 2011.

Hayes, M. and Lowrey, J.: Drought indices, Intermountain West Climate Summary, pp. 1–6, 2007.

Hazewinkel, M.: Encyclopedia of mathematics, Springer (Kluwer Academic Publishers), 2001.

Heim, R.: A review of the twentieth-century drought indices used in the United States, B. Am. Meteorol. Soc., 83, 1149–1165, 2002.

Herrera, S., Fita, L., Fernández, J., and Gutiérrez, J. M.: Evaluation of the mean and extreme precipitation regimes from the ENSEMBLES regional climate multimodel simulations over Spain, J. Geophys. Res., 115, D21 117, 2010.

Hisdal, H., Stahl, K., Tallaksen, L., and Demuth, S.: Have streamflow droughts in Europe become more severe or frequent?, Int. J. Climatol., 21, 317–333, 2001.

Holman, I., Tascone, D., and Hess, T.: A comparison of stochastic and deterministic downscaling methods for modelling potential groundwater recharge under climate change in East Anglia, UK: implications for groundwater resource management, Hydrogeol. J., 17, 1629–1641, 2009.

Jacob, D., Van den Hurk, B., Andrae, U., Elgered, G., Fortelius, C., Graham, L. P., Jackson, S. D., Karstens, U., Köpken, C., Lindau, R., Podzun, R., Rockel, B., Rubel, F., Sass, B. H., Smith, R. N. B., and Yang, X.: A comprehensive model intercomparison study investigating the water budget during the BALTEX-PIDCAP period, Meteorol. Atmos. Phys., 77, 19–43, 2001.

Jacobi, J., Perrone, D., Duncan, L. L., and Hornberger, G.: A tool for calculating the Palmer drought indices, Water Resour. Res., 49, 6086–6089, 2013.

Jaeger, E., Anders, I., Lüthi, D., Rockel, B., Schär, C., and Seneviratne, S.: Analysis of ERA40-driven CLM simulations for Europe, Meteorol. Zeitung, 17, 349–367, 2008.

Keyantash, J. and Dracup, J. A.: The quantification of drought: An evaluation of drought indices, B. Am. Meteorol. Soc., 83, 1167–1180, 2002.

Kilsby, C., Jones, P., Burton, A., Ford, A., Fowler, H., Harpham, C., James, P., Smith, A., and Wilby, R.: A daily weather generator for use in climate change studies, Environ. Mod. Software, 22, 1705 – 1719, 2007.

Kim, B. S., Park, I. H., and Ha, S. R.: Future projection of droughts over South Korea using representative concentration pathways (RCPs), Terr. Atmos. Ocean Sci., 25, 673–688, 2014.

Kirono, D., Kent, D., Hennessy, K., and Mpelasoka, F.: Characteristics of Australian droughts under enhanced greenhouse conditions: Results from 14 global climate models, J. Arid Environ., 75, 566–575, 2011.

Kumar, R., Musuuza, J. L., van Loon, A. F., Teuling, A. J., Barthel, R., Broek, J., Mai, J., Samaniego, L., and Attinger, S.: Multiscale evaluation of the standardized precipitation index as a groundwater drought indicator, Hydrol. Earth Syst. Sci. Discuss, 12, 7405–7436, 2015.

Leng, G., Tang, Q., and Rayburg, S.: Climate change impacts on meteorological, agricultural and hydrological droughts in China, Global Planet. Change, 126, 23–34, 2015.

Li, H., Sheffield, J., and Wood, E.: Bias correction of monthly precipitation and temperature fields from Intergovernmental Panel on Climate Change AR4 models using equidistant quantile matching, J. Geophys. Res., 115, D10 101, 2009.

Masud, M., Khaliq, M., and Wheater, H.: Analysis of meteorological droughts for the Saskatchewan River Basin using univariate and bivariate approaches, J. Hydrol., 522, 452 – 466, 2015.

Mavromatis, T.: Drought index evaluation for assessing future wheat production in Greece, Int. J. Climatol., 27, 911–924, 2007.

McKee, T. B., Doesken, N. J., and Kleist, J.: The relationship of drought frequency and duration to time scales, Eighth Conference on Applied Climatology, Anaheim, California,, 1, 179–184, 1993.

Meehl, G., Stocker, T., Collins, W., Friedlingstein, P., Gaye, A., Gregory, J., Kitoh, A., Knutti, R., Murphy, J., Noda, A., Raper, S., Watterson, I., Weaver, A., and Zhao, Z.: Global climate projections, in: The physical science basis. Contribution of working group I to the fourth assessment report of the Intergovernmental Panel on Climate Change, edited by Solomon, S., Qin, D., Manning, M., Chen, Z., Marquis, M., Averyt, K., Tignor, M., and Miller, H., Cambridge University Press, Cambridge, United Kingdom and New York, NY, USA, 2007.

Merchán, D., Causapé, J., and Abrahao, R.: Impact of irrigation implementation on hydrology and water quality in a small agricultural bassin in Spain, Hydrolog. Sci. J., 58, 1400–1413, 2013.

Mishra, A. and Singh, V.: A review of drought concepts, J.Hydrol., 391, 202–216, 2010.

Nakićenović, N., Davidson, O., Davis, G., Grübler, A., Kram, T., Rovere, E. L. L., Metz, B., Morita, T., Pepper, W., Pitcher, H., Sankovski, A., Shukla, P., Swart, R., Watson, R., and Dadi, Z.: Emission scenarios - Summary for policymakers, Intergovernemental Panel on Climate Change - Special Report, 2000.

Nash, J. and Sutcliffe, V.: River flow forecasting through conceptual models, part I- A discussion of principles, J. Hydrol., 10, 282–290, 1970.

Niemeyer, S.: New drought indices, Options Méditerranéenes, Séries A:, 80, 267–274, 2008.

Palmer, W.: Meteorological drought, Office of Climatology, U.S. Departement of commerce, 45, 1–58, 1965.

Park, C.-K., Byun, H.-R., Deo, R., and Lee, B.-R.: Drought prediction till 2100 under RCP 8.5 climate change scenarios for Korea, J. Hydrol., 526, 221–230, 2015.

Plata-Torres, J.: Informe sobre la campaña de sondeos eléctrico verticales efectuados en el barranco de Lerma (Zaragoza), Grupo de Geofísica del Instituto Geológico y Minero de España, 2012.

Prudhomme, C., Reynard, N., and Crooks, S.: Downscaling of global climate models for flood frequency analysis: Where are we now?, Hydrol. Processes, 16, 1137–1150, 2002.

Quiring, S. and Papakryiakou, T. N.: An evaluation of agricultural drought indices for the Canadian prairies, Agr. Forest Meteorol., 118, 49–62, 2003.

Samaniego, L., Kumar, R., and Zink, M.: Implications of parameter uncertainty on soil moisture drought analysis in Germany, J. Hydrometeorol., 14, 47–68, 2013.

Sánchez, E., Gallardo, C., Gaertner, M., Arribas, A., and Castro, M.: Future climate extreme events in the Mediterranean simulated by a regional climate model: A first approach, Global Planet. Change, 44, 163–180, 2004.

Srikanthan, R. and McMahon, T.: Stochastic generation of annual, monthly and daily climate data: A review, Hydrol. Earth Sys. Sci., 5, 653–670, 2001.

Stahl, K., Kohn, I., Blauhut, V., Urquijo, J., de Stefano, L., Acacio, V., Dias, S., Stagge, J., Tallaksen, L. M., Kampragou, E., van Loon, A., Barker, L., Melsen, L., Bifulco, C., Musolino, D., de Carli, A., Massarutto, A., Assimacopoulos, D., and van Lanen, H.: Impacts of European drought events: insights from an international database of text-based reports, Nat. Hazards Earth Syst. Sci. Discuss., 3, 5453–5492, 2015.

Svoboda, M., Hayes, M., and Wood, D.: Standardized precipitation index user guide, World Meteorological Organization, 1090, 1–24, 2012.

Szép, I., Mika, J., and Dunkel, Z.: Palmer drought severity index as soil moisture indicator: physical interpretation, statistical behaviour and relation to global climate, Phys. Chem. Earth, 30, 231–245, 2005.

Therrien, R.: HydroGeoSphere - A three-dimensional numerical model describing fully-integrated subsurface and surface flow and solute transport., Ph.D. thesis, Université Laval and University of Waterloo, 2006.

Therrien, R., McLaren, R., Sudicky, E., and Panday, S.: HydroGeoSphere: A three-dimensional numerical model describing fully-integrated subsurface and surface flow and solute transport - user manual, University of Waterloo, 2010.

Toews, M. and Allen, D.: Evaluating different GCMs for predicting spatial recharge in an irrigated arid region, J. Hydrol., 374, 265–281, 2009.

Tsakiris, G. and Vangelis, H.: Establishing a drought index incorporating evapotranspiration, European Water, 9, 3–11, 2005.

Tue, V. M., Raghavan, S. V., Minh, P., and Shie-Yui, L.: Investigating drought over the Central Highland, Vietnam, using regional climate models, J. Hydrol., 526, 265–273, 2015.

van der Linden, P. and Mitchell, J.: ENSEMBLES: Climate change and its impact: Summary of research and results from the ENSEMBLES project, Met Office Hadley Centre, UK, 1, 1–160, 2009.

van Genuchten, M.: A closed-form equation for predicting the hydraulic conductivity of unsaturated soils, Soil. Sci. Soc. Am. J., 44, 892–898, 1980.

Vicente-Serrano, S., Beguería, S., and López-Moreno, J. I.: A Multiscalar drought index sensitive to global warming: The standardized precipitation evapotranspiration index, J. Climate, 23, 1696–1718, 2009.

Vicente-Serrano, S. M., Beguería, S., Lorenzo-Lacruz, J., Camarero, J., López-Moreno, J., Azorin-Molina, C., Revuelto, J., Morán-Tejeda, E., and Sanchez-Lorenzo, A.: Performance of drought indices for ecological, agricultural, and hydrological applications, Earth Interact., 16, 1–27, 2012a.

Vicente-Serrano, S. M., López-Moreno, J. I., Beguería, S., Lorenzo-Lacruz, J., Azorin-Molina, C., and Morán-Tejeda, E.: Accurate computation of a streamflow drought index, J. Hydrol. Eng., 17, 318–332, 2012b.

Vicente-Serrano, S. M., van der Schrier, G., Beguería, S., Azorin-Molina, C., and López-Moreno, J. I.: Contribution of precipitation and reference evapotranspiration to drought indices under different climates, J. Hydrol., 526, 42–54, 2015.

von Gunten, D., Wöhling, T., Haslauer, C., Merchán, D., Causapé, J., and Cirpka, O.: Efficient calibration of a distributed *pde*-based hydrological model using grid coarsening, J. Hydrol., 519, 3290–3304, 2014.

von Gunten, D., Wöhling, T., Haslauer, C., Merchán, D., Causapé, J., and Cirpka, O.: Estimating climate-change effects on a Mediterranean catchment under various irrigation conditions, J. Hydrol. Reg. Stud., in press, 2015.

Wanders, N., Wada, Y., and van Lanen, H.: Global hydrological droughts in the 21st century under a changing hydrological regime, Earth Syst. Dynam., 6, 1–15, 2015.

Wilhite, D. A. and Glantz, M. H.: Understanding the drought phenomenon: The role of definitions, in: Planning for drought: Toward a reduction of societal vulnerability, edited by Wilhite, D. A., Easterling, W. E., and Wood, D. A., pp. 11–27, Westview Press, 1985.

Wu, H., Hayes, M. J., Wilhite, D. A., and Svoboda, M. D.: The effect of the length of record on the standardized precipitation index calculation, Int. J. Climatol., 25, 505–520, 2005.

Zarch, M. A. A., Sivakumar, B., and Sharma, A.: Droughts in a warming climate: A global assessment of standardized precipitation index (SPI) and reconnaissance drought index (RDI), J. Hydrol., 526, 183 –195, 2015.

Zargar, A., Sadiq, R., Naser, B., and Khan, F. I.: A review of drought indices, Environ. Rev., 19, 333–349, 2011.

Table 1. A summary of the drought indices used in this study.

Indices	Acronym	Input	Chosen time scale	Reference
Standardized precipitation index	SPI	P	12 months	Svoboda et al. (2012)
Standardized precip. evapo. index	SPEI	P, PET	12 months	Vicente-Serrano et al. (2009)
Rainfall anomaly index	RAI	P	12 months	Keyantash and Dracup (2002)
Effective drought index	EDI	P	12 months	Byun and Wilhite (1999)
Palmer drought severity index	PDSI	P, PET	~ 9 months	Palmer (1965)
Palmer hydrological drought index	PHDI	P, PET	~ 9 months	Palmer (1965)
Reconnaissance drought index	RDI	P, PET	12 months	Tsakiris and Vangelis (2005)

Table 2. Name and acronym of the regional climate models used in this study. - Adapted from Herrera et al. (2010) and von Gunten et al. (2015).

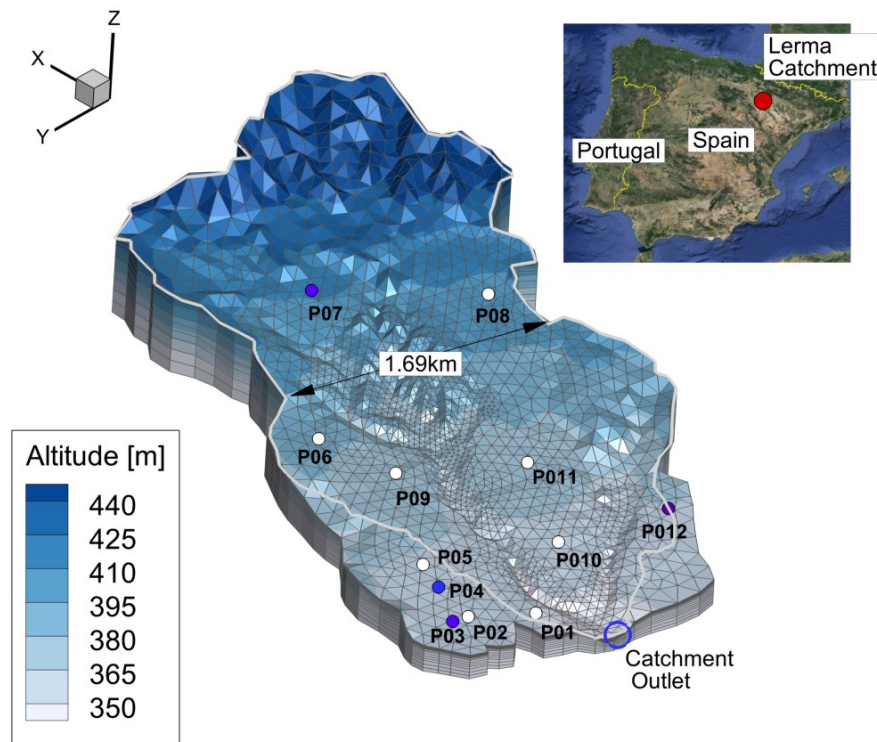| Acronym	RCM	GCM	Reference
ETHZ	CLM	HadCM3	Jaeger et al. (2008)
METO	HadRM3	HadCM3	Collins et al. (2006)
MPI	M- REMO	ECHAM5	Jacob et al. (2001)
UCLM	PROMES	HadCM3	Sánchez et al. (2004)

Figure 1. Surface elevation of the Lerma catchment (masl.). The observation wells drilled in 2010 are indicated by blue circles and the ones drilled in 2008 are indicated by white circles. The gray line represents the limits of the surface flow domain. Vertical exaggeration: 5:1. Modified from von Gunten et al. (2014, 2015).
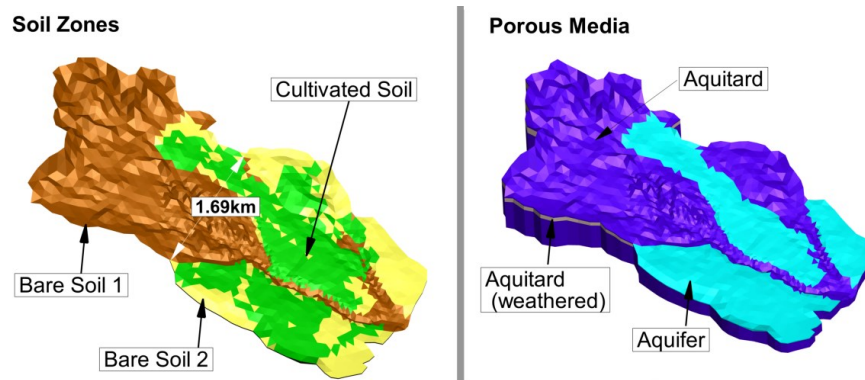
Figure 2. Soil and hydrogeological zones for the year 2009. Vertical exaggeration: 5:1. Modified from von Gunten et al. (2014, 2015).
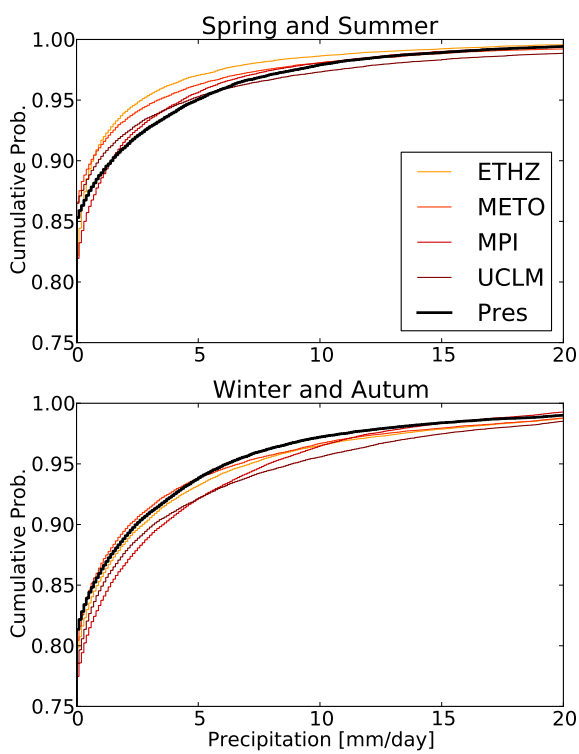
Figure 3. Empirical cumulative distribution function of daily precipitation for present and future climate scenarios.
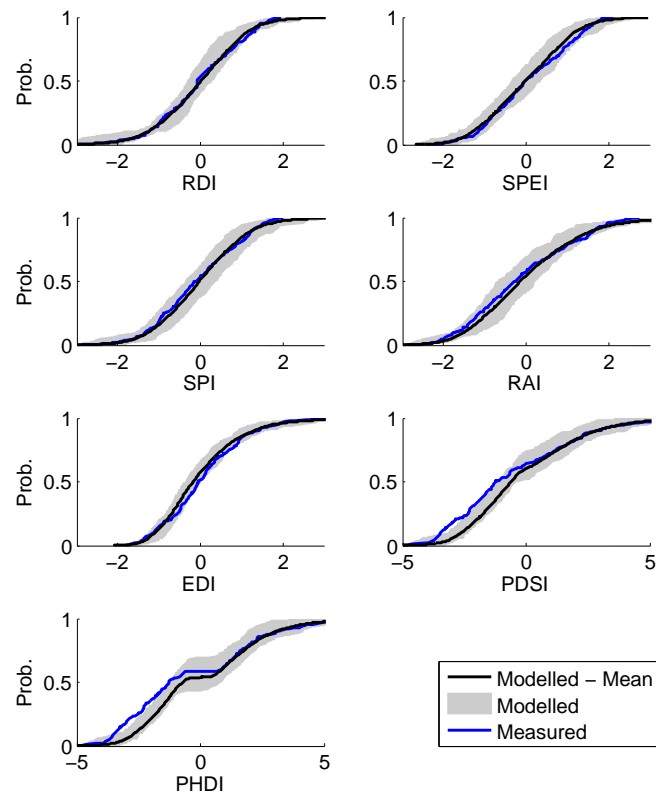
Figure 4. Empirical cumulative distribution function (*ecdf*) of drought indices based on measurement time series (in blue) and based on the outputs from the weather generator (in black). The gray area represents the boundaries of the 15 *ecdf* of drought indices based on the outputs from the weather generator when these outputs are cut at the same length that the measurement time series (23 years).
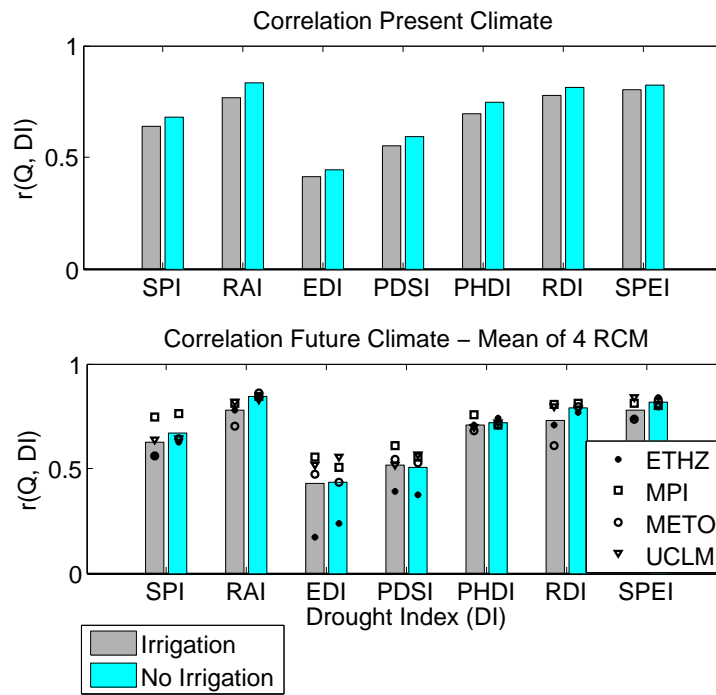
Figure 5. Correlation coefficient r between the drought indices and discharge. In future climate (bottom panel), the plotted bars are the average of the outputs of the four regional climate models. See Table 2 for information about the four regional climate models.
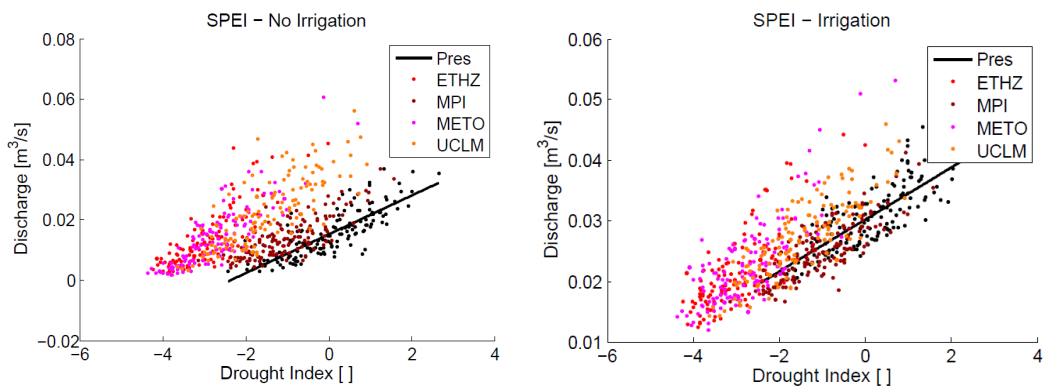

Figure 6. Performance of SPEI in future climate for annual discharge. The black line is the linear regression between SPEI and discharge in present climate. Left panel: NOIRR scenario, large model bias. Right panel: FUTIRR scenario, no significant model bias.
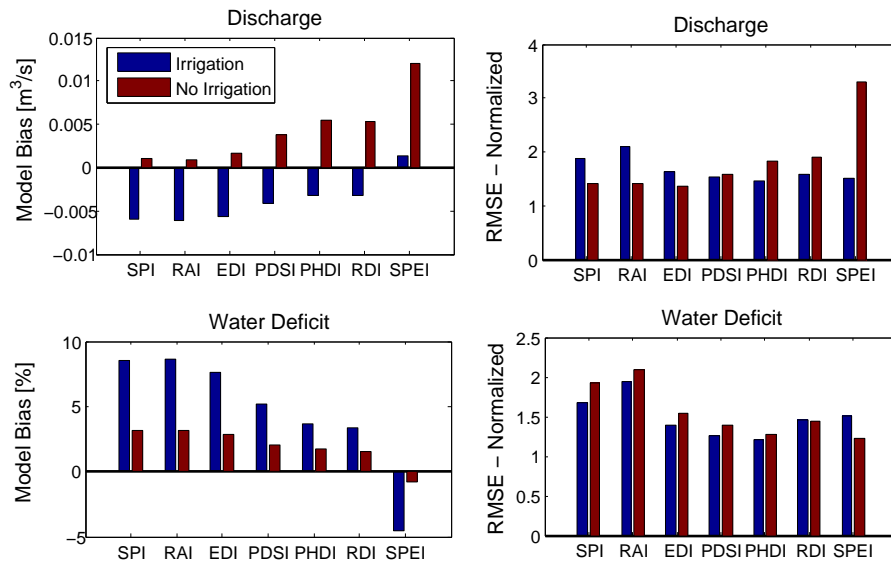
Figure 7. Model bias and NRMSE in the NOIRR and PIRR/FUTIRR irrigation scenarios.
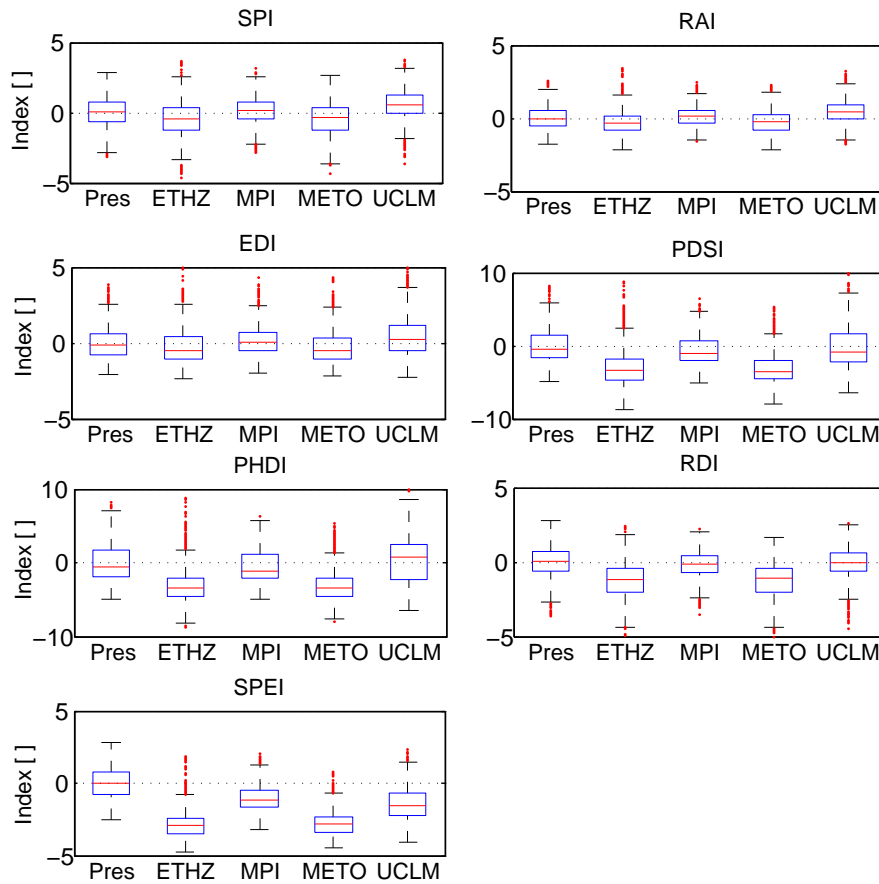

Figure 8. Present and future (2040-2050) droughts predicted by the seven drought indices, using the outputs from the weather generator. See Table 2 for information about the four regional climate models.

7 Discussion and Conclusion

7.1 Integrated hydrological models in climate-impact studies

The main goal of this thesis has been to estimate the usefulness of integrated hydrological models in climate-impact studies. My conclusion is that integrated hydrological models have three main advantages over other types of models, when studying the hydrological effects of climate change:

- Firstly, integrated hydrological models allow a joint study of the different components of the water balance. In the majority of previous studies, impacts of climate change on surface and subsurface flow are studied separately (Goderniaux, 2011), neglecting important feed-backs between surface and subsurface. I have estimated climate-change impacts on the hydrology coherently over all component of the water balance. For example, the dependence of the relationship between actual evapotranspiration and hydraulic heads on the water-table depth can be understood more precisely using an integrated hydrological model than a simpler conceptual model (Section 5).

- Secondly, integrated hydrological models are useful tools to study catchments forced by different types of anthropogenic pressures. It would have been difficult (if not impossible) to reproduce the transition toward irrigated agriculture of the Lerma catchment using other types of hydrological models. These environmental or management changes interact with climate change (Section 5) and might have more impacts on the catchment hydrology than climate change alone. In the Lerma catchment, a better understanding of irrigation and climate change lead to a more detailed prediction of future discharge changes. In this study, the irrigation onset increases total discharge, increases the sensitivity to base flow to climate change, and decreases the sensitivity of peak flow to climate change. A study using a model calibrated only on a single irrigation scenario could not have studied the different discharge responses between the irrigation scenarios. However, these differences are important to understand of the implications of the increase in irrigated areas planned in the Ebro region.

- Finally, integrated hydrological models can be useful to improve our understanding of the evolution of extreme events, such as droughts, in a changing climate. For instance, changes in drought indices are often used to study future droughts. However, this approach neglects changes in potential evapotranspiration in many cases and it does not include any variations in the hydrological processes. These simplifications might result in large biases in the estimation of hydrological impacts of future droughts (Section 6). Integrated hydrological models can help to identify these biases and their causes more efficiently than other hydrological models. Indeed, using simple methods, such as the comparison of drought indices, can be attractive because it saves time. However, it is difficult to test these methods and the effects of the various simplifications. Because integrated hydrological models simulate many of the hydrological processes, a comparison between their outputs and the outputs from simpler methods can lead to a deeper understanding of the consequences of particular simplifications, even if the comparison is limited by the quality of the (inexact) hydrological simulation.

The major practical disadvantage of integrated hydrological models is that they have long simulation times, which complicates their parameter calibration. In this thesis, this problem is overcome by using a set of grids of increasing resolution during the calibration. It decreases the duration of the calibration by a factor of eight in the chosen case study (Section 4). Hence, this procedure significantly simplifies the model calibration. However, it is still a relatively long procedure (about one month) and no detailed estimation of parameter uncertainties is included. Therefore, further improvements of the calibration procedure should be developed before integrated hydrological model can be used as easily as conceptual hydrological models. However, this study shows that parameter calibration of integrated hydrological models is manageable. Hence, integrated hydrological models can be applied and calibrated under realistic conditions on the catchment scale. Because they bring practical advantages for the predictions of hydrological impacts of climate change, I conclude that integrated hydrological models are useful to study climate-change impacts.

7.2   Climate change impacts for the Lerma catchment (2040-2050)

Even if large uncertainties are still present in the climate predictions, climate change will have important hydrological impacts on the Lerma catchment. All considered climate scenarios, based on the A1B emission scenario (Nakićenović et al., 2000), point towards drier summers, wetter winters, and higher temperature, resulting in higher potential evapotranspiration. For 2040-2050, the decrease in summer and spring precipitation is between 3% and 39% of the current (summer and spring) precipitation, depending on the regional climate model. The increase in winter and autumn precipitation is between 1% and 55% of the current (winter and autumn) precipitation. The increase in annual potential evapotranspiration is predicted to be between 9% and 22% of annual current potential evapotranspiration.

The increase in potential evapotranspiration will likely result in a small increase in actual evapotranspiration in the irrigated zones of the catchment. This augmentation of evapotranspiration and the decrease in summer precipitation will likely result in increased irrigation needs. Based on precipitation and potential evapotranspiration changes, I estimate this increase to amount about 9% of the current irrigation volumes, even though this estimate is very uncertain. Indeed, possible future changes in irrigation techniques, crop types, or in the timing of the growing season were not considered. Regardless of the uncertainties, the probable increase in irrigation needs will complicate the allocation of water resource, because of the limited volume of available water and competing water uses such as urban water needs.

Discharge during low-flow periods[2] will probably decrease (between 21% and 33% of current annual low flows). Because water in the Lerma stream is not directly used for agriculture or drinking water purpose, this decrease might not have direct social or economic impacts. However, a decrease in streamflow will indirectly result in an increase in nitrate concentration, because of the lower dilution effect. Current nitrate concentration in the streamflow at the Lerma outlet is about 80mg/l (Merchán et al., 2013) and an increase in concentration might increase eutrophication risks. A decrease

---

[2]Low-flow periods are defined here as days with no precipitation on this day and the previous day.

in annual mean hydraulic heads is also predicted, especially in the lower part of the catchment. No noticeable change in flood risk has been found under irrigated conditions.

Droughts are a serious natural threat for the Lerma catchment and their frequency and intensity will likely increase in the next thirty years. In addition, droughts will probably have different impacts in present and future climates. In other words, the same lack of precipitation could have different hydrological impacts in future climate than currently. For example, discharge could decrease more during future droughts than during present ones, because of the higher mean evapotranspiration. These changes also mean that the meteorological drought indices currently used to diagnose drought conditions could become less efficient in the future, and that the threshold for drought alert might have to be adapted.

7.3   Outlook

This thesis could be expanded in various directions. The major research questions arising from this work are as follows:

1. Most results presented depend on the outputs of large regional or global climate models. Using newer climate scenarios and other GCMs/RCMs might bring new insights in the prediction of hydrological effects of climate change, if the outputs from the newer climate models in present climate are closer to the measurements than the current ones. For example, this study could be updated using predictions of future climate based on the new RCP emission scenarios (Section 2.1). Moreover, it could be extended to later periods, such as 2080-2100. Indeed, intensity of climate change will probably increase toward the end of the century (Collins et al., 2013).

2. I only used a single hydrological model. However, it is often advantageous to compare the outputs from various models (Velázquez et al., 2011) to obtain an estimation of between-model uncertainty. It would be relatively simple to calibrate a conceptual model on discharge or a MODFLOW model (Harbaugh et al., 2000) on the hydraulic heads, at least during periods where irrigation is similar. It is possible that other hydrological models would have difficulties to simulate the transition to irrigated agriculture. However, comparing the outputs from these models during periods with "stable" conditions with the outputs from the current hydrological model would bring more confidence into the current predictions if these models can reproduce the observations adequately.

3. The calibration method that I proposed in Section 4 heavily relies on manual calibration, where parameter sets are selected manually. However, various automatic calibration methods exist, e.g., PEST (Doherty et al., 2010). These methods obtain reproducible parameter estimates and often provide estimates of the parameter uncertainty (Doherty et al., 2003). However, simulation time of the model using a coarse computational grid (about 40 minutes per simulated year for the current Lerma hydrological model) is still too long to consider automatic calibration on a desktop computer. On a medium-size cluster, automatic calibration would be feasible. A more practical option could be to further simplify the hydrological model, at least during the preliminary steps of the model calibration.

4. Plants are not explicitly considered in the hydrological model. The modeled transpiration depends on the chosen leaf area index and root depth, but the relationship between these parameters and transpiration is based on simple empirical expressions (Therrien et al., 2010). Soil-plant interactions are very much simplified in the current model even if these interactions can have a large impact on the water balance. For example, the root depth is considered constant during the year. Hence, a more accurate vegetation model, which would take into account changes in the growing season length, CO_2 influence on stomata, and root depth, would represent the hydrological processes more realistically. Moreover, the future irrigation demand could be modeled in more details, resulting in new insights for agricultural management in the study area.

5. No concern was given to water quality. I focused on water flow. Nevertheless, water quality highly depends on the climate and irrigation conditions. For example, the irrigation onset in the Lerma catchment was accompanied with increased fertilization and strongly influenced the nitrate concentration in the streams (Merchán et al., 2013). Climate change will probably also influence water quality in semi-arid regions (e.g., Bovolo et al., 2010). It would be interesting to investigate the possible impacts of climate change on water quality, notably on nutriment concentrations.

6. In the Lerma catchment, no groundwater is used for irrigation. However, this is common practice in other Mediterranean regions, such as Majorca, a Spanish island on the east of Iberian Peninsula (Candela et al., 2009). If groundwater was used as source for irrigation water, the impact of the irrigation onset on the hydrology of the Lerma catchment would likely be vastly different. Hence, the differences in the hydrological responses of the irrigated/non-irrigated catchment to climate change would also be different (Section 5). Investigating these differences would improve our understanding of the interactions between climate and irrigation changes even if it is not planned to use groundwater for irrigation in the Lerma catchment in the near future.

7. Another possible direction for future studies would to analyze water resources on the regional scale. Various studies have focused on the future of the Pyrenees, notably on the hydrological impacts of climate changes and reforestation (e.g., López-Moreno et al., 2014). As the water used for irrigation in the Lerma catchment originates from this mountain range, it would be interesting to connect this study with hydrological models of the Pyrenean Mountains. In addition, as the irrigation water is stored in the Yesa reservoir, at the foot of the Pyrenees, a further connection with a model of this reservoir could also lead to a better understanding of the possible water management options at regional scale.

8. In general, similar studies could be conducted in other climates or in larger catchments. In this case, an additional challenge would be to estimate subsurface parameters efficiently. Indeed, the computational grids representing larger catchments would impose stronger simplifications on the topography and on the soil parameters than the one used in the Lerma catchment. On the continental scale, coupling between climatological models and integrated hydrological models could also be envisaged (Davison et al., 2015) to study the feed-backs between atmosphere and irrigation. For instance, irrigation leads to higher relative humidity.

The influence on summer storms of the more humid atmosphere could be interesting to analyze.

8 Annexes

8.1 Previous investigations in the Lerma catchment

This thesis is centered on the Lerma catchment, situated in north-east Spain. The main characteristics of this catchment are presented in Section 4, 5 and 6. In addition, I present here a short review of previous studies conducted in the catchment complementing this thesis.

The Lerma catchment underwent a transition from rainfed to irrigated agriculture from 2006 to 2008 and various studies have been conducted to document the consequences of this evolution. Abrahao et al. (2011a) and García-Garizábal et al. (2012) compared the water balance of two un-irrigated year (2004 and 2005) with the water balance of the transitional years (2006-2008). An increase in streamflow, evapotranspiration and a decrease in water table depth were observed. Merchán et al. (2013) confirmed these findings for the years 2009-2010 and then for the years 2011-2013 (Merchán et al., 2015a). The efficiency of water use and the irrigation needs were also analyzed. The irrigation volume was about 10% higher than the hydric needs.

The influence of irrigation on water quality and on soil contamination was also investigated. Soil samples were collected in 2008 in irrigated and non-irrigated fields by Abrahao et al. (2011b). Water samples were also collected in different parts of the streams, which are variably influenced by irrigation. The concentration of 11 organochlorinated compounds, 17 polycyclic aromatic hydrocarbons (PAHs), 13 polychlorinated biphenyls (PCBs), 44 pesticides and metabolites, and several metals and metalloids (Cd, Cr, Cu, Ni, Pb, Zn, As, Se and Hg) were measured in soil and water samples. Traces of insecticides (notably pp'-DDT in the water and endrin in the soil) were found as well as elevated value of nickel and zinc. However, these values were low, compared to regulatory limits, and no difference could be observed between the irrigated and non-irrigated zones. Skhiri et al. (2011) measured phosphorus concentration in the Lerma catchment in 2007. They found that monthly phosphorus concentration is linked with irrigation volume and with the timing of fertilizer application on corn. Urdanoz et al. (2011) compared soil and water salinity before and after the onset of irrigation. Drainage water salinity increased of about 10% between 2006 (pre-irrigation) and 2008 (post-irrigation). Irrigation induced salt leaching from the soils and therefore soil salinity decreased (of about 15%). Merchán et al. (2015a) investigated the sources of soil salinity, notably the dissolution of the material forming the local aquitard (buro). The same author (Merchán et al., 2013) confirmed the existence of a significant relationship between salinity and irrigation for the years 2004-2011 and also found a significant relationship between irrigation and nitrate. Moreover, Merchán et al. (2014) analyzed processes affecting dissolved nitrate and sulfate on the catchment scale, notably denitrification. Stable isotope analysis suggested a low degree of denitrification in water transported from the fields to the main stream in the subsurface. A summary study looking at the 10-years of measured nitrate and salt was conducted in addition (Merchán et al., 2015b).

Pérez et al. (2011) developed an early model of the Lerma catchment using HydroGeoSphere and could reproduce the impact of irrigation on discharge and hydraulic heads. However, the modeling of evapotranspiration, notably the feedbacks with soil moisture, was problematic in the original model. Moreover, new geophysical investigations were conducted by Plata-Torres (2012) in the Lerma catchment and the estimated depth of the aquifer was consequentially reduced. Therefore, the development of a new model was subsequently necessary.

8.2   The RainSim and the EARWIG weather generators

To downscale future precipitation, the RainSim weather generator (Burton et al., 2008) is used in this thesis. RainSim is based on a spatial temporal Neyman-Scott rectangular pulses process. Neyman-Scott pulse process is a point process model. Specifically, the start of this process is the occurrence of storms. Storm origins have an uniform Poisson distribution (Figure 3, top panel). Each storm generates rain cells using β, a parameter which represents the mean waiting time for a rain cell after the storm origin. Each rain cell then produces a constant rain intensity and a duration, based on two exponential distributions. The total rain intensity is the sum of all active rain cells (Figure 3, bottom panel) (Burton et al., 2008). Neyman-Scott rectangular pulses model is an improvement over methods used by other weather generators to simulate precipitation because it provides correlation between the precipitation amounts of each day. In addition, rain events are clustered which helps to reproduce daily variability (Kilsby et al., 2007).

After the production of precipitation time series, the mean temperature and the temperature range are generated by the EARWIG model, using a first-order autoregressive process. To this end, temperature of the last day, precipitation, and a standard normal (Gaussian) variable are used in a linear relationship. For instance, for wet days with a precipitation P_i, temperature T_i of a particular day i is :

$$T_i = a_1 T_{i-1} + a_2 P_i + a_3 + e \tag{3}$$

where e is a standard normal variable. Parameters of this regression (a_1, a_2, a_3) are different for each state of the system (wet-wet, wet-dry, dry-wet, and dry-dry transitions). The other variables needed to simulate potential evapotranspiration (water vapor, sunshine duration, and wind speed) are generated based on a linear relationship between the precipitation on this day, temperature on this day, and value of the variable on the last day (Kilsby et al., 2007).
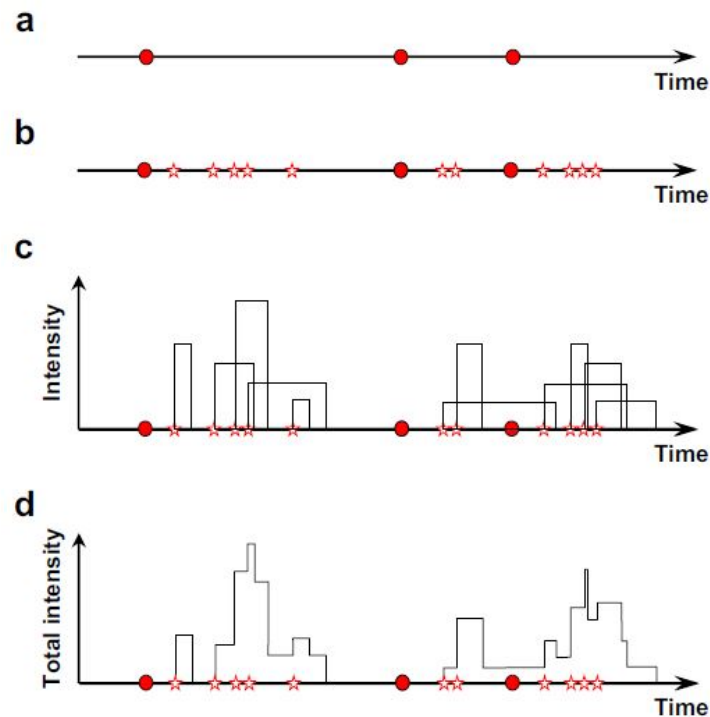
Figure 3: *Schematic of the Neyman-Scott rectangular pulses model. The top panel represent the storm origins, the second panel shows the generation of rain cells, the third panel is the duration and intensity of the rain cells, and the bottom panel presents the final precipitation time series. - Figure from Burton et al. (2008).*

References

Abrahao, R., J. Causapé, I. García-Garizábal, and D. Merchán (2011a). "Implementing irrigation: Water balances and irrigation quality in the Lerma basin (Spain)". In: *Agricult. Water Manag.* 102, pp. 97–104.

Abrahao, R., J. Sarasa, J. Causapé, I. García-Garízabal, and J. L. Ovelleiro (2011b). "Influence of irrigation on the occurrence of organic and inorganic pollutants in soil, water and sediments of a Spanish agrarian basin (Lerma)". In: *Span. J. Agric. Res.* 9, pp. 124–134.

Bovolo, C.I., S. Blenkinsop, B. Majone, M. Zambrano-Bigiarini, H.J. Fowler, A. Bellin, A. Burton, D. Barceló, P. Grathwohl, and J.A.C. Barth (2010). "Climate change, water resources and pollution in the Ebro Basin: Towards an integrated approach". In: *The Ebro river basin.* Ed. by D. Barceló and M. Petrovic. Springer-Verlag.

Burton, A., C.G. Kilsby, H. Fowler, P. S. P. Cowpertwait, and P.E. O'Conell (2008). "RainSim: A spatial-temporal stochastic rainfall modelling system". In: *Environ. Model. Softw.* 23, pp. 1356–1369.

Candela, L., W. von Igel, F.J. Elorza, and G. Aronica (2009). "Impact assessment of combined climate and management scenarios on groundwater resources and associated wetland (Majorca, Spain)". In: *J. Hydrol.* 376, pp. 510–527.

Collins, M., R. Knutti, J. Arblaster, J.-L. Dufresne, T. Fichefet, P. Friedlingstein, X. Gao, W.J. Gutowski, T. Johns, G. Krinner, M. Shongwe, C. Tebaldi, A.J. Weaver, and M. Wehner (2013). "Long-term climate change: Projections, commitments and irreversibility". In: *Climate Change 2013: The physical science basis. contribution of Working Group I to the fifth assessment report of the Intergovernmental Panel on Climate Change.* Ed. by T.F. Stocker, D. Qin, G.-K. Plattner, M. Tignor, S.K. Allen, J. Boschung, A. Nauels, Y. Xia, V. Bex, and P.M. Midgley. Cambridge University Press, Cambridge, United Kingdom and New York, NY, USA.

Davison, J. H., H. Hwang, E. A. Sudicky, and J. C. Lin (2015). "Coupled atmospheric, land surface, and subsurface modeling: Exploring water and energy feedbacks in three-dimensions". In: *Adv. Water Resour., submitted.*

Doherty, J.E. and R. Hunt (2010). "Approaches to highly parameterized inversion: A guide to using PEST for groundwater-model calibration". In: *U.S Geological Survey*, pp. 1–59.

Doherty, J.E. and John M. Johnston (2003). "Methodologies for calibration and predictive analysis of a watershed model". In: *J. Am. Water Resour. As.* 39, pp. 251–265.

García-Garizábal, I., R. Abrahao, and J. Causapé (2012). "Watershed monitoring for the assessment of irrigation water use and irrigation contamination". In: *Irrigation and Water Management, Pollution and Alternative Strategies*, pp. 21–38.

Goderniaux, P. (2011). "Impacts of climate change on groundwater reserves". PhD thesis. University of Liège.

Harbaugh, A.W., E.R. Banta, M.C. Hill, and M.G. McDonald (2000). *MODFLOW-2000, The U.S. Geological Survey modular groundwater model - User guide to modularization concept and the groundwater flow process.* U.S. Geological Survey.

Kilsby, C.G., P.D. Jonesand A. Burton, A.C. Ford, H.J. Fowler, C. Harpham, P. James, A. Smith, and R.L. Wilby (2007). "A daily weather generator for use in climate change studies". In: *Environ. Model. Softw.* 22, pp. 1705–1719.

López-Moreno, J.I., J. Zabalza, S. Vicente-Serrano, J. Revuelto, M. Gilaberte, C. Azorin-Molina, E. Morán-Tejeda, J.M. García-Ruiz, and C. Tague (2014). "Impact of climate and land use change on water availability and reservoir management: Scenarios in the Upper Aragón River, Spanish Pyrenees". In: *Sci. Total eviron.* 493, pp. 1222–1231.

Merchán, D., J. Causapé, and R. Abrahao (2013). "Impact of irrigation implementation on hydrology and water quality in a small agricultural bassin in Spain". In: *Hydrolog. Sci. J.* 58, pp. 1400–1413.

Merchán, D., J. Causapé, R. Abrahao, and I. García-Garizábal (2015a). "Assessment over a decade of a newly implemented irrigated area (Lerma Basin, Spain). I: Water balances and irrigation performance (submitted)". In: *Agr. Water Manage.*

— (2015b). "Assessment over a decade of a newly implemented irrigated area (Lerma Basin, Spain). II: Salts and nitrate exported (submitted)". In: *Agr. Water Manage.*

Merchán, D., N. Otero, A. Soler, and J. Causapé (2014). "Main sources and processes affecting dissolved sulphates and nitrates in a small irrigated basin (Lerma Basin, Zaragoza, Spain): Isotopic characterization". In: *Agr., Ecosyst. Environ.* 195, pp. 127–138.

Nakićenović, N., O. Davidson, G. Davis, A. Grübler, T. Kram, E. Lebre La Rovere, B. Metz and T. Morita, W. Pepper, H. Pitcher, A. Sankovski, P. Shukla, R. Swart, R. Watson, and Z. Dadi (2000). "Emission scenarios - Summary for policymakers". In: *Intergovernemental Panel on Climate Change - Special Report.*

Pérez, A.J., R. Abrahao, J. Causapé, O.A. Cirpka, and C.M. Bürger (2011). "Simulating the transition of a semi-arid rainfed catchment towards irrigation agriculture". In: *J. Hydrol.* 409, pp. 663–681.

Plata-Torres, J. (2012). "Informe sobre la campaña de sondeos eléctrico verticales efectuados en el barranco de Lerma (Zaragoza)". In: *Grupo de Geofísica del Instituto Geológico y Minero de España.*

Skhiri, A. and F. Dechimi (2011). "Irrigation return flows and phosphorus transport in the Middle Ebro River Valley (Spain)". In: *Span. J. Agric. Res.* 9, pp. 938–949.

Therrien, R., R.G. McLaren, E.A. Sudicky, and S.M. Panday (2010). *HydroGeoSphere: A Three-dimensional Numerical Model Describing Fully-integrated Subsurface and Surface Flow and Solute Transport.* University of Waterloo.

Urdanoz, V. and R. Aragüés (2011). "Pre- and post-irrigation mapping of soil salinity with electromagnetic induction techniques and relationships with drainage water salinity". In: *Soil Sci. Soc. Am. J.* 75.1, pp. 207–215.

Velázquez, J. A., F. Anctil, M. H. Ramos, and C. Perrin (2011). "Can a multi-model approach improve hydrological ensemble forecasting? A study on 29 French catchments using 16 hydrological model structures". In: *Adv. Geosci.* 29, pp. 33–42.